The genetic control of microtubule-mediated tip-growth stability in the liverwort *Marchantia polymorpha*

Clement Henry Martin Champion

Somerville College

Department of Plant Sciences

University of Oxford

Thesis submitted for the Degree of Doctor of Philosophy.

Michaelmas 2017

The genetic control of microtubule-mediated tip-growth stability in the liverwort *Marchantia polymorpha*

Clement Henry Martin Champion

Somerville College, Department of Plant Sciences, University of Oxford

Thesis submitted for the Degree of Doctor of Philosophy.

Abstract

Polar growth is an important mechanism for plant cell morphogenesis. Tip-growth represents an extreme mode of polar growth where cell expansion is stably restricted to a narrow domain of the cell periphery resulting in the formation of a tubular cell projection. The microtubule cytoskeleton controls the stable positioning of the growth region in tip-growing cells of flowering plants and mosses. I show that this holds true in the earliest diverging clade of land plants, the liverworts. In *Marchantia polymorpha*, pharmacological destabilization of the microtubule cytoskeleton leads to the formation of wavy or bifurcating rhizoids, a tip-growing cell type analogous to root hairs of flowering plants and to caulonema cells of mosses. Characterization of the organisation of the microtubule cytoskeleton in growing rhizoids of *Marchantia polymorpha* revealed longitudinally oriented microtubules that grow towards and converge into the apical dome. Because microtubule-associated proteins (MAPs) control the organisation of the microtubule cytoskeleton I generated the first *de novo* genome assembly of *Marchantia polymorpha* and compared the MAP repertoire of the liverwort model with that of existing model organisms of the green lineage. A mutant screen in *Marchantia polymorpha* identified the function of Mp*WAVE DAMPENED LIKE* (Mp*WDL*) and Mp*NIMA-RELATED KINASE* (Mp*NEK*) in microtubule-mediated tip-growth stability. MpWDL localizes preferentially to microtubules in the shank of growing rhizoids, where it promotes the longitudinal orientation of the microtubule cytoskeleton. These results are discussed in the context of the evolution of microtubule-mediated tip-growth stability and the tentative hypothesis that the underlying mechanism differs between flowering plants and bryophytes is proposed.

My thanks to…

To Liam for his supervision, support and encouragement; for the opportunities, past and future, he made available to me. To Steve Kelly for his patient training and assistance with the genome assembly. To Ian Moore and my graduate committee, Lee Sweetlove, Nick Kruger and Mark Fricker: your feedback kept me on track each step of the way. To Nick Harberd and John Doonan for their feedback on this manuscript. To Gem, Roni, Debra, Dharshani and Helen, for their friendly assistance with administrative "hassles". To the Clarendon fund and the XX fund for funding my scholarship.

I also wish to thank those who provided resources that sped up the progression of my work. My thanks to Henrik Buschmann for sharing the microtubules reporter constructs and to Takashi Ueda and Ian Moore for the endomembrane compartment reporter constructs. Thanks to Holger for sharing cloning plasmids of his own design. Thanks to Denis for sharing his gene prediction curating script. Thanks to Suvi, Victor and Giulia for sharing the T-DNA mutant lines they generated. Thanks to students who embarked on my project: to Jasper for putting RhiSin together, to Laura for investigating the etiolation phenotype of *wdl* mutants and to Simon for trying to standardize rhizoid growth from gemmae. And of course, to Liam and the Plant Sciences department for providing the space and equipment required for the conduct of my research.

My thanks also go to postdocs and students who have made the department a friendly place of work. To Reka, for countless valuable discussions on cell biology. To Giulia and Hélène for their teaching and technical training. To Holger and Anna for their advice on cloning. To Sandy, Holger, Denis and Reka for working me through the ins and outs of academia. To Charlotte and Sandy for their emulating enthusiasm and professionalism. To Charlotte, Reka, Victor and Liam for feedback on this manuscript. To Anna, Reka

and Sandy for their friendly and critical perspective on my work. To Ana, Bea, Josh and all the Dolan lab members, past and present, for…good times in and out of the lab!

I finally wish to thank those that indirectly enabled me to complete my PhD. To my parents: your love, faith and support carried me this far; I'm grateful beyond measure. To Hélène: your exemplary sense of ethics and kindness stuck with me as a moral compass; I cherish that. To Alexis: your affection, calming presence and refreshing perspective have kept me standing through challenging times and allowed me to give the best of myself at work, thank you.

Table of abbreviations

ARK1 ARMADILLO REPEAT KINESIN 1

MOR1 MICROTUBULE ORGANISATION 1

MRH2 MORPHOLOGY OF ROOT HAIRS

KLCR1 KINESIN LIGHT CHAIN RELATED

NEK NIMA-RELATED KINASE

SPR SPIRAL

EB1 END-BINDING

MIDD1 MICROTUBULE DOMAIN1

MDP microtubule depleting protein

PCaP plasma membrane-associated cation binding protein

WDL WAVE DAMPENED2 LIKE

TPX2 targeting protein for Xlp2

MAP microtubule-associated protein

LCA last common ancestor

ROP Rho GTPase OF PLANTS

REN ROP GTPase ENHANCER

RIC ROP interacting factor

RhoGEF ROP guanidine exchange factor

CMA cortical microtubule array

CMF cortical microfibrils of cellulose

PPB preprophase band

GDP/GTP guanosine diphosphate/guanosine triphosphate

GFP/YFP green fluorescent protein/ yellow fluorescent protein

WT wild type

Contents

Chapter 1 Introduction

1.1 Summary

With this literature review, I show that root hairs, pollen tubes and caulonema cells expand by a specific mode of growth, called tip-growth. In tip-growing cells, growth is restricted to a narrow domain of the cell periphery, thereafter referred to as the apical dome, where the apoplast shows a chemical composition typical of a primary cell wall that can be stretched, in contrast with the stiffer secondary cell wall localized in the basal and subapical region of the cell.

Furthermore, I show that the actin cytoskeleton mediates the trafficking of secretory vesicles containing the cell wall materials required for growth in the expanding apical dome. I then present the evidence in support of the view that the Rho GTPase (ROP) signalling pathway orchestrates the actin cytoskeleton dynamics and, as a result, tip-growth.

In a third section, I turn to the role of microtubules in stabilizing tip-growth. Specifically, I review the evidence supporting the stabilizing role of microtubules in tip-growth. In order address the mechanism of microtubule-mediated tip-growth stability, I summarize the concepts of microtubule dynamics and microtubule array organisation and emphasize the role of microtubule-associated proteins in controlling them and tip-growth stability.

Ultimately, this literature review highlights the knowledge gap that constitutes the molecular mechanism of microtubule-mediated tip-growth stability. I conclude with the notion that the emerging liverwort model *Marchantia polymorpha* is a powerful gene discovery tool and propose to use it to identify the molecular players of microtubule-mediated tip-growth stability.

1.2 Deposition of cell wall material with anisotropic properties controls cell growth polarity in diffuse and tip-growing cells

1.2.1 The balance between turgor pressure and cell wall deformability determines where growth occurs

Plant cells are constricted by a cell wall and cell growth requires its expansion. The cell wall is commonly modelled as a viscoplastic material. The plastic behaviour of the cell wall means that it deforms irreversibly when turgor pressure is applied above a certain threshold, the yield stress. The viscous behaviour of the cell wall means that the extent of the deformation is proportional to its elasticity and the excess of stress applied.

In this model, cell expansion should take place homogenously in all directions along the plane of the cell wall. However, many cell types exhibit patterns of cell expansion where one direction is preponderant, a property that is crucial to acquire their functional shape. Such anisotropic growth can be in principle achieved by introducing a component of resistance to the stress in one preferential direction.

This is typically illustrated by the example of diffuse growing cells, where cortical microfibrils of cellulose (CMF) oppose a resistance to stress in their longitudinal direction, when cross-linked by hemicellulose polymers (reviewed in (Bashline et al. 2014)). In primary cell walls, CMFs are deposited in all directions of the cell wall plane: a situation referred to as transverse isotropy. Consequently, cell expansion is isotropic in the plane of the cell wall. By contrast, in secondary cell walls, CMFs are deposited as layers of parallel-arranged fibres, which confer them a preferential orientation of stress resistance. In other words, the anisotropic orientation of CMFs causes the anisotropic growth in diffuse growing cells. One example of diffuse growing cell type where growth anisotropy is achieved by controlling the orientation of CMFs is epidermal hypocotyl cells of vascular plants. These cells have the particularity that they change their growth

pattern in response to environmental conditions in order to expose photosynthetic tissues to light. Simply put, epidermal hypocotyl cells expand more longitudinally when grown in darkness by promoting the deposition of circumferential parallel-arranged CMF layers in the longitudinal cell walls.

1.2.2 Secretion of new cell wall material controls cell wall integrity and cell wall deformability

As a direct consequence of cell wall expansion in the plane of the cell wall, it should follow that the cell wall is thinning as it is expanding. In their viscoplastic model, Dumais *et al* ((Dumais 2013; Dumais et al. 2006)) link cell wall thickening and cell wall lateral expansion. Assuming a constant cell wall thickness, it implies that an equal amount of new cell wall material is being secreted as the original cell wall material is being translocated laterally. A corollary of this rule is that, if cell wall expansion exceeds the capacity of the cell to secrete replacing cell wall material, the thinned wall may no longer be stiff enough to sustain turgor pressure and the cell may burst. In other words, secretion of cell new wall material is required to translate cell wall expansion into sustainable cell growth.

In addition to sustaining cell growth, secretion of cell wall material contribute to the control of cell wall rheological properties (reviewed in (Bashline et al. 2014)). Sugar polymers other than CMFs, such as pectins and hemicellulose, are synthesized in the Golgi apparatus and secreted in the apoplast, where their crosslinking can reversibly stiffen the cell wall matrix. Hydroxyproline-rich glycoproteins are also secreted to the apoplast where some, such as pectin methyl esterases (PMEs) or expansins, increase or decrease the level of cell wall polymers cross-linking in order to rigidify or loosen the cell wall, respectively.

Unlike CMFs, the mechanical properties of the secreted components of the cell wall matrix are poorly understood and how exactly they contribute to the cell wall anisotropic expansion remains to be clarified. In principle, anisotropy can be achieved by the polar secretion of stiffening or loosening cell wall matrix components (Dumais et al. 2006). It is however challenging to test such hypothesis in diffuse growing cells because of the contribution of parallel-arranged CMFs to the anisotropy of the cell wall.

1.2.3 Tip-growing projection of cells grow by secreting cell wall material in their primary cell wall at their tip

A number of plant cell-types, such as trichoblasts or pollen vegetative cells, can stably restrict growth to a narrow domain of their surface and form a tubular projection such as a root hair, a rhizoid or a pollen tube. This is qualitatively observed by simply recording their growth trajectory over time, which shows that the tip is the only growing region. Quantitative methods, such as cell wall labelling with fluorescent microspheres, unequivocally confirm that growth is limited to the apical dome in root hairs (Shaw, Dumais, and Long 2000), pollen tubes (Rojas, Hotton, and Dumais 2011) and protonema apical cells (Menand, Calder, and Dolan 2007).

This growth pattern coincides with a different cell wall composition in the apical dome and in the shank of tip-growing cells. At the tip, the composition of the apoplast is that of a primary cell wall (Murata and Wada 1989; Newcomb and Bonnet 1965; Reiss, Schnepf, and Herth 1984). By contrast, a secondary cell wall is formed further basally by the successive deposition of parallel-arranged CMF layers oriented along intersecting directions in root hairs (Emons and van Maaren 1987; Murata and Wada 1989; Newcomb and Bonnet 1965; Reiss, Schnepf, and Herth 1984; Wada and Staehelin 1981) or by the deposition of callose in pollen tubes ((Chebli et al. 2012; Lampugnani et al. 2013; Wang

et al. 2011). As a result, the cell wall is more deformable at the tip than in the shank, which could be in principle sufficient to explain the growth polarity in tip-growing cells.

However, modelling of tip-growth in the viscoplastic framework predicts that this simplistic opposition between a homogeneously deformable tip and a stiffer shank would result in a nearly flat apical dome (Dumais et al. 2006). This conflicts with the observation that rhizoids, root hairs and pollen tubes typically have a nearly hemispherical apical dome. It was proposed that the primary cell wall in the apical dome must display some degree of anisotropy. Consistently with this hypothesis, introducing cell wall anisotropy in the apical dome so that extensibility decreases away from the tip results in the prediction of an apical dome much closer to observed morphologies. In the absence of a parallel-arranged CMF array or callose, anisotropy must therefore be achieved by secretion of another cell wall material. In principle, stiffening cell wall material at the base of the apical dome and/or loosening cell wall material at the tip would result in such anisotropy.

Here, the case of angiosperm pollen tube provides an enlightening model. Digestion of the pectins by pectinases results in the flat apical dome morphology predicted for a homogeneous apical cell wall (Rounds and Bezanilla 2013), suggesting a pivotal role of pectins in the formation of an extensibility gradient in the apical cell wall. Moreover, the pectin homogalacturonan is secreted in esterified form into the apical cell wall, but is found in deesterified form further down in the subapex and shank (Bosch, Cheung, and Hepler 2005; Bosch and Hepler 2005; Jauh and Lord 1996). This transition to a cross-linkable form of pectin requires PME activity, as suggested by compromised cell wall integrity in loss-of-function mutants (Jiang et al. 2005; Tian et al. 2006). PME and PME inhibitors are secreted in the tip of the apical dome (Bosch and Hepler 2005; Jiang et al. 2005; Röckel et al. 2008) and, while class I PME persist in the base of the apical dome

and in the shank, PME inhibitors disappear from the cell wall at the transition point (Röckel et al. 2008). Because of these distinct localization patterns, PME activity becomes restricted at the base of the apical dome. This permits the crosslinking of pectins and rigidification of the cell wall in the base of the apical dome, while leaving the cell wall at the tip thick and extensible.

Cross-linking of cell wall polymers is further regulated by another class of proteins : expansins. A number of expansin genes are preferentially expressed in root hairs (Cho and Cosgrove 2002; Kwasniewski and Szarejko 2006; Won et al. 2010) and are thought to control tip-growth. Alpha-expansins, a subfamily of expansins, are secreted to the apical cell wall of root hairs (Baluška et al. 2000), where they soften the primary cell wall by transiently dissociating the CMFs from their hemicellulosic cross-link. Consequently, alpha-expansins promote cell elongation (Cosgrove et al. 2002; C. Lin, Choi, and Cho 2011) and polar growth (Cho and Cosgrove 2002) in root hairs. The role of alpha-expansins in other tip-growing cell types remains to be addressed, but a divergent class of beta-expansins reduces cell wall yield stress and promote pollen tube elongation (Cosgrove, Bedinger, and Durachko 1997; Tabuchi, Li, and Cosgrove 2011). This advocates for a role of both alpha and beta expansins in controlling cell wall loosening in tip-growing cells.

In addition to remodelling the pectin or cellulosic arrays, secreted proteins can act as structural components of the cell wall. Hydroxyproline-rich glycoproteins (HRGP) are glycosylated in the ER and Golgi before being secreted into the apical cell wall of root hairs, pollen tubes or protonema apical cells (Jauh and Lord 1996; Lee et al. 2005; Shpak, Leykam, and Kieliszewski 1999; Yuasa et al. 2005). Two subclasses of HRGPs are known regulators of tip-growth extensins (S M Velasquez et al. 2011; Silvia M. Velasquez et al. 2015) and arabinogalactan proteins (AGPs) (Lee et al. 2005). While the

mode of action of AGPs is largely unknown (Nguema-Ona et al. 2012; Seifert and Roberts 2007), extensins act as scaffolding proteins in the pecto-cellulosic cell wall by cross-linking with each other (Cannon et al. 2008; Held et al. 2004) and possibly with pectins upon oxidation by extensin peroxidases (Cannon et al. 2008; Valentin et al. 2010). The effect of this extensin scaffold on the rheological properties are however unknown.

In conclusion, the anisotropic properties of the apical cell wall is largely determined by both the secretion of structural components of the cell wall, such as pectins, hemicelluloses and extensins, and their subsequent rearrangement by remodelling secreted proteins, such as PMEs or expansins. It follows that the mechanism controlling targeted secretion to the apical cell wall is key to the polar expansion of tip-growing cells.

1.3 The endomembrane compartments of the secretory pathway are polarly distributed towards the apical dome by the actin cytoskeleton under the regulation of ROP signalling

1.3.1 Tip-growing cells show a polar distribution of endomembrane compartments that is specialised for secretion in the apical dome

Correct targeting of vesicles containing this cell wall component thus plays an important role in controlling polar growth in tip-growing cells. Indeed, secretion of pectins, hemicellulose polymers as well as remodelling and structural proteins in the cell wall results in patterns of cell wall anisotropy and polar growth in tip-growing cells. Secreted cell wall proteins are synthesized in the rough endoplasmic reticulum (RER) and later glycosylated in Golgi dictyosomes before being targeted to the plasma membrane inside of secretory vesicles, also containing Golgi-synthesized pectins and hemicelluloses.

The apical region of tip-growing cells is characteristically non-vacuolated, free of plastids and enriched in vesicles (Cheung and Wu 2008; Derksen et al. 1995; Galway, Heckman, and Schiefelbein 1997). It is commonly called the "clear zone", referring to its smoother aspect in DIC micrographs compared to the more basal cytoplasm. The abundance of vesicles reflects the secretion of new cell wall material at the extending tip (Sherrier and VandenBosch 1994). In parallel, endocytosis is observed at the apical membrane (Parton et al. 2001), presumably as a result of the large amount of excessive membrane being inserted during exocytosis (Ketelaar et al. 2008).

Just behind the clear zone, in the so-called subapex, the organelle distribution is remarkably enriched in mitochondria, Golgi stacks and RER in all types of tip-growing cells (Derksen et al. 1995; Galway, Heckman, and Schiefelbein 1997; Furt et al. 2012; Lovy-Wheeler et al. 2007), while, in the shank, the remaining cytoplasm is highly vacuolated and enriched in plastids and peroxisomes (Furt et al. 2012). Although mitochondria may provide the energy required for ATP-dependent mechanisms effecting cell growth in the apical dome, cellular processes taking place in the sub-apex and the shank, are less likely to participate directly to cell elongation.

1.3.2 The actin cytoskeleton controls the cytological zonation of tip-growing cells

The apical accumulation of vesicles in the apical dome is mediated by the actin cytoskeleton. Shortly following the application of actin-depolymerizing drugs, the gradient of vesicles dissipates (Parton et al. 2001; de Graaf et al. 2005; T. Chen et al. 2007).

The presence of a subapical to apical F-actin structure was consistently observed using a broad range of techniques in almost every species and tip-growth model studied

(Foissner, Grolig, and Obermeyer 2002; Lovy-Wheeler et al. 2005; Vidali et al. 2009). Only the pollen tube of *Picea abies* seems to lack such structure (Anderhag, Hepler, and Lazzaro 2000). However, different shapes of this F-actin structure have been reported depending on plant species, cell-types and methodologies. Lily pollen tubes show a cortical actin structure restricted to the base of the clear zone (Lovy-Wheeler et al. 2005; Lovy-Wheeler et al. 2007; Vidali et al. 2009). By comparison, the actin structure at the tip of root hairs of *A. thaliana* and pollen tube of *Nicotina tabaccum* extends further towards the tip and even forms a focal point at the very apex of caulonemal cells in *Physcomitrella patens* (Baluška et al. 2000; Cheung and Wu 2008; Vidali et al. 2009). The first type was referred to as a cortical fringe and the second type as mesh-like actin structures although such dichotomy seems somewhat artificial : moss caulonemal cells, tobacco pollen tubes and lily pollen tubes all have a cortical-biased localization of actin filaments, which simply appears more strongly biased in lily pollen tubes (Vidali et al. 2009). Thus it appears that a common feature of tip-growing cells is the presence of an apical F-actin structure that is required for the accumulation of vesicles in the apical dome.

Consequently, the formation of this apical F-actin structure is of particular importance for polarizing cell growth in tip-growing cells. The organization of the actin cytoskeleton in the apical dome is controlled by a family of regulatory small GTPases. Rho GTPases of Plants (ROP) indirectly control actin assembly and disassembly of filamentous actin in the apical dome of pollen tubes via ROP effectors *At*RIC3 and *At*RIC4 (Hwang et al. 2005) and in protonemal cells (Burkart, Baskin, and Bezanilla 2015). This implies that controlling the pattern of ROP activity, and so the pattern of activity of its actin-remodeling effectors, is critical to polarize the distribution of secretory vesicles and cell growth.

1.3.3 ROP activity is sufficient to polarize growth in tip-growing cells

ROPs have been identified as regulators of polar growth and their subcellular localization pattern is consistent with a role in polarizing growth. For instance, *At*ROP2, *At*ROP4, *At*ROP6, *At*ROP10 (Bloch et al. 2005; M. A. Jones et al. 2002; Molendijk et al. 2001) and *Nt*ROP10 (M.-J. Lei et al. 2015) localise to the apical plasma membrane of growing root hairs. Similarly, *At*ROP1 and *At*ROP5 to that of growing pollen tubes (Kost et al. 1999; Hai Li et al. 1999). This shows that a polar localization of ROPs coincides with polar growth in tip-growing cells.

Consistently, when the pattern of ROP activity is blurred, the polarity of growth is decreased in tip-growing cells. In transgenic lines expressing a constitutively active form of *At*ROP2, *At*ROP6, *At*ROP11 or *Nt*ROP10 the plasma membrane localization of the protein products extends to the shank of root hairs, which are short and swollen. Similarly, a loss of polar ROP localisation and polar growth in transgenic lines expressing the constitutively active form of AtROP1 or AtROP5 has been shown in pollen tubes (Kost et al. 1999; Hai Li et al. 1999). Moreover, lines overexpressing *At*ROP2 have branching root hairs, suggesting that an excess of ROP activity results in the formation of ectopic growth points (Bloch et al. 2005; M. A. Jones et al. 2002; Molendijk et al. 2001). Taken together, these observations strongly suggest that ROP activity is sufficient to polarize growth in root hairs and pollen tubes.

Moreover, ROP activity is not only sufficient but also required to polarize growth in tip-growing cells. Indeed, constitutive expression of the dominant negative form of ROP genes results in shorter tubular pollen tubes and root hairs (Hwang et al. 2010; M. A. Jones et al. 2002; M.-J. Lei et al. 2015). This suggests that ROP activity at the apical plasma membrane is required to sustain tip-growth.

Consistently with the role of ROP signalling in pollen tube and root hairs growth polarity, *Pp*ROP GUANIDIN EXCHANGE FACTOR 3 (*Pp*RopGEF3), a putative activator of ROPs of the moss Physcomitrella patens, localizes to the apical membrane of growing caulonemal cells and transgenic lines overexpressing *Pp*ROP2 have short and swollen chloronemal cells and no caulonema (Burkart, Baskin, and Bezanilla 2015; Ito, Ren, and Fujita 2014). This suggests that the role of ROP signalling in polarizing tip-growth is conserved between mosses and flowering plants.

In differentiating tracheary elements, a diffuse growing cell-type where cell wall deposition is polarized, the interaction between *At*ROP11 and the ROP effector *At*MICROTUBULE DEPLETION DOMAIN 1 (MIDD1) defines domains of cell wall formation (Oda et al. 2010; Oda and Fukuda 2012; Oda and Fukuda 2013a). *At*MIDD1 binds to microtubules, which as a result maintain the patterning cell wall deposition by preventing lateral diffusion of the ROP-MIDD1 complex. Although no evidence suggest that this mechanism is at play in tip-growth, this provide an example of how the microtubule cytoskeleton may participate in stabilizing the domain of cell wall deposition in tip-growing cells. In the next section, I review the evidence supporting a role of microtubules and microtubule-associated proteins in defining the domain of cell growth in tip-growing cells.

1.4 Tip-growth stability requires a dynamic microtubule cytoskeleton organised by microtubule-associated proteins

1.4.1 Stabilization and reorientation of tip-growth requires to modulate microtubule dynamics

Treatments with microtubule-destabilizing drugs result in wavy-growing root hairs (Bibikova, Blancaflor, and Gilroy 1999), bifurcating protonemal cells (Schwuchow,

Sack, and Hartmann 1990; Hiwatashi, Sato, and Doonan 2014) and wavy-growing and bifurcating pollen tubes in gymnosperms (Anderhag, Hepler, and Lazzaro 2000). This suggests that stabilizing tip-growth requires regulating microtubule dynamics.

Tip-growing cells not only have the ability to restrict growth to a narrow domain at their tip, they can also reorient it in response to environmental stimuli. Phototropism in protonema of mosses (Demkiv et al. 1999; Jenkins and Cove 1983) and ferns (Etzold 1965), gravitropism in moss protonema (Demkiv et al. 1999; Sack 1993) or chemotropism in leguminous root hairs (Esseling 2003), all exemplify the adaptability of the tip-growth mechanism in response to environmental stimuli.

The ability of tip-growing cells to redirect their growth implies that polarity cues, such as ROP activity, can be redistributed. Consistently, the reorientation of growth requires ROP activity (Ke et al. 2016; W. Liu et al. 2010) and active ROP is relocalized from the tip to the base of the apical dome in Nod factor-responding root hairs (M.-J. Lei et al. 2015).

The mechanism underlying tip-growth reorientation is largely unknown. It has been proposed to act through the microtubule cytoskeleton. Tip-growth reorientation involves a transient and local depolymerisation of the endoplasmic microtubules (Sack 1993; Schwuchow, Sack, and Hartmann 1990; Sieberer, Timmers, and Emons 2005) or a decrease in microtubule polymerization (Vassileva 2005). Consistently, root hairs with taxol-stabilized microtubules are unable to reorient their growth in response to thigmotropic stimuli (Bibikova, Blancaflor, and Gilroy 1999). This suggests that reorientation of tip-growth in response to environmental stimuli requires microtubules depolymerisation.

1.4.2 Microtubule-associated proteins control the polymerisation and depolymerisation of microtubules

The structure of microtubules and mechanism of microtubule polymerization is reviewed in (Hashimoto 2015). Microtubules are made of 13 protofilaments associated laterally into a 24 nm wide hollow cylinder (Figure 1.1). Each protofilament consists of a linear assembly of tubulin heterodimers. Tubulin heterodimers are made of one alpha-tubulin and one beta-tubulin. The beta-tubulin subunit possess a nucleotide-binding site where GDP or GTP can bind. When beta-tubulin is GTP-bound, it can associate with the alpha-tubulin of a tubulin dimer by hydrolysing GTP into GDP. As a result, protofilaments and microtubules are polar polymers with two structurally and functionally distinct extremities. The plus-end, characterised by the exposure of beta-tubulins, alternates between polymerization and depolymerisation; the minus-end, characterized by the exposure of alpha-tubulins, undergoes slow depolymerisation. Microtubule depolymerisation results from the relatively unstable protofilament association when the beta-tubulin is GDP-bound. Thus, if the GTP-bound beta-tubulin cap at the plus-end is compromised the plus-end of microtubules switches from polymerization to rapid depolymerisation.

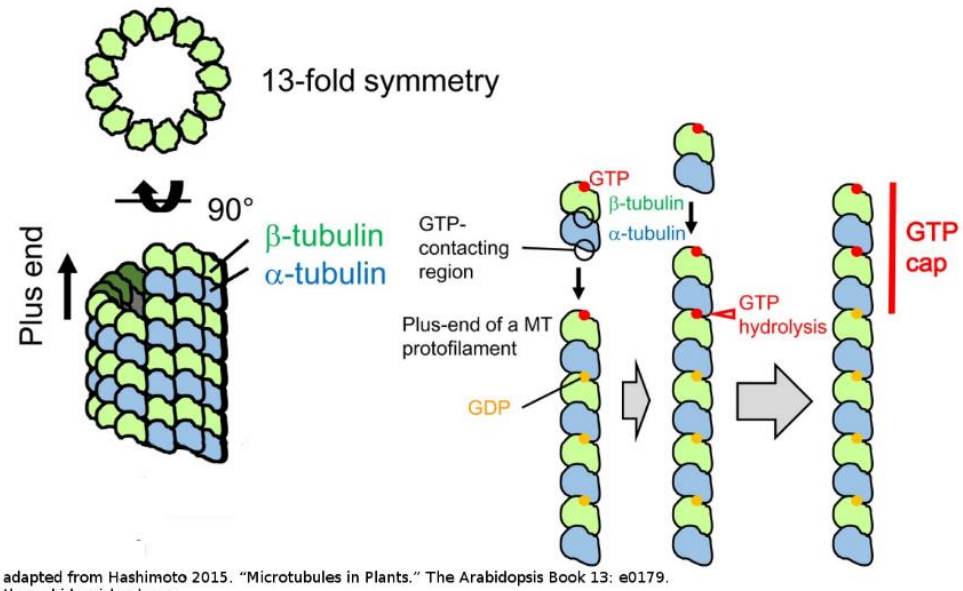

adapted from Hashimoto 2015. "Microtubules in Plants." The Arabidopsis Book 13: e0179.
thearabidopsisbook.org

Figure 1.1: Mechanism of microtubule polymerisation

Polymerisation and depolymerisation rates are partly controlled by microtubule-associated proteins (MAPs). Strictly speaking, MAPs define a group of proteins that bind to microtubules as evidenced by co-immunoprecipitation or pull-down assays. In animals, MAP215 binds to microtubules and is proposed to recruit free tubulin dimers and facilitate their integration to the microtubule plus-end (Ayaz et al. 2012; Ayaz et al. 2014). MICROTUBULE ORGANIZATION 1 (MOR1) is the plant homolog of the animal MAP215 protein. In *Arabidopsis thaliana*, microtubules grow slower in the *mor1-1* temperature sensitive mutant at the restrictive temperature (Kawamura and Wasteneys 2008), suggesting that a role of MAP215/MOR1 proteins in promoting microtubule polymerization is conserved between plants and animals. Paradoxically, the rate of microtubule depolymerisation is also increased in *mor1-1* at the restrictive temperature. This suggests that *At*MOR1 controls microtubule dynamicity rather than polymerisation or depolymerisation solely.

By contrast with the general role of MOR1 in controlling microtubule dynamicity, some MAPs promote or inhibit microtubule depolymerisation specifically. In *Arabidopsis thaliana,* KINESIN-13A promotes microtubule depolymerisation at both the minus-end and the plus-end (Oda and Fukuda 2013a; Oda and Fukuda 2013b). In addition, plasma membrane-associated cation binding (PCaP) proteins MAP18 and MICROTUBULE DEPOLYMERIZING PROTEIN 25 (MDP25) are plant-specific MAPs that predominantly localise to the plasma membrane (J. Li et al. 2011; Zhu et al. 2013). *In vitro, At*MAP18 and *At*MDP25 bind to microtubules and promote microtubule depolymerisation at high Ca2+ concentrations (X. Wang et al. 2007; J. Li et al. 2011). This suggests that *At*MAP18 and *At*MDP25 may control the dynamics of microtubules in high cytosolic Ca2+ concentrations *in vivo*. Consistently, AtMAP18 colocalizes to microtubules *in vivo,* and overexpression and downregulation of At*MAP18* causes microtubules to become oryzalin hypersensitive and resistant respectively. Similarly, at*mdp25* and At*MDP25* overexpressing mutants have resp. more and fewer microtubules in hypocotyl epidermal cells (J. Li et al. 2011). This suggests that PCaP proteins may promote microtubule depolymerization *in vivo*. Opposite to Kinesin13A and PCaPs, *At*MAP65-1 and *At*MAP65-5 proteins decrease microtubule depolymerization rate (Damme et al. 2004).

Taken together, these examples illustrate the role of MAPs in controlling the polymerization rate, the depolymerisation rate of microtubules, or both.

1.4.3 Microtubule-associated proteins control the frequency of pausing microtubules and the frequency of catastrophe and rescue events

The transition from polymerisation to rapid depolymerisation, called catastrophe, occurs *in vivo* when the plus-end of a microtubule encounters an obstacle with a steep angle, such as another microtubule. Rapidly depolymerizing plus ends randomly switches back

to polymerisation, possibly when the depolymerizing plus-end reaches an isolated GTP-bound beta-tubulin (Dimitrov et al. 2008). This transition is called a rescue event. Occasionally but rarely in plants, the plus-end of microtubules is neither polymerising nor depolymerising, which defines the pause state.

MAPs partly control the frequency of catastrophe and rescue events. *At*ARMADILLO REPEAT KINESIN 1 localizes to the plus-end of microtubules and promotes catastrophe events (Eng and Wasteneys 2014), while *At*WDL3 localizes to entire microtubules and prevents catastrophe events (X. Liu et al. 2013).

Another example is the evolutionary conserved family of CYTOPLASMIC LINKER ASSOCIATED PROTEIN (CLASP) proteins. In *Arabidopsis thaliana, At*CLASP localizes preferentially to the plus-end of microtubules (J. C. Ambrose et al. 2007), where it prevents catastrophe in the event of the plus-end encountering a cell edge (C. Ambrose et al. 2011). Consistently, CLASP homolog in fission yeast prevents catastrophe events and promote microtubule rescue (Al-Bassam et al. 2010). This suggests that the role of CLASP proteins in preventing catastrophe event is conserved between animals and plants.

Moreover, MAPs can also promote the repression of the pause state. *At*SPIRAL2 (*AtSPR2)* and *At*SPIRAL2 LIKE (*At*SPR2L*)* decorate microtubules and *in vitro* polymerisation assays suggest that *At*SPR2 and *At*SPR2L decrease the frequency of the pause state (Yao et al. 2008).

Taken together, these examples illustrates that MAPs not only control the rates of microtubule polymerisation and depolymerisation, but also the transition between this two states.

1.4.5 Microtubule associated proteins control the organisation of the cortical microtubule array

Microtubules may interact with each other directly or in a MAP-mediated manner, resulting in their bundling or intersecting. According to the model of microtubule array self-organisation by microtubule-microtubule encounter (Wasteneys and Ambrose 2009), when the plus-end of a microtubule encounters the flank of another with a shallow angle, it is likely to become bundled with the encountered microtubule and grow parallel to it. On the contrary, when if the angle of encounter is steep, the plus-end may either undergo rapid depolymerisation or cross over and continue polymerisation in the same direction as before the encounter.

In addition to this self-organization mechanism, MAPs control the bundling of microtubules. *At*MAP65-1 and *At*MAP65-5 preferentially localize to bundled microtubules *in vivo* (Damme et al. 2004) and possibly cross-link microtubules, as suggested by *in vitro* assays for many MAP65 proteins (Chan et al. 1999; Fache et al. 2010; Mao et al. 2006; Smertenko et al. 2004). Similarly, *At*MOR1 and its tobacco homolog *Nt*TMBP200 bind to microtubules and form cross-bridges *in vitro* (Yasuhara et al. 2002). MAPs of the WDL and MAP70 families also localize to microtubule bundles *in vivo* and promote the formation of microtubule bundles *in vitro* (Korolev et al. 2005; Korolev et al. 2007; Pesquet et al. 2010; X. Liu et al. 2013; Sun, Ma, and Mao 2015; Perrin et al. 2007).

Furthermore, microtubules may be severed by katanins. In animals, katanin subunit p60 binds to the microtubule lattice and associate into a hexamer in an ATP-dependent (Hartman and Vale 1999). The association of the katanin hexamer with microtubules destabilize tubulin-tubulin interactions thus locally breaking the interactions holding the protofilaments together (Roll-Mecak and Vale 2008). In *Arabidopsis thaliana*,

*At*KATANIN1 controls the organisation of the cortical microtubule array (Burk et al. 2001; Bichet et al. 2001) by severing microtubules at specific sites, including intersecting microtubules or microtubules nucleated with an angle from a parent microtubule (Zhang et al. 2014; Lindeboom et al. 2013; Nakamura, Ehrhardt, and Hashimoto 2010).

Taken together, these examples illustrate that MAPs control microtubule bundling and severing. In addition to the mechanism of self-organizing property of microtubules, MAPs thus participate to the formation of a variety of higher-order architectures of the microtubule cytoskeleton, called microtubule arrays. During interphase, the majority of microtubules is localized in the close vicinity of the plasma membrane and together they constitute the cortical microtubule array (CMA). According to the alignment hypothesis, cortical microtubules act as directional cues for cellulose synthase complexes as they synthesize cellulose microfibrils (reviewed in (L. Lei et al. 2014)). As such, the organisation of the CMA plays a crucial role in the control of cell wall anisotropy, and ultimately in polar growth and cell differentiation in diffuse growing cells.

1.4.6 Microtubule-associated proteins control microtubule-mediated tip-growth stability

Much like in polar growth of diffuse growing cells, microtubules are not distributed evenly between growing and non-growing parts of tip-growing cell (C. Ambrose and Wasteneys 2014; Anderhag, Hepler, and Lazzaro 2000; Eng and Wasteneys 2014a; Hiwatashi, Sato, and Doonan 2014; Schwuchow, Sack, and Hartmann 1990; Sieberer, Timmers, and Emons 2005). Cortical microtubules are arranged in a sub-axial array in the shank and typically absent from the apical dome. By contrast, a common feature of

all tip-growing cells is the presence in the apical dome of endoplasmic microtubules, which are interphase microtubules that run throughout the cytoplasm.

Endoplasmic microtubules in the apical dome have been proposed to control microtubule-mediated tip-growth stability (Eng and Wasteneys 2014a; Sieberer, Timmers, and Emons 2005; Hiwatashi, Sato, and Doonan 2014). In root hairs, endoplasmic microtubules polymerize towards and reach the apical plasma membrane, before undergoing rapid depolymerisation (Sieberer et al. 2005; Eng and Wasteneys 2014). The polymerization rate of endoplasmic microtubules is decreased in the wavy-growing or bifurcating root hairs of at*ark1* mutants (Eng and Wasteneys 2014). *At*ARK1 binds preferentially to the growing ends of cortical microtubules where it promotes catastrophe events resulting in rapid depolymerisation (Eng and Wasteneys 2014). Whether this holds true for endoplasmic microtubules could not be tested due to technical limitations. The authors propose that upon rapid depolymerisation of microtubules the concentration of tubulin monomers increases in the cytosol, which may in turn indirectly promote rapid polymerisation of cortical and endoplasmic microtubules. Consistently, treatments with the microtubule destabilizing drug oryzalin could rescue the polymerization rate and growth phenotypes of at*ark1* root hairs. Altogether, this suggests that *At*ARK1-promoted catastrophe events in the apical dome may be required to maintain a concentration of free tubulin dimers sufficient for the polymerisation of endoplasmic microtubules in the apical dome. Similarly, PpKINID1 and PpKINID2 are required for the stability of endoplasmic microtubules that converge in the tip of moss caulonema cells and loss-of-function mutants form wavy caulonema cells (Hiwatashi, Sato, and Doonan 2014). This suggests that the endoplasmic microtubules in the apical dome of caulonema cells are required to stabilize tip-growth in moss.

Other MAPs that control microtubule dynamics also control tip-growth stability. at*mor1-1* forms wavy root hairs at the restrictive temperature, while at*map18* forms wavy pollen tubes (Whittington et al. 2001; D. Lin et al. 2013). The causal relationship between their activity on microtubule dynamics and their role in tip-growth stability is however more elusive than for ARK1 and KINID proteins. A detailed characterisation of the microtubule phenotype of at*mor1-1* root hairs is unfortunately lacking. at*map18* mutant pollen tubes have however received more attention (Zhu et al. 2013; Kang et al. 2017). Surprisingly, *At*MAP18 promotes tip-growth stability by severing actin filaments in the apical dome, but does not appear to control the organisation of the cortical microtubule array in pollen tubes. Indeed, cortical microtubules of at*map18* pollen tubes are indistinguishable from WT in terms of bundling and the microtubule dynamics in at*map18 pollen* tubes have not been characterised. By contrast, at*map18* pollen tubes have actin cables protruding in the apical dome, suggesting that *At*MAP18 destabilises the actin cytoskeleton in the apical dome. Consistently, *At*MAP18 binds to and severs actin filaments in high Ca2+ conditions *in vitro*. Moreover, the actin severing activity of *At*MAP18 is required for transgenic complementation of at*map18* mutants and rescue of their wavy pollen tube phenotype. While these results do not exclude a role of *At*MAP18 in regulating microtubule dynamics in pollen tubes, they clearly support a role of *At*MAP18 in organising the apical actin meshwork.

Finally, identifying further genetic regulators of microtubule-mediated tip-growth stability is required to elucidate the mechanism controlling it. It is likely that MAPs that control microtubule dynamics and/or the organisation of interphase microtubule arrays in diffuse growth have similar functions in tip-growing cells. Consequently, other MAPs than *At*ARK1 and *At*MOR1 are likely to control microtubule-mediated tip-growth

stability and I aim to identify them from a mutant screen in the emerging model for genetic studies, *Marchantia polymorpha*.

1.5 Marchantia polymorpha: a model organism for genetic studies of tip-growth

1.5.1 Marchantia polymorpha *is amenable to both reverse and forward genetics*

Liverworts are an early-diverging phylum of land plants that have a gametophytic dominated life cycle. In *Marchantia polymorpha*, the liverwort model organism, the mature gametophyte is haploid and dioiceous. Male and female gametes are respectively produced in antheridiophores and archegoniophores formed on the upper side of the thallus, called dorsal side. Upon fertilization, the diploid sporophyte develops into an axial structure consisting of a foot that anchors it to the maternal tissue, a stalk and a capsule where sporogenesis takes place. The short-lived sporophyte remains nutritionally dependent on the female gametophyte until it releases the haploid spores and dies. Upon germination, spores finally grow into a thallus completing a 14 weeks-long life cycle.

Because of the small stature, the short life cycle and the haploidy of *Marchantia polymorpha*, the liverwort model is an excellent system for forward genetics. Moreover, *Marchantia polymorpha* is amenable to T-DNA mutagenesis. Mutant screens can thus be performed in a shorter time and at a larger scale than in other land plant model organisms.

In addition to reproducing sexually, *Marchantia polymorpha* also reproduces by forming vegetative propagules called gemmae. Gemmae develop from epidermal cells on the dorsal side within specialized dorsal structures called gemmae cups. Combined with the ease of generating mutants in *Marchantia polymorpha*, gemmae provide an excellent way of propagating mutant or transgenic lines.

Building on the advantages of *Marchantia polymorpha* for mutant screens, tip-growth defective T-DNA mutants were generated and the resulting T-DNA mutant collection is propagated, making it an extremely useful resource for this project.

1.5.2 Smooth rhizoids are tip-growing cells analogous to root hairs and homologous to moss rhizoids that form throughout the gametophytic phase

The liverwort model *Marchantia polymorpha* forms tip-growing cells at several stages of the gametophyte development. The first cell division of the spore is asymmetric: one daughter cell terminally differentiate into a rhizoid cell, while the other regenerate a thallus. On the bottom side of the thallus, called the ventral side, smooth rhizoids grow perpendicular to the plane of the epidermis and penetrate the substratum where they provide anchorage and function in nutrient and water uptake. Thus, they share a common rooting function with rhizoids of mosses and root hairs of vascular plants.

Young gemmae have a biradial symmetry and develop rhizoids on both sides. Thus, young gemmae are a convenient developmental stage to study tip-growth in *Marchantia polymorpha* because their production does not require crossing and their rhizoids can be observed from above.

The genetic mechanism controlling the early stages of development of filamentous rooting cells is conserved between liverworts to flowering plants. Indeed, RSL class I genes are required for epidermal cells to differentiate into rhizoid cells in *Marchantia polymorpha* and *Physcomitrella patens* or to form root hairs in *Arabidopsis thaliana* (Menand et al. 2007; Proust et al. 2016; Jang et al. 2011; Masucci and Schiefelbein 1994). Thus, rhizoids of *Marchantia polymorpha* and *Physcomitrella patens* are homologous

cell types, while rhizoids and root hairs are strictly speaking analogous cell types because they form in different generation of their life cycle.

Here, I investigate the role of microtubules in stabilizing tip-growth in the rhizoids of *Marchantia polymorpha*. I show that the role of microtubules in stabilizing tip-growth is conserved between flowering plants and liverworts. Because MAPs control microtubule dynamics and the organization of microtubule arrays, I first characterize the MAP repertoire in *Marchantia polymorpha* by homology with known MAPs in flowering plants and analyze the diversification of MAP gene families during the course of the evolution of the land plants. Finally, I identify by forward genetics two new MAPs controlling tip-growth stability and charactize the function of *Mp*WDL on the organization of the microtubule cytoskeleton in growing rhizoids.

Chapter 2: Evolution of Microtubule Associated Proteins gene families during the colonisation of the terrestrial environment

2.1 Summary

The mechanisms that control the organisation of microtubule arrays by microtubule-associated proteins (MAP) evolved during the evolution of streptophyte as plants transitioned from an aquatic to a terrestrial environment. With this chapter, I present the first *de novo* genome assembly of the liverwort *Marchantia polymorpha* and investigate the diversification of microtubule associated protein gene families during the course of streptophyte evolution. I show that there was a diversification of pre-existing structural MAP orthogroups and the origin of new ones during the course of streptophyte evolution. Furthermore, I show that *Marchantia polymorpha* provides a simpler genetic model than *Arabidopsis thaliana* for MAP gene discovery from mutant screens.

2.2 Introduction

During the course of streptophyte evolution, the mechanisms of cell division and differentiation mechanisms underwent significant changes and so did the organization of microtubule arrays. The innovation of 3D tissues in the last common ancestor (LCA) of land plants was a key innovation that contributed to the radiation of land plants. It was proposed that the constraints on deformability within plant 3D tissues strengthen the need for a tight spatial coordination of cell division orientation, which would involve a specialized organization of the cortical microtubule array : the preprophase band (PPB) (Pickett-heaps et al. 1999). The PPB is a ring of parallel cortical microtubules that forms during preprophase and predicts the future cortical division site (reviewed in (Buschmann and Zachgo 2016)). The vast majority of dividing cells of land plants form a PPB (Figure 2.1), but parallel rings of cortical microtubules forming at the site of the future division plane also form in the zygnematales. Whether the latter microtubule structure, referred to as the isthmus band, participates in the mechanism of cell division plane orientation is however unknown. Nonetheless, this supports the parsimonious hypothesis that, in the LCA of land plants or in the LCA of zygnematales and land plants, the cortical microtubule array (CMA) acquired a new function in cell division, mediated by a specialized CMA organization.

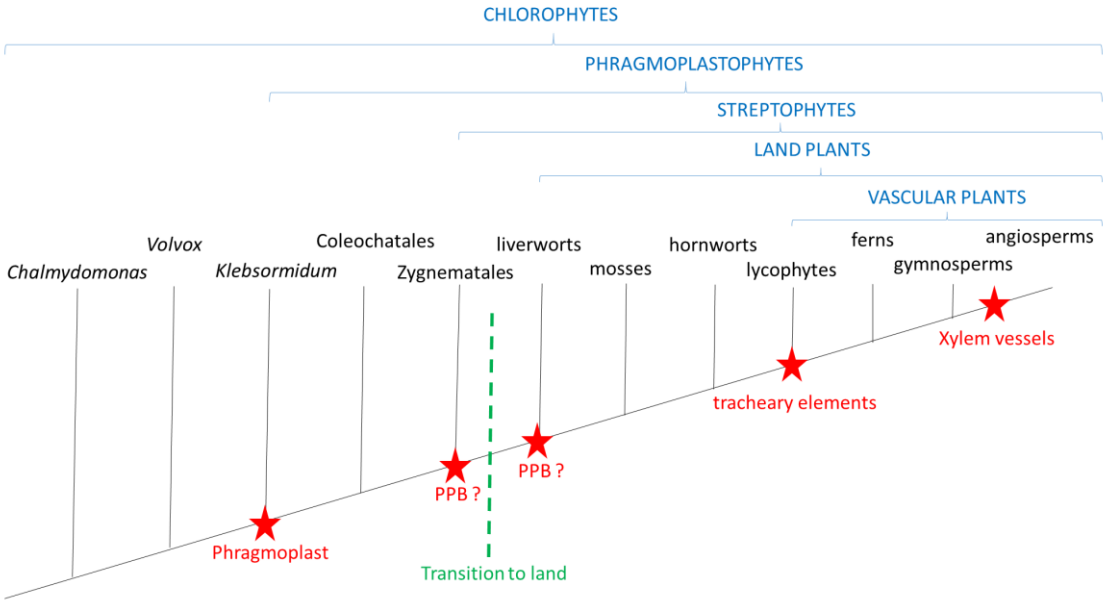

Figure 2.1: Microtubule-related biological innovations during the evolution of chlorophytes.

During the course of land plant evolution, the innovation of new cell-types correlated with the innovation of specialized CMA organizations participating in their differentiation. For instance, the formation of secondary cell wall pits in tracheary elements in *Arabidopsis thaliana* relies on the formation of a specialized CMA organisation characterised by local depolymerisation of microtubules in the future pit regions and bundling of microtubules around them (Oda, Mimura, and Hasezawa 2005). Because tracheary elements represent a key innovation of tracheophytes, it is tempting to assume that this specialised CMA organization originated in the last common ancestor of tracheophytes. However, it is unknown whether a similar CMA organization can be observed in analogous cell-types from non-vascular plants, such as hydroids of mosses or pitted cells of liverworts. Nevertheless, we can safely hypothesise that during land plant evolution the CMA acquired a new function in tracheary element differentiation mediated by a specialized CMA organization.

Taken together, these examples suggest that new CMA organisations required for cell division and cell differentiation were innovated during the course streptophyte evolution.

The molecular mechanism controlling the organisation of the CMA is largely operated by microtubule-associated proteins (reviewed in (Struk and Dhonukshe 2014)). Microtubule-associated proteins (MAPs) define a diverse group of phylogenetically unrelated proteins that bind to microtubules. A distinction can be made between structural MAPs and motor MAPs to highlight a functional difference. While structural MAPs control microtubule dynamics and array organisation, motor MAPs typically function in microtubule-based transport of vesicles, organelles or cytoskeleton elements (Mandelkow and Mandelkow 1995).

The question remains of how the structural MAP gene families whose members control these innovative mechanisms of CMA organization evolved. Two simple hypotheses are conceivable: 1) neofunctionalisation of pre-existing MAP genes or 2) innovation of new MAP gene families. Building on these hypotheses we have the following corollaries: the loss of a given MAP function could cause 1) the recruitment of the obsolete MAP gene to another function, or 2) its loss. While causation is challenging to prove, we can test whether the diversification or loss of MAP gene families is consistent with either hypothesis.

By comparing land plant genomes with the recently released genome assemblies of streptophyte algae, we can investigate the genetic gains and losses that have taken place when plants transitioned from an aquatic to a terrestrial environment. To increase the resolution of this phylogenetic analysis, I generated a *de novo* genome assembly of the liverwort *Marchantia polymorpha*, a representative of the earliest diverging clade of land plants. This allowed me to generate a hypothetical repertoire of genes present in the last

common ancestor of land plants, where some of the key innovations in CMA organization may have occurred.

2.3 Material and methods

2.3.1 De novo *genome assembly*

De-novo sequencing of wild-type *Marchantia polymorpha* genomic DNA was performed with Illumina's HiSeq technology by the Beijing Genome Institute, using three 2 x 100 bp paired-end libraries (170bp, 500bp and 800bp insert size) and two 2 x 50 bp mate pair libraries (2kb and 5kb insert size). Reads were quality trimmed using Trimmomatic-0.32 [37] and normalised using Khmer-0.7.1 [38] with a khmer size of 31. Scaffolds were assembled using Allpaths-LG-4832 [39] set with haploidify parameters. Resulting scaffolds were corrected using Pilon-1.6 [40] and further gap-filling and scaffolding steps were carried out using SGA [41] and SSPACE-v3 [42] respectively. Reads that did not align against the assembled scaffolds were independently assembled using SGA [41] and resulting contigs were added to the core assembly before a final step of scaffolding, gap filling and correction.

2.3.2 Gene prediction

CDS model predictions were generated using Augustus-3.0.1 [43]. A training set of 9600 *Marchantia polymorpha* sequences was generated by aligning the *Marchantia polymorpha de-novo* transcriptome against the draft genome using exonerate-2.2.0 [44] and aligned transcripts were verified using BLASTp searches against the NCBI plants peptide databases. Predicted CDSs were finally searched for contamination using a BLAST-2.2.29-based filtering pipeline. A CDS was considered ambiguous if none of its three best

hits obtained by BLASTn belonged to the Archeaplastida clade; only hits longer than 225bp with e-value lower than 1e-15 and with more than 35% identity were taken into account. Ambiguous CDS and CDS with no hits were further analysed by BLASTx. Those CDS that met the above thresholds and had none of their best three hits belonging to Archeaplastida were considered contaminations. Any genome scaffold including more than 10% contaminating CDS was removed from the assembly together with all associated predicted CDS. Remaining contaminating CDS were hard-masked.

2.3.3 Protein sequence datasets retrieval

Protein sequences inferred from genome assemblies of *Chlamydomonas reinhardtii* (Creinhardtii_281_v5.5.protein_primaryTranscriptOnly.fa, Merchant *et al.* 2007), *Volvox carteri* (Vcarteri_317_v2.1.protein_primaryTranscriptOnly.fa, Prochnik *et al.* 2010), *Marchantia polymorpha* NCBI GenBank accession LVLJ00000000.1, Honkanen *et al.* 2016), *Physcomitrella patens*, *Selaginella moellendorffii (Smoellendorffii_91_v1.0.protein_primaryTranscriptOnly.fa*, Banks *et al.* 2011) *Oryza sativa* (Osativa_323_v7.0.protein_primaryTranscriptOnly.fa, Ouyang *et al.* 2007) and *Arabidopsis thaliana* (Athaliana_167_TAIR10.protein_primaryTranscriptOnly.fa, Lamaesch *et al.* 2012)were obtained from Phytozome (Goodstein et al. 2012).

Klebsormidium nitens (160614_klebsormidium_v1.1_AA.fasta, Hori *et al.* 2014) was obtained from http://www.plantmorphogenesis.bio.titech.ac.jp/~algae_genome_project/klebsormidium/

2.3.4 MAP gene identification

Protein sequences from all aforementioned proteomes were categorised based on sequence similarity into orthogroups as defined by (Emms and Kelly 2015)using Orhofinder-0.7.1 default settings. Orthogroups were screened for the presence of at least *Arabidopsis thaliana* gene coding for a protein empirically demonstrated to bind to microtubules resulting in the following list of MAP families: class I formins, QWRF domain-containing proteins, MAP65 proteins, NIMA RELATED KINASE (NEK) proteins, SPIRAL1 proteins (SPR1), MAP70 proteins, SPIRAL2 proteins (SPR2), EB1 proteins, gama-tubulins, TONNEAU1 proteins (TON1), CYTOPLASMIC LINKER ASSOCIATED PROTEINs (CLASP), TPX2 domain-containing proteins, RUNKEL proteins (RUK), MICROTUBULE ORGANISATION 1 proteins (MOR1), katanin p60 subunits (KTN1), MICROTUBULE ASSOCIATED STRESS PROTEINs (MASP1), TRANSLATIONALLY CONTROLLED TUMOR PROTEINs (TCTP), AUXIN INDUCED IN ROOT 9 proteins (AIR9), TRICHOME CELL SHAPE1 proteins (TCS1), COMPANION OF CELLULOSE SYNTHASE1 proteins (CC1), MICROTUBULE DESTABILISING PROTEIN 40 proteins (MDP40), PLASMA MEMBRANE LOCALISED CALMODULIN CALCIUM PROTEINs (PCaP), TONNEAU RECRUITING MOTIF proteins (TRM), MICROTUBULE DEPLETION DOMAIN 1 proteins (MIDD1), TANGLED proteins (TAN1) and GROWING PLUS-END TRACKING1 proteins (GPT1).

Kinesins and kinesin-like proteins were voluntarily excluded from the analysis because of the difficulty to resolve kinesins families.

2.4 Results

2.4.1 Marchantia polymorpha *draft de novo genome assembly covers 75% of expected genome size and includes 18 000 hypothetical protein-coding genes* [1]

Total genome size is estimated to be 310 Mb. We used 117 518 377 sequence reads generated by Illumina Hiseq from genomic DNA extractions (Table 1). Over 95% of those reads were assembled into 4137 scaffolds, 90% of which are larger than 50kb. The total assembly length covers 206 Mb of the nuclear genome, with a N50 of 376 kb.

We identified 17 956 protein-coding genes, suggesting that the gene density is one gene per 11 kb on average (Table 2.1). To assess the accuracy of the gene predictions, we compared the set of gene predictions with a control training set of 9600 transcripts. We estimated that 87% of all exons from genes represented in the control dataset were identified with no error. Furthermore, we estimated that 46% of control genes were predicted with no error, meaning that 54% of gene predictions had an error in at least one exon.

[1] The first version of the genome assembly was made in collaboration with Steve Kelly and Sandy Hetherington using DNA sequencing data obtained from Hélène Proust and Giulia Morieri. I repeated the genome assembly to improve the quality of input reads and generated gene predictions under Steve Kelly's supervision. Denis Saint-Marcoux helped me with the curation of the genome assembly to remove chloroplastic DNA and putative contaminations, and I finally formatted the 4th version of the assembly for release to NCBI Whole Genome Shotgun database.

statistics for the *de novo* genome assembly	
Illumina HiSeq, 100 bp paired-end reads	84 554 420 reads
Illumina HiSeq, 50 bp mate-pair reads	32 963 957 reads
estimated genome size	310 Mb (Nasu *et al.*, 1997)
depth of sequencing coverage	65x
number of scaffolds	4 137
scaffold N50 (L50)	376 kb (174)
scaffold NG50 (LG50)	190 kb (364)
total assembly length (of which % gaps)	206 Mb (12%gap)
% total assembly length in scaffolds > 50 kb	90.00%

statistical analysis of gene predictions	
number of predicted protein-coding genes	17 956
exon-level specificity / sensitivity	70% / 87%
gene-level specificity / sensitivity	35% / 46%

Table 2.1: Descriptive output variables of the *Marchantia polymorpha* de novo genome assembly and gene prediction (Honkanen *et al*, 2016[2])

2.4.2 The repertoire of structural MAP genes diversified during the evolution of streptophytes

To characterize a draft repertoire of structural MAP genes in *Marchantia polymorpha*, I generated groups of orthologous genes, termed hereafter orthogroups, using the most recent genome annotations from selected plant models and this assembly. I then screened for orthogroups that include at least one *Arabidopsis thaliana* gene empirically demonstrated to bind to microtubules (*i.e.* a total of 26 families). This resulted in the identification of 24 gene models in 22 orthogroups in *Marchantia polymorpha* (Table 2.2).

[2] The figure and the data presented in this figure are of my own making and were published in Honkanen *et al* 2016.

To pinpoint when MAP orthogroups originated during Archeaplastida evolution, I compared the repertoires of structural MAP orthogroups from all selected plant genomes. 31 orthogroups were identified in total (Table2). 15 originated during the evolution of streptophytes, including 10 that originated during Embryophyte evolution, of which 7 originated during Tracheophyte evolution. This suggests that half of the MAP gene repertoire of flowering plants has been innovated during the evolution of streptophytes, two third of which during the colonization of the terrestrial environment by land plants.

Representative gene member	At	Os	Sm	Pp	Mp	Kf	Vc	Cr
AtFH14	11	7	8	2	2	3	2	2
AtEDE1	10	10	2	4	1	1	1	1
AtMAP65-1	9	11	9	6	1	1	1	1
AtNEK1	6	6	3	1	1	1	3	3
AtSPR1	6	4	1	8	1	2	2	2
AtMAP70-5	5	4	1	9	1	1	1	1
AtSPR2	5	2	2	4	1	1	1	1
AtEB1a	3	2	3	4	2	1	1	1
AtTUBG1	2	1	1	2	1	1	1	1
AtTON1	2	2	1	1	1	1	1	1
AtCLASP	1	3	2	3	1	1	1	1
AtTPX2	1	1	1	3	1	1	1	1
AtRUK	1	1	1	2	1	1	1	1
AtMOR1	1	1	1	2	1	1	1	1
AtKTN1	1	1	1	2	1	1	2	2
AtMASP1	2	4	2	1	1	1	0	0
HsTCTP	2	1	1	2	1	1	0	0
AtAIR9	1	1	2	3	1	2	0	0
AtWVD2	8	6	3	14	1	0	0	0
AtTCS1	9	8	5	11	1	0	0	0
AtCC1	4	5	2	2	1	0	0	0
AtMDP25	1	2	0	1	1	0	0	0
AtMDP40	7	4	1	0	0	0	0	0
AtTRM1	4	3	0	0	0	0	0	0
AtGPT1	3	1	0	0	0	0	0	0
AtTRM8	3	2	1	0	0	0	0	0
AtMIDD1	2	1	0	0	0	0	0	0
AtTAN1	1	1	0	0	0	0	0	0
AtMAP18	1	0	0	0	0	0	0	0
Total	**112**	**95**	**55**	**87**	**24**	**22**	**20**	**20**

Table 2.2: Number of genes from MAP orthogroups in selected plant taxa.

At, *Arabidopsis thaliana* ; Os, *Oryza sativa* ; Sm, *Selaginella moelendorfii* ; Pp, *Physcomitrella patens* ; Mp, *Marchantia polymporpha* ; Kf, *Klebsormidium flacidum* ; Vc, *Volvox carteri* ; Cr, *Chlamydomona reinhardtii*. Darker blue highlighting indicates chlorophyte-wide orthogroups. Lighter blue, lighter green and darker green highlighting represent orthogroups that originated in the LCA of streptophytes, land plants and vascular plants, respectively.

The number of structural MAP genes within orthogroups increased during Archeaplastida evolution ($p=1.358e^{-09}$), ranging from 1.1 gene per orthogroup in *Marchantia polymorpha* to 3.9 in *Physcomitrella patens* (Figure 2.2). With the exception of *Selaginella moellondorfii*, the stomatophytes taxa are not significantly different from each other ($p>0.05$) but significantly differ from previously diverging taxa ($p<0.05$). This suggests that MAP gene duplications occurred during the evolution of stomatophytes and is consistent with known whole genome duplication events in the LCA of angiosperms (De Bodt, Maere, and Van De Peer 2005) and in mosses (Rensing et al. 2007).

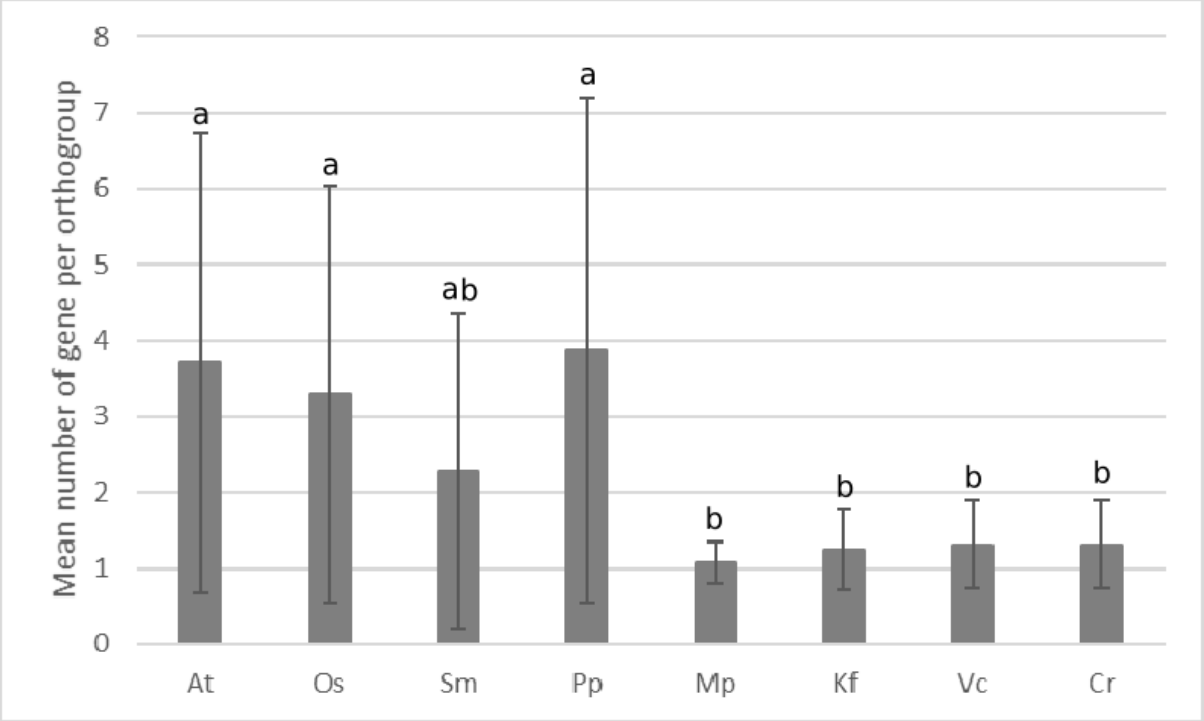

Figure 2.2: Mean number of genes in MAP orthogroups in selected plant taxa. A Kruskal-Wallis test showed a statistically significant effect of the taxa (p=1.358e-09). A Dunn test with Benjamini-Hochberg adjustment method identified pairs of taxa that are statistically dissimilar ($p<0.05$). At, *Arabidopsis thaliana* ; Os, *Oryza sativa* ; Sm, *Selaginella moelendorfii* ; Pp, *Physcomitrella patens* ; Mp, *Marchantia polymporpha* ; Kf, *Klebsormidium flacidum* ; Vc, *Volvox carteri* ; Cr, *Chlamydomona reinhardtii*.

Altogether, these data indicate that there was a diversification of pre-existing and the origin of new structural MAP orthogroups during the course of streptophyte evolution.

2.4.3 Most multigenic MAP orthogroups include genes that are ubiquitously expressed

To test if some genes from multigenic MAP orthogroups were likely to exhibit functional redundancy in *Arabidopsis thaliana*, I analysed their pattern of expression as documented by the *Arabidopsis* eFP browser database (http://bar.utoronto.ca/efp/cgi-bin/efpWeb.cgi, (Winter et al. 2007)). I extracted absolute gene expression values for all 50 samples available and computed the coefficient of variation, a value of the standard deviation normalized by the mean. On average, the coefficient of variation for genes from multigenic orthogroups is significantly higher than for housekeeping genes ($p = 0.03$) (Figure 2.3 A). This suggests that genes from multigenic orthogroups are on average more heterogeneously expressed than housekeeping genes. Nonetheless, 90% of multigenic MAP orthogroups (*i.e.* all except GROWING PLUS-END TRACKING 1 (GPT1), EB1 and MIDD1) include at least one gene that is more ubiquitously expressed than the most heterogeneously expressed housekeeping gene (TUBULINB6 (TUB6)) (Figure 2.3 B-V). This suggests that several genes from the same multigenic MAP orthogroups are likely to be expressed in the same tissues and is consistent with the hypothesis that genes from multigenic MAP orthogroups may exhibit functional redundancy.

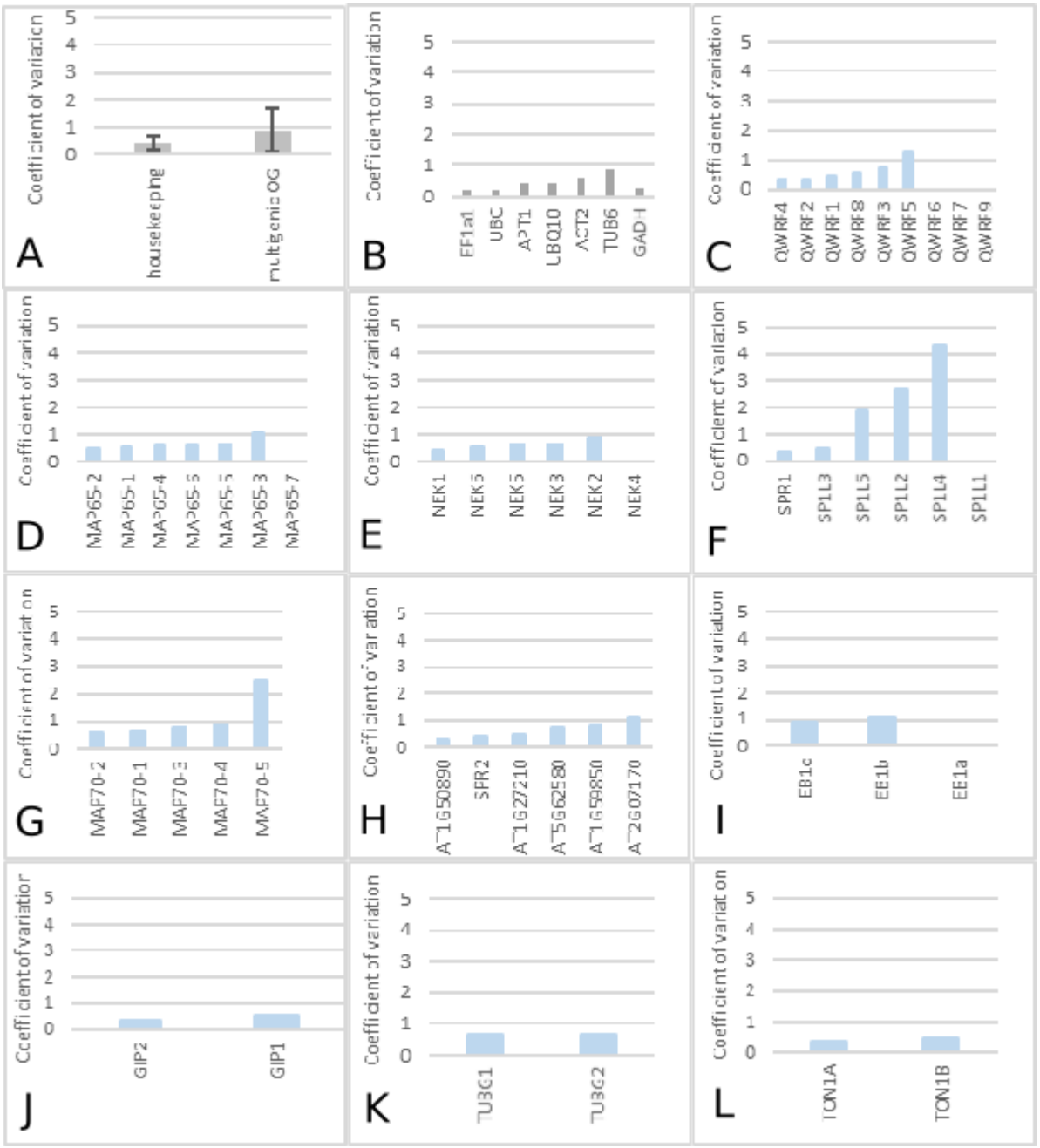

Figure 2.3: Coefficient of variation for the absolute expression values of housekeeping genes and genes from monogenic or multigenic MAP orthogroups in *Arabidopsis thaliana*. A, mean coefficient of variation of housekeeping genes and genes from multigenic orthogroups; B, housekeeping genes; **C-L** genes from multigenic orthogroups found throughout Archeaplastida: **C**, EDE1 orthogroup; **D**,MAP65 orthogroup; **E**, NEK orthogroup; **F**,SPR1 orthogroup; **G**, MAP70 orthogroup; **H**,SPR2 orthogroup; **I**,EB1 orthogroup; **J**, GPI orthogroup; **K**, TUBG orthogroup; **L**, TON1 orthogroup

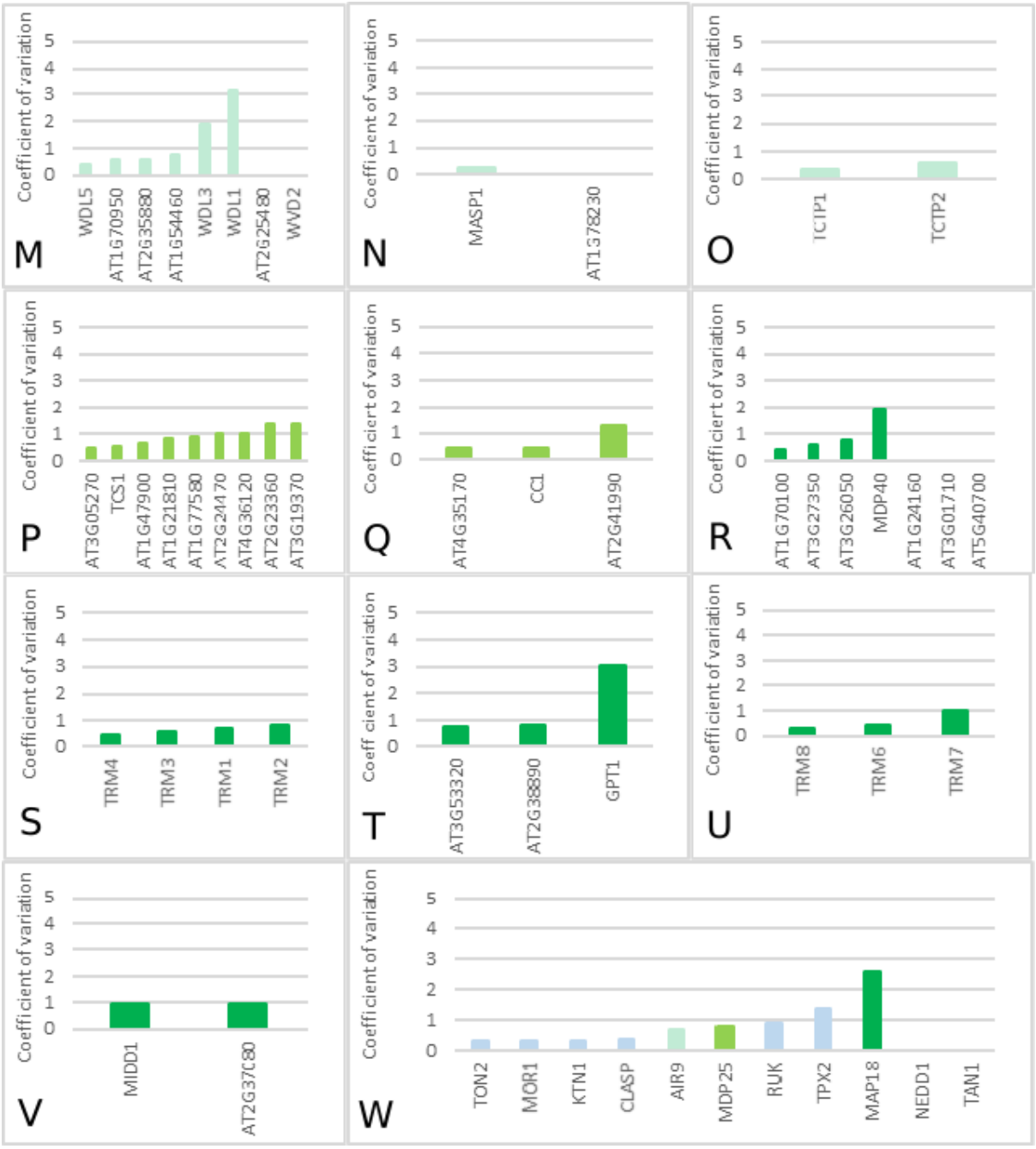

Figure 2.3 (continued): Coefficient of variation for the absolute expression values of housekeeping genes and genes from monogenic or multigenic MAP orthogroups in *Arabidopsis thaliana*. ; **M-V**, genes from multigenic orthogroups that originated during streptophyte evolution: **M**, WVD2 orthogroup; **N**, MASP1 orthogroup; **O**, TCTP; **P**, TCS1 orthogroup; **Q**, CC1 orthogroup; **R**, MDP40 orthogroup; **S**, TRM1 orthogroup; **T**, GPT1; **U**, TRM8; **V**, MIDD1. **W**, genes from monogenic orthogroups.

2.4.4 All orthogroups of the axonemal dynein regulatory complex are absent in taxa that lack flagellated cells

To test whether the loss of a particular microtubule array resulted in the loss of genes controlling its organization, I identified the orthogroups that include at least one *DYNEIN REGULATORY COMPLEX* (*DRC*) gene. DRC are a group of protein that control the function of the axonemal microtubule array in motile sperm cells (Maureen Wirschell 2013, Rupp 2003, Lin 2011, reviewed in Viswanadha 2017), a cell type absent from angiosperms. I identified 10 *DRC* orthogroups, all of which were absent in *Arabidopsis thaliana* and *Oryza sativa* (Table 2.3). By contrast, 8 to 10 orthogroups were present in plant taxa that have motile sperm cells. This suggests that *DRC* genes became obsolete and were lost when the axonemal microtubule array was lost in the last common ancestor of Angiosperms.

Representative gene member	At	Os	Sm	Pp	Mp	Kf	Vc	Cr
DRC4	0	0	3	1	1	1	1	1
DRC7	0	0	2	1	1	1	1	1
DRC3	0	0	2	1	1	1	1	1
DRC11	0	0	2	1	1	1	1	1
DRC1	0	0	1	1	1	1	1	0
DRC2	0	0	1	1	1	1	1	1
DRC5	0	0	1	1	1	1	1	1
DRC6	0	0	1	1	1	1	1	1
DRC10	0	0	0	1	1	1	1	1
DRC9	0	0	0	0	1	1	1	1
Total	**0**	**0**	**13**	**9**	**10**	**10**	**10**	**9**

Table 2.3: Number of genes from DRC orthogroups in selected plant taxa.

At, *Arabidopsis thaliana* ; Os, *Oryza sativa* ; Sm, *Selaginella moelendorfii* ; Pp, *Physcomitrella patens* ; Mp, *Marchantia polymporpha* ; Kf, *Klebsormidium flacidum* ; Vc, *Volvox carteri* ; Cr, *Chlamydomona reinhardtii*.

2.5 Discussion

2.5.1 Our draft de novo *assembly of* Marchantia polymorpha *genome compares well with the JGI genome assembly pre-release*

The genome assembly generated as part of this work was the first publicly released genome assembly for *Marchantia polymorpha* (https://www.ncbi.nlm.nih.gov/Traces/wgs/?val=LVLJ01#contigs, Honkanen *et al* 2016). It provided a tool for the study of the evolution of development in the early years of the *Marchantia polymorpha* research community and remains today a resource that compares well with the pre-released genome assembly on the JGI website in terms of coverage, fragmentation and gene predictions (Appendix A1) (https://phytozome.jgi.doe.gov/pz/portal.html#!info?alias=Org_Mpolymorpha). It must however be said that the JGI genome assembly outperforms ours on every aspects and should be preferred in future studies.

2.5.2 Structural MAP genes from orthogroups that originated during land plant evolution control functions of cortical microtubule arrays adapted to the terrestrial environment

The total number of MAP orthogroups considered in this chapter is higher than the number of MAP gene families in previous reviews (Gardiner 2013). This is mostly due to the identification of new MAPs in recent literature, namely TRM , MASP1, CC1, TCS1, MDP40, GPT (Drevensek et al. 2012; Bhaskara et al. 2017; Endler et al. 2015; L. Chen et al. 2016; Wong and Hashimoto 2017). To a lesser extent, the sampling method also explains this difference: while previous reviews restricted the scope to certain MAPs arbitrarily considered being “predominantly microtubule-related” (Gardiner 2013), I

chose a more systematic and conservative sampling method based on experimentally proven microtubule-binding properties of at least one member of an orthogroup.

A third of structural MAP orthogroups originated during the evolution of land plants. This indicates that the progressive colonisation of the terrestrial environment was concomitant with the innovation of a substantial MAP genetic toolkit. The adaptation of plants to the terrestrial environment included key morphological innovations, one such innovation being the formation of xylem vessel elements in angiosperms. Interestingly, MIDD1 originated after the split between lycophytes and angiosperms and controls the formation of cell wall pits in tracheary elements by organising cortical microtubules in a specialised array characteristic of metaxylem vessels. This suggest that new MAP orthogroups were innovated to control the rearrangement of the CMA during cell differentiation of cell-types that have an adaptive value for living on land. Taken together, this suggest that the colonisation of land by plants may have prompted or required the innovation of new MAP orthogroups to shape adaptive organizations of the CMA in the context of cell differentiation.

The corollary of this conclusion is that the loss of a given microtubule function would prompt or be caused by the loss of MAPs controlling it. The example of axonemal DRC proteins is consistent with this hypothesis. Indeed, a large majority of DRC orthogroups are conserved in all taxa that have flagellated cells and all are lost in angiosperms, which lack flagellated cells. Moreover, this is consistent with recent studies showing the simultaneous loss of axonemal dynein heavy chain proteins (Kollmar 2016). Hence, the corollary holds true and further substantiate this conclusion.

2.5.3 *Structural MAP genes from Archeaplastida-wide orthogroups acquired functions adapted to the terrestrial habitat during the evolution of land plants*

In addition to the innovation of new MAP orthogroups, plants may have recruited genes from previously existing MAP orthogroups to control organizations of the CMA that represent adaptations to living on land. Considering MAP orthogroups that predated the origin of the streptophytes and subsequently diversified, we find that they include genes that control the same adaptive traits as mentioned in 2.5.2. *Ze*MAP65-1 controls the formation of microtubule bundles characteristic of differentiating tracheary elements when expressed in *Arabidopsis* xylogenic suspension cells (Mao et al. 2006). Similarly, *At*MAP70-1 and *At*MAP70-5 promote the formation of microtubule bundles in *Arabidopsis* xylogenic suspension cells, and MAP70-5 promotes the formation of tracheary elements *in vivo* (Keech et al. 2010). This suggests that these proteins were recruited during the evolution of streptophytes to control the organisation of the CMA characteristic of differentiating xylem tracheary elements.

Taken together, the example of the MAP65 and MAP70 orthogroups suggests that genes from previously existing MAP orthogroups were recruited during the course of land plant evolution to shape specialized organizations of the CMA that represent adaptations to living on land.

Finally, this analysis demonstrates that the MAP repertoire of plants evolved during the course of land plant evolution as they adapted to the terrestrial environment by two distinct means: i) innovation/loss of MAP orthogroups with adaptive/obsolete functions, and ii) recruitment of genes from pre-existing MAP orthogroups to control adaptive functions of the cortical microtubule array.

2.5.4 Functional *redundancy occurs between genes of multigenic orthogroups in* Arabidopsis thaliana

The gene expression data extracted from the eFP browser database reveals that some genes from multigenic orthogroups have overlapping expression patterns. This suggests that functional redundancy may occur between those co-expressed genes.

Mutants in genes from the MAP65 orthogroup display mutant phenotypes that are often aggravated by mutations in other MAP65 genes. In *Arabidopsis thaliana,* the cytokinesis defect in *map65-3* mutants is aggravated in *map65-1;map65-3* , *map65-2;map65-3* and *map65-4;map65-3* double mutants ,while *map65-1/2/4* single mutants have no noticeable cytokinesis mutant phenotype (Haoge Li et al. 2017; Sasabe et al. 2011). Similarly, the decreased hypocotyl etiolation phenotype in *map65-2* is aggravated by the mutation of *map65-1*, which alone does not cause a mutant etiolation phenotype (Lucas et al. 2011). This suggests that some members of the MAP65 orthogroup in *Arabidopsis thaliana* are partially functionally redundant.

A similar situation is observed in the case of *Arabidopsis* genes from the SPR1 orthogroup. The root epidermal bulging phenotype of *spr1* mutant is aggravated in *spr1;spr1l3,* and further aggravated in the quadruple mutants *spr1;spr1l3;spr1l2;spr1l4,* while none of the mutations in *spr1l2/3/4* cause root epidermal bulging phenotype on their one (Nakajima, Kawamura, and Hashimoto 2006). Moreover, the *spr1;spr1l3* double mutant shows a twisted hypocotyl phenotype that neither single mutants exhibits (Nakajima, Kawamura, and Hashimoto 2006). Similarly, *spr1l4* shows a weak twisted stem phenotype which is aggravated in the quadruple mutant, while none of the mutations in *spr1*, *spr1l2* and *spr1l3* cause a noticeable twisted stem phenotype on their own (Nakajima, Kawamura, and Hashimoto 2006). This suggests that some members of the SPR1 orthogroup in *Arabidopsis thaliana* are at least partially functionally redundant.

Lastly, the three genes *TONNEAU RECRUITING MOTIF 6* (TRM6), *TRM7* and *TRM8* of the TRM8 orthogroup provide further evidence of functional redundancy between genes from the same orthogroup. The impaired PPB formation phenotype of *trm7* is aggravated in *trm7;trm6* and *trm7;trm8*, and no PPB forms in the triple mutant (Schaefer et al. 2017). This suggests that all members of the TRM8 orthogroup in *Arabidopsis thaliana* are partially functionally redundant.

Taken together with the overlap of expression patterns of genes from the same orthogroups, these three examples support the hypothesis that functional redundancy is likely to occur between genes from multigenic orthogroups in *Arabidopsis thaliana*.

2.5.5 The simple repertoire of structural MAP gene in Marchantia polymorpha *suggests that mutant screens may be a successful route to discover MAP function*

The occurrence of functional redundancy within gene families in *Arabidopsis thaliana* is problematic in forward genetic approaches aiming to identify new genes regulating any given process. It has recently prompted ambitious and innovative approaches such as the systematic generation of double mutant libraries (Su and Krysan 2016). This is however undoubtedly a very logistically demanding and time-consuming endeavour and bypassing the issue of functional redundancy altogether would be preferable.

The genome assembly presented here reveals that 77% of *Arabidopsis thaliana* MAP orthogroups are represented in *Marchantia polymorpha*. In contrast to all other land plant models, 92% of these orthogroups contain a single gene. Although this trend of genetic simplicity has been reported for families of transcription factors (Catarino et al. 2016), it should not be assumed to be systematically the case for all gene families. Indeed, the total number of genes predicted from the genome assembly is comparable to *Arabidopsis*

thaliana and the simplicity of certain gene families in *Marchantia polymorpha* is likely to be counterweighted by increased complexity of other gene families.

In conclusion, the simplicity of the MAP gene repertoire in *Marchantia polymorpha* makes it likely that a mutation in MAP genes would cause an observable mutant phenotype and that a forward genetic screen in the liverwort model will reveal new functions of MAP genes in land plants.

Chapter 3: Identification of new genes regulating microtubule-mediated tip-growth stability in *Marchantia polymorpha.*

3.1 Summary

Plant cells display diverse and specialised morphologies that result from different patterns of cell growth. Filamentous rooting cells represent an extreme case of cell growth polarity. In root hair cells of vascular plants and rhizoid cells of mosses, cell growth is restricted to a narrow domain of the cell periphery resulting in the formation of a tubular projection called root hair and rhizoid respectively. The position of the growing region in filamentous rooting cells is highly stable, resulting in the formation of a straight tube. When this spatial stability is perturbed, the morphology of filamentous rooting cells changes to wavy and bifurcating tubes. The spatial stability of tip-growth relies on finely-tuned microtubule dynamics controlled by microtubule-associated proteins (MAPs). Because functional redundancy of genes from multigenic MAP gene families in *Arabidopsis thaliana* may have prevented the identification of MAP genes controlling tip-growth stability, I aimed to identify new genes regulating tip-growth stability in *Marchantia polymorpha* where the large majority of MAP gene families are monogenic. First, I demonstrated that, similarly to other tip-growing cell-types, tip-growth stability is mediated by microtubules in *Marchantia polymorpha* rhizoids. Then, I screened T-DNA and UV-B mutant collections and isolated 29 independent mutant lines showing a defect in tip-growth stability. Finally, I developed a mutation discovery pipeline that identifies causal mutation by comparing SNPs from independent non-allelic M0 generation of UV-B mutagenized lines. Altogether, this work permitted the discovery of two new regulators

of tip-growth stability in *Marchantia polymorpha*, *NIMA-RELATED* KINASE (Mp*NEK)* and *WAVE DAMPENED2-LIKE* (Mp*WDL*).

3.2 Introduction

A very large proportion of the interface between land plants and the soil is constituted of filamentous cells, such as root hairs of vascular plants, rhizoids of non-vascular plants and ferns or caulonema cells of mosses. They provide rooting functions, such as anchorage, water and nutrient uptake (V. a S. Jones and Dolan 2012). Their tubular shape is key to this function as evidenced by morphological mutants that are defective in anchorage (Appendix A2). Filamentous rooting cells form by tip-growth, a mechanism where growth is stably restricted to a narrow domain of the cell periphery in order to form a straight tubular projection.

In filamentous rooting cells, growth requires the accumulation in the apical dome of secretory vesicles containing cell wall material to be deposited at the tip ((Dumais et al. 2006), reviewed in (Rounds and Bezanilla 2013)). This polar distribution of vesicles relies on the actin cytoskeleton but the stability of the position of the growing tip is mediated by microtubules (Parton et al. 2000; de Graaf et al. 2005; Bibikova, Blancaflor, and Gilroy 1999). Microtubules are distributed unevenly in root hairs. In the non-growing shank, cortical and endoplasmic microtubules are oriented longitudinally and grow towards the tip (C. Ambrose and Wasteneys 2014; Anderhag, Hepler, and Lazzaro 2000; Eng and Wasteneys 2014; Hiwatashi, Sato, and Doonan 2014; Schwuchow, Sack, and Hartmann 1990; Sieberer et al. 2005; Timmers et al. 2007). However, cortical microtubules are not typically seen in the apical dome of growing root hairs and only a few endoplasmic microtubules transiently penetrate the apical dome before entering rapid depolymerisation from their plus-end(Sieberer et al. 2005; Eng and Wasteneys 2014a). By contrast with root hairs, the apical dome of caulonema cells exhibits an abundance of endoplasmic microtubules that converge into an apical bundle (Hiwatashi, Sato, and Doonan 2014).

Tip-growing cells exposed to drugs that stabilize or destabilize microtubules display wavy tubular morphologies, suggesting that the growth region is shifted laterally from an apical position to a subapical position (Bibikova, Blancaflor, and Gilroy 1999; Schwuchow, Sack, and Hartmann 1990). Branching root hairs are also observed following the application of microtubule stabilizing drugs, suggesting that dynamic microtubules are required to maintain a single growth point. This suggests that a tight regulation of microtubule dynamics is required to control the integrity and the stable positioning of the growing region in tip-growing cells. Confirming this interpretation, mutations in MAPs often lead to loss of tip-growth spatial stability. In *Arabidopsis thaliana*, MICROTUBULE ORGANISATION 1 (MOR1) enhances the dynamic instability of microtubules, and the temperature-sensitive mutant *mor1-1* forms wavy root hairs at the restrictive temperature (Whittington et al. 2001). Similarly, the plus-end tracking ARMADILLO-REPEAT KINESIN 1 (ARK1) promotes the transition of microtubules from polymerizing to depolymerizing state (catastrophe) as well as microtubule polymerisation, and root hairs are wavy in the *ark1* loss-of-function mutant (Eng 2014). In pollen tubes, tip-growth regulators include MAP18, a plasma membrane Calmodulin-Ca2+ binding protein that binds to microtubules *in vitro* (Zhu et al. 2013). MAP18 promotes microtubule depolymerisation *in vitro* and increases oryzalin sensitivity or resistance in *MAP18* overexpressing lines or RNAi lines respectively (X. Wang et al. 2007).

Interestingly, MAP18 and MOR1 are single copy genes. This is consistent with the view that functional redundancy in the larger MAP gene families may have prevented the identification of remaining tip-growth stability regulators. To further our understanding of the mechanism controlling microtubule-mediated tip-growth stability, I aim to identify genetic regulators of tip-growth stability in *Marchantia polymorpha*, which mostly has

monogenic MAP gene families. The liverwort model forms rhizoids at different stages of gametophyte development from bicellular spores to the ventral epidermis of mature gametophyte or the outer cell layer of vegetative propagules called gemmae. I first showed that *Marchantia polymorpha* rhizoids present a cytological organisation resembling most that of moss caulonema, and that they rely on microtubule dynamics to control tip-growth stability. I then selected existing T-DNA mutant lines with wavy rhizoids, carried out a UV irradiation mutant screen for mutants with wavy rhizoids and developed a novel mutation discovery pipeline that bypasses the need for crossing mutants. This resulted in the identification of two new genetic regulators of tip-growth stability in land plants: Mp*WDL* and Mp*NEK*.

3.3 Material and methods

3.3.1 Plant growth

Male and female *Marchantia polymorpha* accessions Takaragaike-1 (tak1) and Takaragaike-2 (tak2) provided by K. Ishizaki (Kobe University, Japan) were used as wild-type. T-DNA mutant lines were selected from a T-DNA mutant collection generated by Suvi Honkanen, Victor Jones and Giulia Morieri. Plants were grown horizontally and under continuous white light (~60 PPFD) on a Johnson's medium modified as detailed in Honkanen *et al.*, 2016. To induce the formation of reproductive organs, one month-old gemmelings were transferred to a 1:3 mixture of medium vermiculite : John Innes No. 2 compost and grown under 150 PPFD white light supplemented with GreenPower LED research modules FR (8727900 809336 00, Phillips).

3.3.2 Drug treatments

Gemmae were placed on modified Johnson's medium (Honkanen *et al,* 2016) supplemented with Oryzalin or DMSO and mature rhizoids where imaged two days later.

Oryzalin was dissolved in pure DMSO to produce 0.1mM and 0.75mM 1000X stock concentrations. Treatment plates were compared to 0.1% DMSO control plates.

3.3.3 Cloning and plant transformation

Reporter constructs $_{pro}$Mp*EF1α*:*GFP*-Mp*TUB1* and $_{pro}$Mp*EF1α*:*GFP*-AtEB*1A* were kindly provided by Henrik Buschmann (Osnabruck University, Germany) (Buschmann et al. 2016). Reporter construct $_{pro}$Mp*EF1α*:*YFP*-Mp*RabA4* was kindly provided by Ian Moore (Oxford University, UK) (unpublished). GW compatible vectors MpGWB207 (Ishizaki et al. 2015), HB444 *(*Mp*EF1a:*GW:term in pCambia1300 harbouring *ACETO LACTATE SYNTHASE* chlorsulfuron resistance gene), *HB39 (*pENTRY3C-3x-*NLS-YFP*) were kindly provided by Kimitsune Ishizaki (Kobe University, Japan) and Holger Breuninger (Oxford University, UK).

The open reading frame of Mp*WDL* was amplified from genomic DNA using Phusion High-Fidelity DNA polymerase (NEB) and gene-specific primers (WDL_infusion _F1: ACCAATTCAGTCGACATGAGTGAAGCCGGA and WDL_infusion_GS1_R1: GCCCTTGCTCACCATGGATCCTGATGCAACAGCCA) designed to introduce a 15bp sequence homologous to HB39 and to replace the stop codon by a glycine-serine C-terminal linker. The YFP C-term entry vector HB39 was linearized using the restriction enzymes NcoI and SalI (NEB). The PCR product was gel purified and recombined with double digested HB39 using the In-Fusion kit (#638910, Clonetech). Finally, the *WDL*

fusion entry vector was recombined by LR reaction (#12538-200, ThermoFisher) with the destination vector HB444 to produce a constitutive expression construct.

A 5kb region upstream of the start codon of Mp*WDL* was defined as the promoter region and amplified from genomic DNA using Phusion High-Fidelity DNA polymerase (NEB) and gene-specific primers (pWDL_F1: AAACGACGCCCAGTGCCACCCAATGCTTCAAAGTTTGAAG and pWDL_SmaI_R1:) designed to introduce a 15 bp sequence homologous to MPGWB207 and a SmaI restriction site downstream of the 5'UTR. Destination vector MPGWB207 was linearized using the restriction enzymes HindIII and SacI (NEB) to remove the proMp*EF1a* cassette. The promoter amplicon was gel purified and recombined with double digested MPGWB207 using the In-Fusion kit (#638910, Clonetech). The resulting construct was linearized with the restriction enzyme SmaI and ligated with the Gateway Cassette frame A (Invitrogren) to produce a destination vector. The proWDL destination vector was finally recombined by LR reaction (#12538-200, ThermoFisher) with the WDL-GS-YFP and pENTRY-3C-NLS-vYFP entry vectors to produce the $_{pro}$*WDL*::*WDL-GS-YFP* and $_{pro}$*WDL*::(*NLS*-v*YFP*)$_3$.

The expression clones were transformed into *Marchantia polymorpha* spores obtained from a cross between tak1 and tak2 by co-cultivation with *Agrobacterium tumefaciens* GV3101 using a method from Honkanen *et al.*, 2016. Co-cultivated sporelings were plated on modified Johnson's medium supplemented with 100 ppm cefotaxime plus 10 ppm hygromycin, 150 ppm gentamycin or 0,15 ppm chlorsulfuron depending on the constructs.

3.3.4 Reporter lines

Reporter lines for cytoskeleton and endomembrane compartments were generated by transformation of spores obtained from a cross between tak1 and tak2. Transformants were screened for adequate signal strength and absence of aberrant morphological phenotype. Selected reporter lines were then crossed to mutant backgrounds when required. Because the level of expression of certain reporter constructs increased or decreased after sexual reproduction, the F1 progeny with wavy rhizoids was compared with the F1 progeny with straight rhizoids, rather than with the parental reporter line.

3.3.5 Confocal imaging

To image growing rhizoids, I used one-day-old gemmelings. To image growth-arrested rhizoids, I used two-day-old gemmelings. Whether rhizoids were growing was tested by imaging rhizoids over the course of several minutes.

Imaging chambers were designed as described in (Kirchhelle et al. 2016), using cavity slides to allow rhizoids to grow without entering in contact with the cover slid. Gemmae were plated on the agar slice before adding perfluorodecalin and transferring to normal growth conditions. Imaging of rhizoids was finally carried out using a 20X or a 60X water immersion lens.

For the purpose of staining with fluorescent dyes, gemmae were grown on small petri dishes with 10 mL of modified Johnson's medium, rather than in imaging chambers. Gemmelings were immersed in 10uM propidium iodide for 4 minutes and washed once by removing the staining solution and adding 20mL ddH2O. Imaging was then conducted using a 40X water dipping lens. If prior staining with GFP-bound microsphere was needed, gemmelings were exposed for 5 minutes to 0.02% FluoSpheres (F8848,

Invitrogen), washed once in 20 mL ddH2O and left alone for 20 minutes before PI staining.

All imaging was carried out using a TCS SP5 confocal microscope (Leica). Excitation and emission settings were determined empirically to minimize chloroplast and cell wall autofluorescence bleed-through. The same settings were used for EGFP and Venus: excitation with 488nm and emission between 500nm and 570nm. Brightness was adjusted in raw images to reach the point of saturation and the same modifications were applied to all samples to be compared.

3.3.6 Quantification of rhizoid phenotype

Rhizoid sinuosity and rhizoid diameter were measured from the apical most region of growth-arrested rhizoids that would fit in a 200x100 um field of view. The quantification of rhizoid diameter was carried out by measuring manually the shortest diameter along the shank of rhizoids every 5 um. The quantification of rhizoid 3D sinuosity was carried out using a python script written by Jasper Lamers. Here is his description of the method, as written in his Master thesis:

"Software to analyse the waviness of rhizoids in 3D was developed in the Python programming language(Rossum 1995) and uses Python Imaging Library (Lundh, Ellis, and others 2012) (3.3.1), NumPy(van der Walt, Colbert, and Varoquaux 2011) (1.11.2) and scikit-image(Van Der Walt et al. 2014) (0.12.3) to open and read images. Contours of cells and its inner pixels were segmented in each slice by applying a pixel intensity threshold with OpenCV (2.8.4)(Bradski, n.d.). The noise of the image is removed by selecting contours larger than 1% of the total area of the image. The centres of gravity (CoGs) of these contours were calculated and used to sort the contours to represent the

rhizoid in 3D. This order, referred to as the path, is determined by defining the shortest possible route between all central points of the contours using a Simulated Annealing algorithm(Seshadri 2006) modified to deal with a three dimensional distance calculation for a non-circular path with a fixed starting point. After defining the path, the angle to the x-axis between each CoG and its successor was calculated to define the local direction of the path. The path is split when a significant change in direction occurs. The contours of the resulting fragments of the path are used for a non-parametric regression analysis using Locally Weighted Scatterplot Smoothing (LOWESS)(Cleveland 1979), with the Statsmodels(Seabold and Perktold 2010) (0.6.1) module. Parameterized with frac. set as 0.1. After the regression analysis of all parts, the regressions were assembled to one path. The pipeline from angle calculation to assembly of the regression was performed for both the xy and xz axis in order to maintain the 3D dataset. Finally, this assembly is used to calculate sinuosity as defined by the ratio between the total path length after regression by the shortest distance between base and tip of the rhizoid."

3.3.7 Expression studies

Three-weeks-old gemmelings were ground in liquid nitrogen using pestle and mortar. cDNA synthesis and qPCR were carried out as described in Breuninger *et al.* 2016. Absolute levels of expression were normalised using Mp*EF1a* as a reference gene.

Primers used for qPCR were as follows. Mp*EF1a*_forward: CCGAGATCCTGACCAAGG. Mp*EF1a*_reverse: GAGGTGGGTACTCAGCGAAG. Mp*WDL*_forward: GTTGCCTGTCCTCACGATCA. Mp*WDL*_reverse: TCATGACGCTTGGGCAGTAG.

3.3.8 Genomic DNA extraction

Genomic DNA was isolated from one month-old plants grown in axenic conditions. Whole tissue was ground in liquid nitrogen using pestle and mortar. Genomic DNA was extracted with 2% CTAB buffer as described in Porebski *et al.*, 1997.

To assess the suitability downstream applications, the quantity of extracted DNA was measured with a Qubit 2.0 Fluorometer (Invitrogen) and the purity was estimated from absorbance ratios measured with a ND-1000 spectrophotometer (Nanodrop).

3.3.9 TAIL-PCR

TAIL-PCR were carried out as detailed in Honkanen *et al.* 2016. (see attached paper)

3.3.10 UV-B mutagenesis

Fresh sporangia obtained from a cross between tak1 and tak2 were harvested a surface sterilised with 1% NaDCC solution for 4 minutes and subsequently washed three times in ddH20 before plating on square plates with modified Johnson's medium at a density of 2000 spores per plate. Excess of water on the plates was allowed to dry out in the flow hood before opening the plates in a Benchtop 2UV Transilluminator (UVP) set at 302 nm and equipped with 6 G8T5E UV-B fluorescent lamps (Ushio). Spores were placed facing the UV-B light source with no plastic or medium in between and exposed for a duration of time sufficient to yield 50% kill, which was 60s in our experimental conditions. Then, irradiated plates were closed and plates kept in the dark at room temperature overnight before being transferred to normal growth conditions. Finally, irradiated sporelings were assessed for survival and screened for mutant phenotypes 14 days after plating.

3.3.11 Non-allelism based mutation discovery pipeline

The sequencing of UV-B mutants was carried out with Illumina's HiSeq-2000 platform by the Oxford Welcome Trust Center for Human Genomics. Raw reads were quality trimmed using Trimmomatic-0.32 and normalised using Khmer-0.7.1 with a k-mer size of 31. Resulting reads were aligned against the genome assembly using bowtie2-2.1.0 set in --very-sensitive-local mode. Alignments were position sorted and mismatches within reads with q quality higher than 35 were extracted using the function sort and mpileup from bio-samtools-2.0.5. Because they were likely caused by misalignments, mismatches in regions with coverage exceeding 100X were excluded using the varFilter function from bcftools of the samtools-0.1.9 package. Then, mismatches were retained only if they were supported by more than 7 reads and if they appeared sufficiently homozygous based on a negative FQ value or AF1 value higher than 0.5001. Finally, retained mismatches were considered candidate SNPs if they were absent from other sequenced non-allelic lines, tak1 and tak2, if they were G2A or C2T substitutions or INDELs consistently with the expected UV-B mutation signature, and if they caused a change in the amino acid sequence of a predicted gene.

3.4 Results

3.4.1 Microtubule dynamics regulate tip-growth polarity in Marchantia polymorpha

To check that *Marchantia polymorpha* rhizoids present a cytological organization typical of a tip-growing cell, I transformed and analysed vesicle and cytoskeleton reporter lines (Figure 3.1 and Appendix A3). Small GTPases of the RabA4 subfamily are recruited to an endomembrane compartment that localizes preferentially in the apical dome of root hairs (Preuss *et al*, 2004). Consistently, the vesicles labelled by YFP-*Mp*RabA4 accumulated in the apical dome of growing rhizoids (Figure 3.1 A). The endomembrane

compartment labelled by *At*RabA4b in the apical dome of root hairs is distinct from the trans-Golgi network (TGN) (Preuss *et al,* 2004). Consistently, the TGN marker YFP-MpSYP6a labelled vesicles in the shank and in the subapex but not in the apical dome (Appendix A3). This suggests that the zonation of endomembrane compartments is similar in tip-growing cells of angiosperms and liverworts.

In the shank of growing rhizoids, the localization of GFP-*Mp*TUB1 indicates that the microtubule cytoskeleton (Figure 3.1 B) is composed of cortical microtubules (Figure 3.1 C) and endoplasmic microtubules (Figure 3.1 D) that have a net longitudinal orientation. This is similar to tip-growing cells of flowering plants and mosses. Unlike in tip-growing cells of flowering plants, many microtubules extended in the apical dome, and appeared to converge and form a hub-like structure that resembles the apical microtubule bundle of moss caulonema cells (Figure 3.1 E). In the shank as well as in the apical dome, microtubule plus-ends labelled with GFP-*At*EB1a grew toward the tip (Figure 3.1 F-G). This shows that the microtubule cytoskeleton of growing rhizoids in *Marchantia polymorpha* is structurally similar to that of other tip-growing models in the shank but exhibits bryophyte-specific features in the apical dome, where growth takes place.

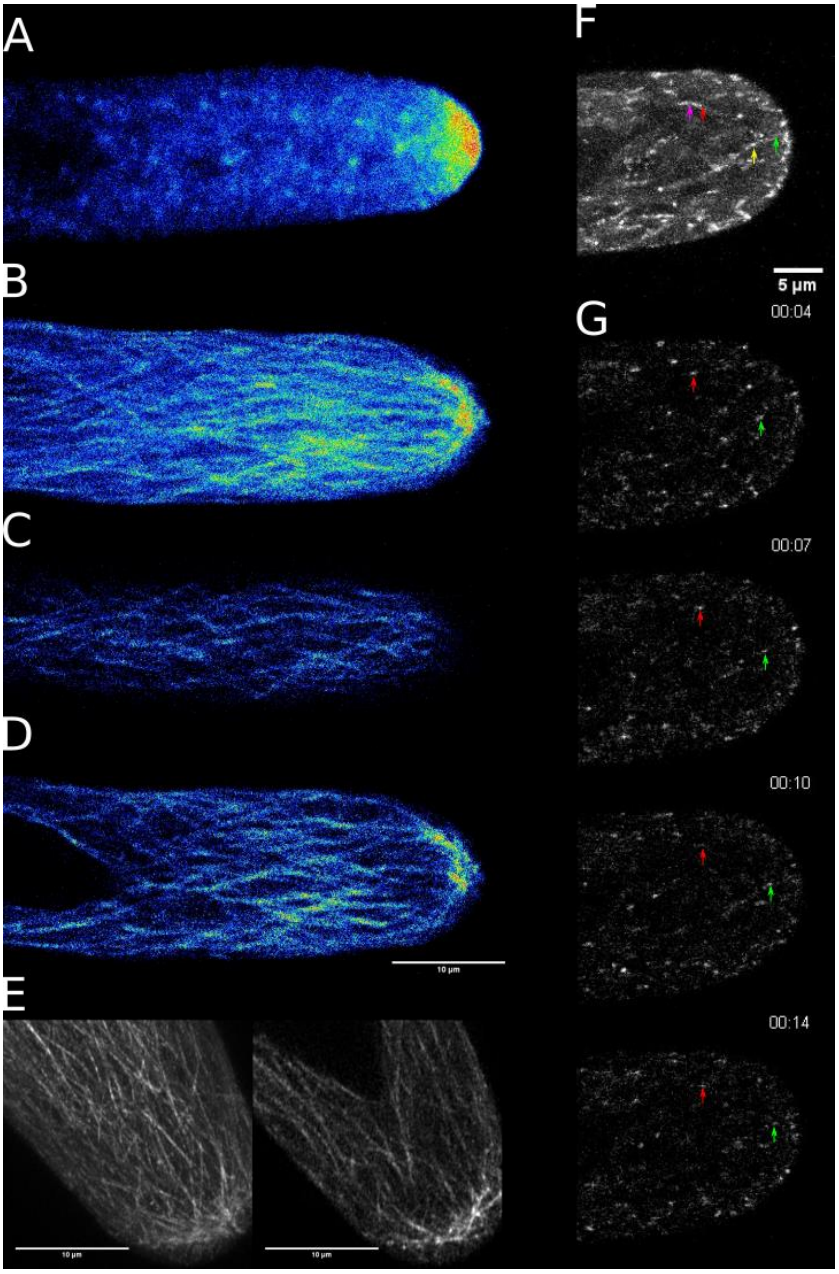

Figure 3.1: Microtubule cytoskeleton and vesicles in actively growing rhizoids in *Marchantia polymorpha*. A: Z-maximum projection of a *proMpEF1a::YFP-MpRabA4* growing rhizoid. Colour code corresponds to 16 colours scale. **B-D:** Z-maximum projection (**A**), cortical plane (**B**) and midplane (**C**) of a *proMpEF1a::GFP-MpTUB1* growing rhizoid. Colour code corresponds to 16 colours LUT. **E:** Z-maximum projection (left) and midplane (right) of the apical dome *proMpEF1a::GFP-MpTUB1* growing rhizoid. **F-G**: 20s temporal projection (**F**) and montage (**G**) in the apical dome midplane of a *proMpEF1a::GFP-AtEB1* growing rhizoid. In **F**, purple and yellow arrows indicate the start position of two EB1 comets; red and green arrows mark the end position of the same two EB1 comets. In **G**, arrows follow the trajectory of EB1 comets marked in **F**.

To test whether the microtubule cytoskeleton shared the same function in stabilizing tip-growth as in other tip-growth models, I treated growing rhizoids with the microtubule-depolymerising drug oryzalin (Figure 3.2). At lower concentrations, oryzalin caused the rhizoids to grow wavy compared to rhizoids grown in control conditions, and at higher concentrations branching was observed in addition to the increased rhizoid sinuosity. This suggests that microtubules stabilize tip-growth in *Marchantia polymorpha*.

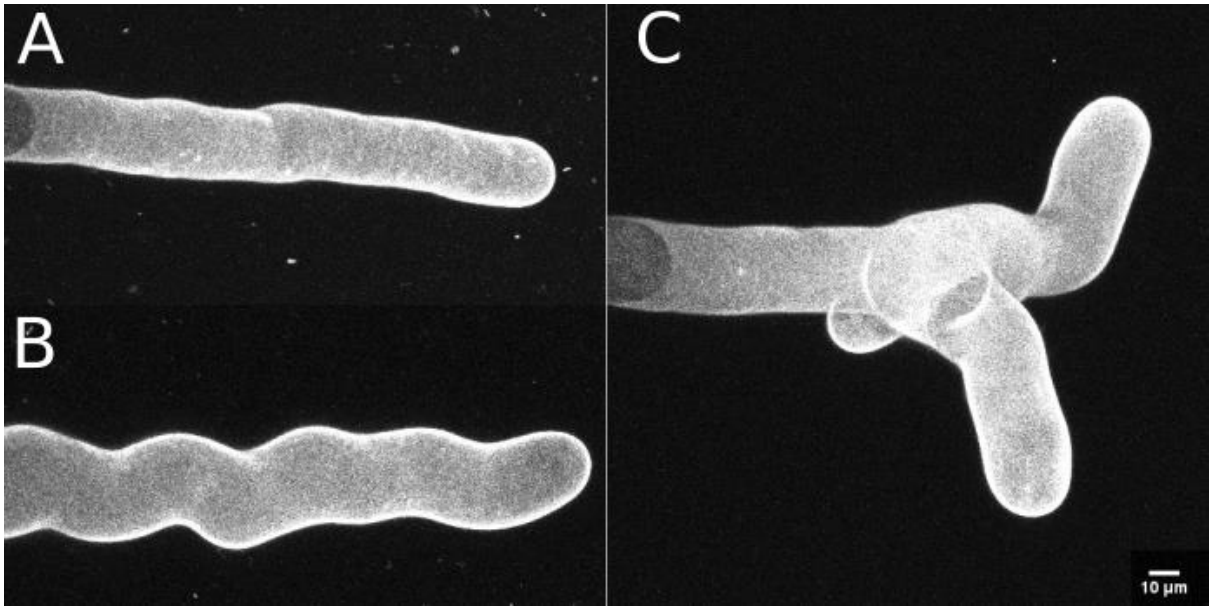

Figure 3.2: Rhizoids grown on the microtubule-destabilizing drug Oryzalin. Z-maximum projection of propidium iodide-stained mature rhizoids grown on 0.1% DMSO (**A**), 0.1 uM oryzalin (**B**) or 0.75 uM oryzalin (**C**).

*3.4.2 Mp*WDL *regulates tip-growth stability*

To identify genetic regulators of microtubule-mediated tip-growth stability, I screened a T-DNA mutant collection generated by Suvi Honkanen and Giulia Morieri for wavy rhizoid phenotypes. Ten independent T-DNA mutant lines had wavy rhizoids. I crossed the T-DNA mutant lines CURLY RHIZOID1 (CR1) and CURLY RHIZOID2 (CR2) with WT and analysed the frequency of plants with wavy rhizoids in the F1 progeny (Table

3.1). Half of the F1 progeny had wavy rhizoids, proving that the mutant phenotype was inherited. Moreover, half of the F1 progeny was hygromycin resistant and hygromycin resistant plants all exhibited the mutant phenotype, suggesting that a single T-DNA insertion caused the wavy rhizoid phenotype.

line	Wavy rhizoids		Straight rhizoids		Total		HygS/HygR ratio
	HygR	HygS	HygR	HygS	HygR	HygS	
CR1/*wdl-3*	131	0	0	122	131	122	1/1.1
CR2/*wdl-2*	117	0	0	116	117	116	1/1.0

Table 3.1: Co-segregation analysis of wavy rhizoid and hygromycin resistance phenotypes CR1xWT and CR2xWT F1 population. HygR: hygromycin resistant. HygS: hygromycin sensitive.

I mapped by TAIL PCR the T-DNA insertions in CR1 and CR2 to a gene predicted to code a TPX2 domain containing protein. The predicted TPX2 domain shares 55% homology with that of *Arabidopsis thaliana* WAVE DAMPENED LIKE (WDL) clade of TPX2-containing proteins and has the KLEEK motif characteristic of the TPX2 domain of WDL proteins (Figure 3.2 A). Consistently, the mutated gene sits within the WDL clade of TPX2 domain containing proteins (Figure 3.2 B). Thus, CR1 and CR2 were named *wdl-3* and *wdl-2* respectively. An additional T-DNA mutant line with an insertion in Mp*WDL* was identified by Suvi Honkanen and named *wdl-1* (Honkanen *et al.* 2016).

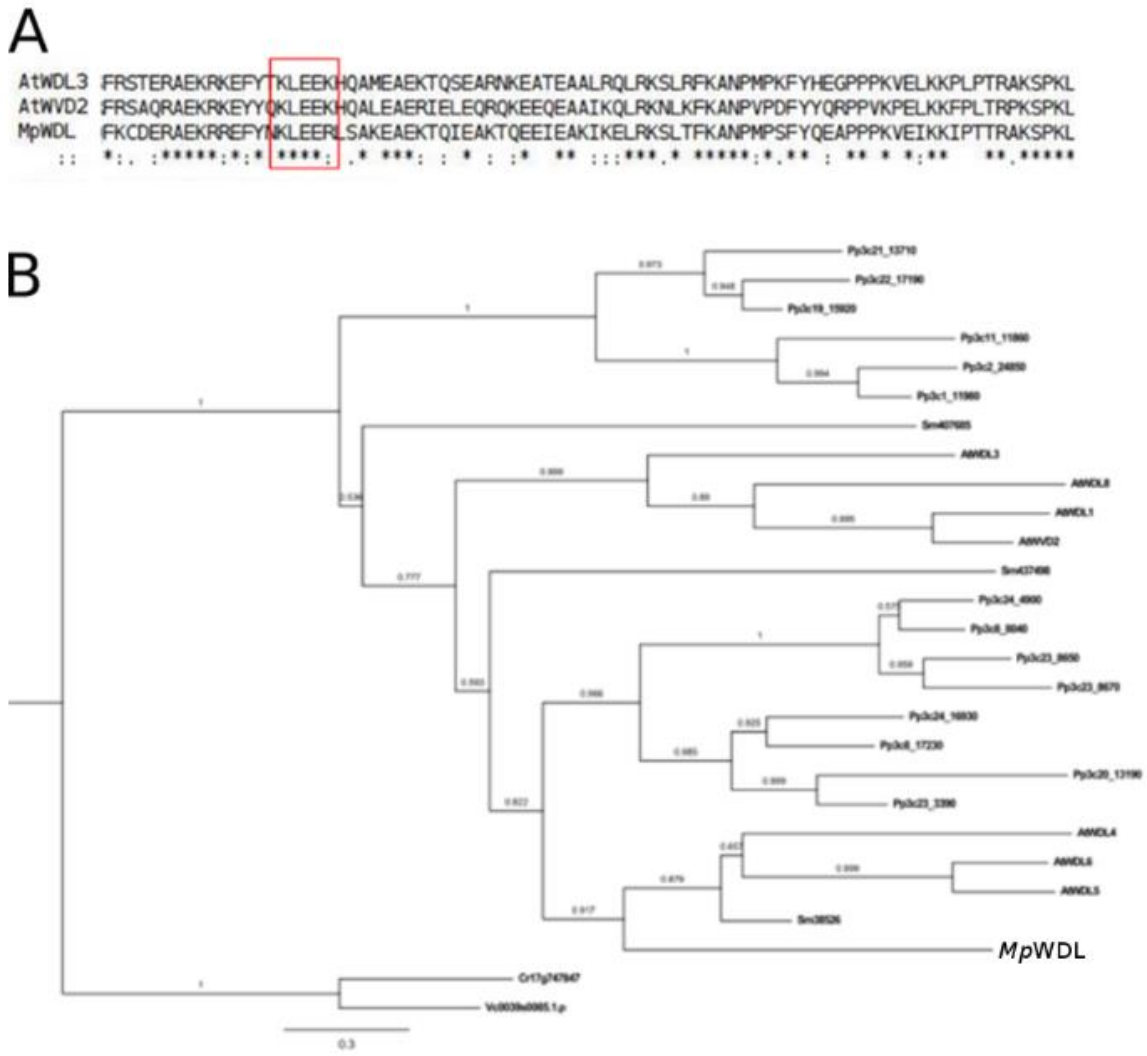

Figure 3.2: WDL clade of TPX2 domain containing proteins. **A:** Alignment of the TPX2 domain of MpWDL and representative members of *Arabidopsis thaliana* WDL proteins. The red box marks the KLEEK motif characteristic of WDL proteins. **B:** Phylogenetic tree inferred from full-protein alignment and rooted with non-KLEEK TPX2 domain-containing proteins of chlorophyte algae. Branch support is shown as p-value from SH test.

Suvi Honkanen and Giulia Morieri tested the remaining T-DNA mutant lines for co-segregation of the hygromycin resistance and the wavy rhizoid phenotype. They showed that the causative mutation was not tagged by the functional hygromycin resistance

cassette of a T-DNA insertion in the following mutant lines: ST33-5, ST47-6, ST50-24, ST50-8, SH21 (unpublished data).

To test whether some of these untagged T-DNA mutant lines might be mutated in Mp*WDL*, I carried out complementation assays. *wdl* mutants were crossed with SH21 and ST33-5. All the progeny from the cross between a *wdl* mutant and ST33-5 or SH21 had wavy rhizoids, suggesting that ST33-5 and SH21 are allelic to *wdl* mutants (Table 3.2).

Parent 1	Parent 2	Wavy rhizoid	Straight rhizoid	Total F1	Genetic distance (cM)
wdl-1	ST33-5/ *wdl*$^{GOF-1}$	237	0	237	0
wdl-3	SH21	242	0	242	0

Table 3.2: Complementation assays between *wdl* tagged and untagged T-DNA mutant lines

The T-DNA insertion in *wdl-2* and *wdl-3* is in an exon and an intron of Mp*WDL* (Figure 3.3 A). This suggests that *wdl-2* and *wdl-3* cannot produce a functional Mp*WDL* transcript. Consistently, the steady state level of *MpWDL* transcript is virtually not detectable in *wdl-2* and *wdl-3* (Figure 3.3 B). Furthermore, the location of the T-DNA insertions in *wdl-2 and wdl-3* at the predicted microtubule-binding domain TPX2 suggests that the truncated protein that may still be produced would not be fully functional. Consistently, the WT rhizoid phenotype was restored by expressing *pro*Mp*WDL::WDL-YFP* in the *wdl-2* background, suggesting that the wavy rhizoid phenotype is caused by the loss of *WDL* function (Figure 3.3 J-L).

By contrast, sequencing of the ST33-5 genome revealed a T-DNA insertion in the promoter region of Mp*WDL*, with the left border of the T-DNA facing the start of the gene. This suggests that ST33-5 may be an Mp*WDL* overexpressing line. Consistently,

the steady state level of *MpWDL* transcript is 4 times higher in ST33-5 than in tak1. Because no mutations were detected in its *WDL* coding sequence, ST33-5 was named WDL^{GOF-1} (Figure 3B). Albeit being weaker and less penetrant, the rhizoid wavy phenotype of WDL^{GOF-1} is similar to that of *wdl*-2 (Figure 3F and Figure 3H). This suggests that fine-tuning of *WDL* expression is required to control tip-growth stability.

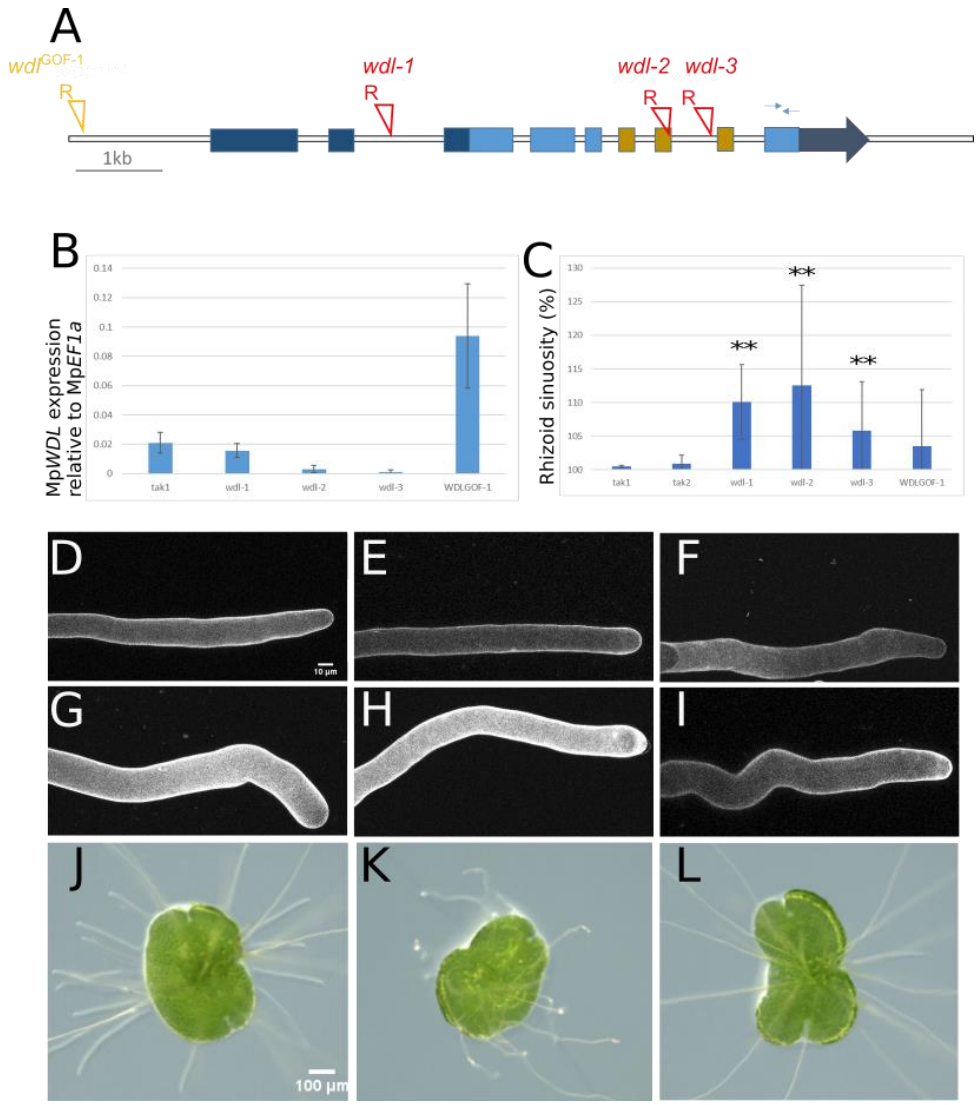

Figure 3.3: *wdl* gain-of-function and loss-of-function mutant lines have wavy rhizoids. A: Schematic representation of *MpWDL* gene model. UTR regions are represented in dark blue, CDS in light blue. The TPX2 domain spans across the 3 exons represented in brown. T-DNA insertion sites are indicated in red with the right border orientation marked with R. The thin arrows on exon9 represent the primers used for qPCR. **B:** Steady state level of expression of *MpWDL* normalised to *MpEF1a*. **C:** Mean rhizoid 3D sinuosity from 10 mature rhizoids. Error bars indicate +/- 1 SD and two stars indicate a Benjamini-Hochberg adjusted p-value from non-parametric Dunn test lower than 0.01. **D-I:** Mature rhizoids of tak1 (D), tak2 (E), *wdl*$^{GOF-1}$ (F), *wdl-1* (G), *wdl-2* (H) and *wdl-3* (I). **J-L :** 2d old gemma of tak1 (J), *wdl-2* (K) and *wdl-2* complemented with *proMpWDL::MpWDL-YFP*.

3.4.3 Mp*WDL-YFP localizes to microtubules*

In *Arabidopsis* thaliana, WAVE DAMPENED LIKE proteins bind to microtubules *in vitro* and localize to cortical microtubules in hypocotyl cells. To test whether *Mp*WDL localizes to microtubules in *Marchantia polymorpha*, I analysed the localization of the *Mp*WDL-YFP protein fusion driven by the Mp*WDL* promoter. *Mp*WDL-YFP localizes to interphase and mitotic microtubules in all cell-types investigated (Figure 3.4). In growing WT rhizoids, the pattern of *Mp*WDL-YFP localization (Figure 3.4 C) resembles that of GFP-*Mp*TUB1 growing rhizoids (Figure 3.1 B), showing microtubules that are longitudinally arranged in the shank of rhizoids and converge in the apical dome. (Figure 3.4 A). However, a noticeable difference is that the *Mp*WDL-YFP signal was predominantly observed in the shank, while the *Mp*TUB1-EGFP signal was either predominantly observed in the apical dome (Figure 3.5 A, Appendix A4 and Appendix A5), or equally observed in the apical dome and the shank and subapex (Appendix A4 and Appendix A5). This suggests that MpWDL-YFP preferentially localizes to microtubules in the shank of growing rhizoids. Co-localisation of *Mp*WDL-YFP and *Mp*TUB1-GFP remains to be investigated to further substantiate this claim.

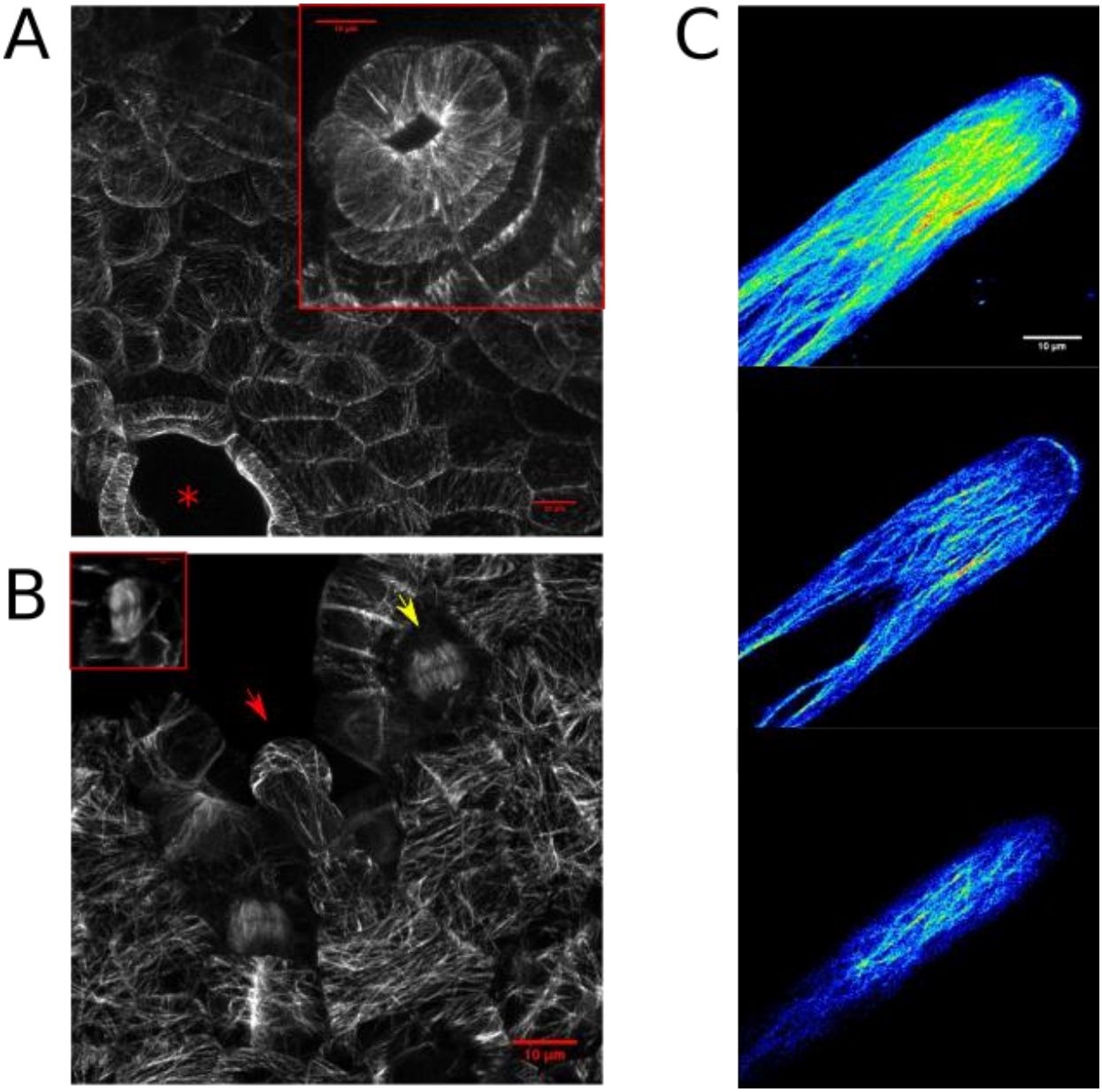

Figure 3.4: Localization of *Mp*WDL-YFP in *Marchantia polymorpha*. A: Dorsal epidermis of *proMpWDL::MpWDL-YFP*. The red star indicates a mature air pore and the inserted red box frames a developing air pore. **B:** Meristematic notch of a *proMpWDL::MpWDL-YFP*. The red arrow points to a mucilage papillae cell directly above the meristematic notch. The yellow arrow points to a phragmoplast, while the red inserted box frames a mitotic microtubules during metaphase. **C:** (top to bottom) Z-maximum projection midplane and cortical plane of a a *proMpWDL::MpWDL-YFP* growing rhizoids.

*3.4.4 Mp*WDL *promotes the formation of a longitudinal array of parallel-arranged microtubules in the shank of growing rhizoids*

To test whether *Mp*WDL controls the organisation of the microtubule cytoskeleton in rhizoids, I compared the *Mp*TUB1-GFP localization in WT and *wdl* loss-of-function backgrounds (Figure 3.5). Due to technical limitations in standardizing rhizoid growth conditions, only seven WT and 6 *wdl-2* growing rhizoids were imaged. The microtubule cytoskeleton in the shank of all *wdl-2* growing rhizoids appeared more randomly organised (*i.e.* isotropic) than in the shank of all WT growing rhizoids (Figure 3.5, Appendix A4 and Appendix A5). This qualitative result suggests that *Mp*WDL promotes the organisation of the microtubule cytoskeleton into an array of parallel-arranged microtubules with a net longitudinal orientation in the shank of growing rhizoids.

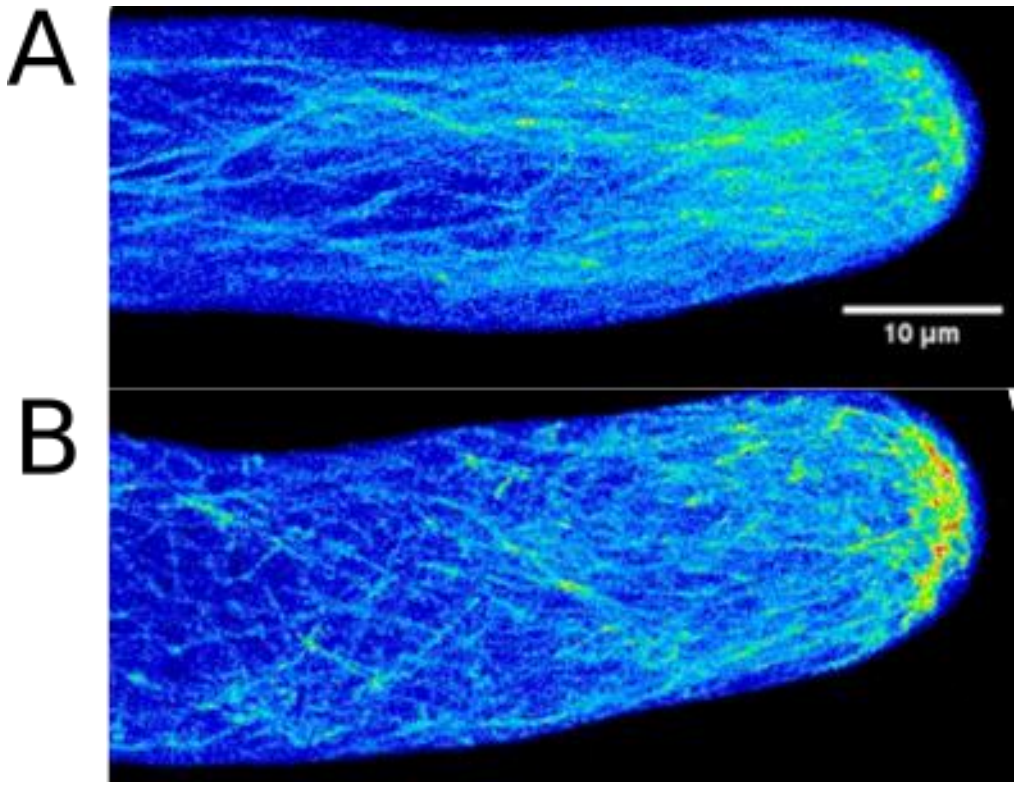

Figure 3.5: Organization of the microtubule cytoskeleton in *wdl-2* growing. Z-maximum projection of *proMpEF1a::GFP-MpTUB1* in WT (**A**) and *wdl-2* (**B**) growing rhizoids. Colour code corresponds to 16 colours scale.

3.4.5 T-DNA mutants with wavy rhizoid that are not allelic to wdl mutants indicate that additional genes regulate tip-growth stability

To test whether other untagged T-DNA mutants may be mutated in *wdl*, I carried out complementation tests between *wdl* mutants and ST47-6, ST50-24 and ST50-8 (Table 3.3). All three lines are segregating independently from the *wdl* mutations, showing that there are other genes than Mp*WDL* that control tip-growth stability in *Marchantia polymorpha*.

Parent 1	Parent 2	Wavy rhizoid	Straight rhizoid	Total F1	Genetic distance (cM)
wdl-3	ST47-6	189	67	256	52.3
wdl-2	ST50-24	202	53	255	40.6
wdl-1	ST50-8	188	47	235	40.0

Table 3.3: Complementation assays between *wdl* mutants and remaining untagged T-DNA mutant lines.

3.4.6 UV-B and T-DNA mutant lines with sinuous rhizoids form 4 complementation groups

3.4.6.1 Morphological phenotypes of mutant lines suggest different classes of mutants

To identify new genes regulating tip-growth stability, I generated a mutant collection by UV-B irradiation of tak1xtak2 F1 spores and screened for wavy rhizoid phenotypes. Out of 120 000 mutagenized sporelings, 97 independent mutant lines with wavy rhizoids were identified. Of those, 22 were retained for further analysis, based on practical criteria such as sufficient gametophyte growth, the production of gemmae and the ability to reproduce sexually.

To characterize in more depth the morphological phenotype of rhizoids in these mutant lines, I imaged mature rhizoids developed on the upper side of two day-old gemmae. Two parameters were considered: rhizoid diameter and rhizoid sinuosity (Table 3.4). Because rhizoid sinuosity and rhizoid diameter were found to statistically depend on genotype ($p_{kruskal\text{-}wallis} < 2.10^{-6}$), these parameters were used to categorize the mutant lines based on their rhizoid morphological phenotype. A group of 8 mutants showed a 5% to 15% increase in rhizoid sinuosity together with a rhizoid diameter similar to WT. To a lesser extent, UV5.8 may be included in this group because it showed a rhizoid diameter similar to WT together with a mild increase in rhizoid sinuosity associated with a high variance, suggesting that the phenotype was weakly penetrant but qualitatively similar. This wavy rhizoid of WT diameter phenotype suggests that these mutants can polarize growth similarly to WT but fail to stabilize growth to a constant position in the apical dome.

By contrast, a distinct group of 6 mutants had a significantly higher rhizoid diameter and showed a weak or undetectable increase in rhizoid sinuosity. This suggests that the growth domain may be larger in rhizoids of these mutants. Moreover, additional phenotypes correlated perfectly with this group of mutants, such as gaping air pores on the dorsal epidermis in the mature gametophyte (Appendix 6).

Upon closer investigation of previously identified T-DNA mutants with wavy rhizoids, *wdl-2* mutant appeared to phenotypically resemble the first group of mutants, while the *ren-1* T-DNA mutant line (Honkanen *et al* 2016) appeared to share all the phenotypic attributes of the latter group of mutants.[3]

[3] Suvi Honkanen generated the *ren-1* mutant line, noted the wavy rhizoid phenotype and identified the T-DNA insertion site in Mp*REN* locus. I quantified the rhizoid sinuosity and diameter, as well as noted the gaping air pore phenotype mentioned in 3.4.5.2.

Lines	Rhizoid sinuosity (%)	Rhizoid diameter (um)
tak1	100.5 +/-0.2	20.8 +/-2.1
tak2	100.9 +/- 1.2	19.5 +/-2.4
*wdl-1***	110.1 +/-5.6**	19.1 +/- 2.0
*wdl-2***	112.6 +/-14.9**	19.5 +/-2.1
*wdl-3***	105.8 +/-7.2**	18.9 +/-1.9
wdlGOF-1	103.5 +/-8.4	18.9 +/-1.4
ren-1	103.2 +/-4.7	32.7 +/-3.7**
SH21	105.0 +/-7.1**	15.7 +/-1.6*
ST47-6	114.8 +/-44.4*	17.7 +/-2.5
VJ72	104.6 +/- 8.0 **	18.0 +/- 2.3
UV3.4	103.6 +/-2.5**	23.2 +/-3.0
UV3.8	136.8 +/-52.7**	22.2 +/-2.5
UV3.13	114.7 +/-9.3**	21.8 +/-4.1
UV4.31	105.4 +/-6.9**	27.6 +/-2.3**
UV4.32	101.5 +/-1.2	25.7 +/-1.5**
UV4.34	105.8 +/-11.4*	29.4 +/-2.4**
UV5.5	108.3 +/-7.2**	19.8 +/-1.4
UV5.8	103.4 +/-4.3	23.1 +/-2.6
UV5.21	NA	NA
UV5.28	100.6 +/-0.4	27.4 +/-4.9**
UV5.30	114.8 +/-16.9**	18.88 +/-2.0
UV5.33	104.6 +/-6.3**	18.5 +/-1.9
UV5.36	112.1 +/-19.2**	20.4 +/-2.3
UV5.37	NA	NA
UV5.38	NA	NA
UV5.39	111.2 +/-11.6**	23.6 +/-2.1*
UV5.42	107.2 +/-8.5**	22.6 +/-2.9
UV6.3	102.9 +/-5.8	25.8 +/-3.7**
UV6.8	103.6 +/-8.5	28.8 +/-7.2**
UV6.9	100.5 +/-0.3	16.8 +/-1.3*
UV6.14	105.6 +/-16.7	21.5 +/-10.4
UV6.16**	115.3 +/-15.4**	22.0 +/-2.1

Table 3.4: Morphological phenotype of T-DNA and UV mutant lines mentioned in this study. The mean values of rhizoid sinuosity and rhizoid diameter were obtained from 10 mature rhizoids per genotype and are given +/- 1 SD. Single or double stars indicate a Benjamini-Hochberg adjusted p-value from non-parametric Dunn test lower than 0.05 and 0.01 respectively. Phenotypes significantly different from WT were highlighted to help visualising the independence of the large rhizoid and wavy rhizoid phenotypes.

3.4.6.2 Complementation assays confirm 4 complementation groups

To test whether the UV mutant lines were allelic to the *wdl* and *ren* mutants, I carried out complementation assays (Table 3.5). UV mutant lines were crossed to a *wdl* mutant or *ren-1* according to phenotypic similarity and the rhizoid phenotype was scored for waviness. All the progeny of the cross between *wdl-2* and UV5.5 or UV5.36 had wavy rhizoids, suggesting that they are allelic to *wdl-2*. By contrast, some F1 plants in the progeny of all other crosses between a *wdl* parent and a UV mutant line had straight rhizoids, proving that the causative mutation was in a gene other than Mp*WDL*. In a majority of cases, the causative mutation was segregating independently from the *wdl* mutations, as indicated by the ca. 50cM genetic distance. However, the genetic distance between the Mp*WDL* locus and the causative mutation of UV3.8, UV3.13, UV5.30, UV5.33, UV5.36, UV5.42, UV5.39, UV6.14 and UV6.16 showed genetic linkage.

Parent 1	Parent 2	Wavy rhizoid	Straight rhizoid	Total F1	Genetic distance (cM)
wdl-2	UV5.5	236	0	236	0
SH21	UV5.36	239	5	247	4.0
wdl-3	UV3.8	244	11	255	8.6
wdl-2	UV3.13	484	13	497	5.2
wdl-2	UV5.30	492	12	504	4.7
wdl-2	UV5.33	272	11	283	7.8
wdl-2	UV5.42	247	9	256	7.0
wdl-2	UV6.16	345	14	359	7.8
wdl-2	UV5.39	218	24	242	20.0
wdl-2	UV6.14	266	21	287	14.6
wdl-2	UV3.1	190	63	253	49.8
wdl-2	UV3.4	250	67	317	42.3
wdl-2	UV3.6	89	30	119	50.4
wdl-2	UV3.7	120	27	147	36.7
wdl-2	UV5.8	194	41	235	34.9
wdl-2	UV5.21	218	67	285	47.0
wdl-2	UV5.37	413	114	527	42.7
wdl-2	UV5.38	164	48	212	45.3
wdl-2	UV6.9	214	82	296	55.4

Table 3.5: Complementation assays between *wdl* mutants and UV-B mutant lines.

To test whether the UV mutant lines that were neither allelic nor independently segregating from the Mp*WDL* locus were allelic, I carried out complementation assays between them (Table 3.6). With the exception of UV3.13, UV5.39 and UV6.14 – which were not tested, UV3.8, UV5.33, UV5.36, UV5.42 and UV6.16 were all allelic to UV5.30. Hence, these six UV mutant lines form a new complementation group.

Parent 1	Parent 2	Wavy rhizoid	Straight rhizoid	Total F1	Genetic distance (cM)
UV5.42	UV5.30	252	0	252	0
UV6.16	UV5.30	240	0	240	0
UV5.33	UV5.30	243	0	243	0
UV3.8	UV5.30	241	0	241	0
UV5.36	UV5.30	233	0	233	0

Table 3.6: Complementation assays between UV-B mutant lines linked to Mp*WDL*

To test whether some of the mutant lines that were independently segregating from the Mp*WDL* locus were allelic with each other, I carried out further complementation assays. All the progeny from the cross between the T-DNA mutant line ST47-6 and UV3.4 had wavy rhizoid Therefore, ST47-6 and UV3.4 form another new complementation group (Table 3.7).

Parent 1	Parent 2	Wavy rhizoid	Straight rhizoid	Total F1	Genetic distance (cM)
UV3.4	ST47-6	156	0	156	0

Table 3.7: Complementation assay between untagged T-DNA mutant line ST47-6 and UV mutant line UV3.4.

Finally, the UV mutant lines that resembled the *ren-1* mutant were considered for complementation assays (Table 3.8). While most had so severe a dorsal epidermis phenotype that they could not be crossed, the female UV4.32 could be crossed to the male *ren-1* and UV4.31. All the progeny from both crosses had wavy rhizoids, suggesting that the causative mutation in UV4.31 and UV4.32 is indeed at the Mp*REN* locus.

Parent 1	Parent 2	Wavy rhizoid	Straight rhizoid	Total F1	Genetic distance (cM)
ren-1	UV4.32	243	0	243	0
UV4.31	UV4.32	116	0	116	0

Table 3.8: Complementation assay between *ren-1* and selected UV-B mutants

3.4.7 SNP filtering pipeline identifies causative mutations after sequencing of the M0 mutant genomes

To identify the causative mutations from the UV mutant lines, I developed a mutation discovery pipeline that bypasses the need for crossing. Several independent UV M0 mutant lines – some with wavy rhizoids, some with straight rhizoids – were selected and

their genome sequenced. Raw reads were aligned against our reference genome and mismatches were identified and taken through the following filtering steps : The pools of mismatches obtained were compared to identify mismatches present in one UV mutant line with wavy rhizoids and absent from any other UV mutant lines with straight rhizoids. This step is later referred to as non-allelism filtering and represents the only novelty of this approach. Following the non-allelism filtering, retained mismatches were further filtered to ultimately end up with SNPs and INDELs that were consistent with the expected UV signature and predicted to change the amino acid sequence of a protein.

To test the efficiency of this method, it was applied to the UV4.32 mutant line, which belongs to the Mp*REN* complementation group. In total, approximately 143 292 mismatches were identified in UV4.32 before any filtering (Figure 3.6 B). By contrast, tak1 and tak2 genomes were re-sequenced and contained 80 000 and 16 000 mismatches respectively (Appendix A7). This suggests that about two third of the mismatches in UV4.32 are tak1/tak2 polymorphisms or misalignments while the remaining 44 000 include UV-induced mutations.

The number of mismatches specific to UV4.32 decreased with the number of UV mutant lines with straight rhizoids used for filtering (Figure 3.6 A). In fact, the number of specific mismatches followed an exponential decay, suggesting that the mismatches information contained in the filtering lines is to some extent redundant. This is certainly due to the tak1-tak2 polymorphisms segregating in the F1 progeny that was mutagenized, and possibly due to UV-induced mutations occurring at the same locus independently in several UV mutant lines. Ultimately, using all 8 filtering lines sequenced, the number of candidate mismatches was reduced to 12 000 mismatches, or more than 90% decrease (Figure 3.6 B). This suggests that non-allelism filtering increased the stringency of candidate mismatches identification, prior to standard filtering steps.

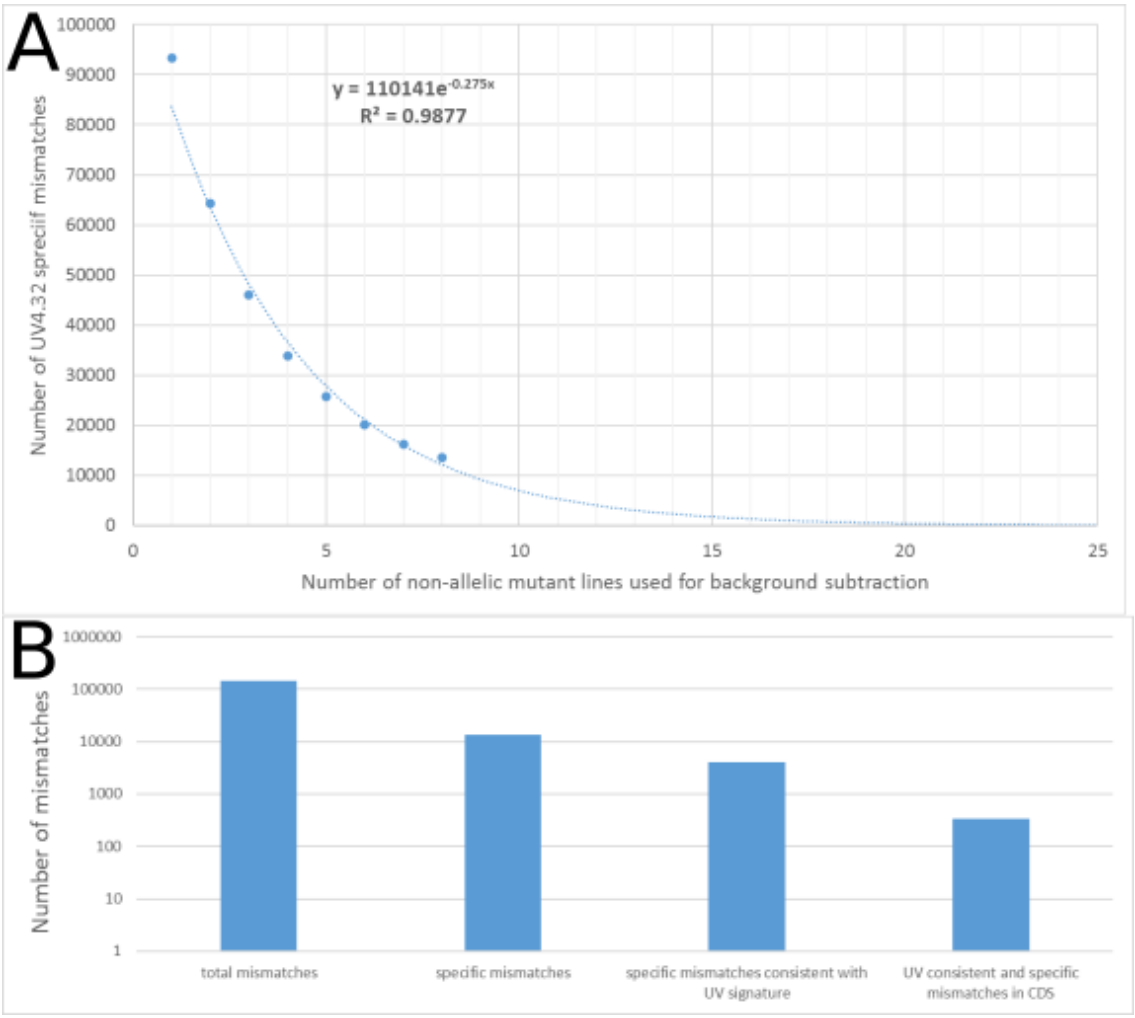

Figure 3.6: Performance and output of non-allelism based mutation discovery pipeline in UV4.32. A: Effect of increasing number of non-allelic mutant backgrounds on filtering efficiency. **B:** Number of UV4.32 mismatches in remaining after each filtering step when using 8 non-allelic UV mutant lines.

Subsequent filtering steps further reduced the number of candidate mismatches to 10 mutations that were consistent with the expected UV mutation signature and were predicted to change the amino acid sequence of a protein (Table 3.10). Of those, one 2 base pair deletion caused an early stop codon in Mp*REN*. This suggests that the subsequent filtering steps were conservative enough.

Altogether, this proves that this non-allelism based mutation discovery pipeline enables the identification of a small number of mutations, including the causative mutation, from UV mutant lines after sequencing of the M0 generation.

Mutated gene model	Arabidopsis homolog	Annotation of Arabidopsis homolog	Type of mutation
Mp*REN*	AT5G12150/PHGAP1	Rho GTPase Activating Protein	Frame shift, early stop
Mp1660s1160	AT5G38840	SMAD/FHA domain containing protein	missense
Mp2415s1240	AT2G29510	hypothetical protein DUF3527	missense
Mp2490s1660	AT1G74410	RING protein	missense
Mp2782s1160	Unresolved	Acyl transferase	missense
Mp3036s1070	AT3G54750	unannotated	missense
Mp3802s1070	AT1G06560	NOP2C, RNA methylation	missense
Mp4605s1070	Unresolved	Glycosyl transferase	missense
Mp773s1730	AT1G73060	LPA3	missense
Mp909s1190	AT2G07360	SH3 domain-containing protein	missense

Table 3.10: Candidate mutations for UV4.32

*3.4.8 Nonsense mutation in Mp*NEK *causes the wavy rhizoid phenotype of UV3.4*

To identify the causative mutation in UV3.4, I applied the non-allelism based mutation discovery pipeline. Out of 190 843 total mismatches, only 6 candidate mutations remained (Appendix A8). Of those, only one mutation resulted in an early stop codon and the nonsense mutation was in a gene homologous to the NIMA RELATED KINASEs (NEKs) (Table 3.11). Because NEK proteins are MAPs that control microtubule dynamics in *Arabidopsis thaliana* (Motose et al. 2011), this mutation thus appeared to be a reasonable candidate and was further investigated.

Mutated gene model	Arabidopsis homolog	Annotation of Arabidopsis homolog	Type of mutation
Mp2834s1300	AT3G37750/NEK6	beta-tubulin phosphorylation	nonsense
Mp2145s1300	AT3G54630/EIF4G	Kinetochore protein-like protein	missense
Mp4343s1080	AT2G1677/bZIP23	Zinc deficiency response transcription factor	missense
Mp2528s1180	AT5G16840	Binding partner of ACD11-1, response to cytokinin	missense
Mp1040s1130	AT5G03900	Iron sulphur cluster biosynthesis family protein	missense
Mp4751s1220	No hit	NA	Missense

Table 3.11: Candidate mutations for UV3.4

Interestingly, Victor Jones carried out a TAIL PCR on the T-DNA mutant line VJ72 and identified a T-DNA insertion in the promoter region of Mp*NEK*. I quantified the rhizoid phenotype of VJ72 revealed a wavy rhizoid phenotype (Figure 3.7 B). This suggests that both the nonsense mutation of UV3.4 in *MpNEK* and the T-DNA insertion of VJ72 in the promoter of Mp*NEK* may cause a wavy rhizoid phenotype.

To test that the T-DNA insertion in the promoter of Mp*NEK* causes the weak wavy rhizoid phenotype, I analysed the progeny of the VJ72 backcross to WT (Table 3.12). Half of the progeny was hygromycin resistant, suggesting that this was the only T-DNA insertion. Moreover, all the hygromycin resistant progeny formed weakly waving rhizoids, suggesting that the T-DNA insertion in the promoter region of Mp*NEK* causes the mutant phenotype.

Line	Wavy rhizoids		Straight rhizoids		Total F1		HygS/R ratio
	HygR	HygS	HygR	HygS	HygR	HygS	
VJ72	136	0	0	145	136	145	1/0.9

Table 3.12: Co-segregation analysis of wavy rhizoid and hygromycin resistance phenotypes VJ72xWT F1 population. HygR: hygromycin resistant. HygS: hygromycin sensitive.

To test that UV3.4 is allelic to VJ72, I carried out a complementation assay (Table 3.13). UV3.4 and VJ72 being both males, I used as the female parent the T-DNA untagged mutant line ST47-6, which I had showed to be allelic to UV3.4 (Table 3.7). All the progeny from the cross between ST47-6 and VJ72 had a wavy rhizoid phenotype. Therefore, UV3.4, ST47-6 and VJ72 form a complementation group. Altogether, this suggests that the nonsense mutation of UV3.4 in Mp*NEK* causes the wavy rhizoid phenotype.

Parent 1	Parent 2	Wavy rhizoid	Straight rhizoid	Total F1	Genetic distance (cM)
UV3.4	ST47-6	156	0	156	0
VJ72	ST47-6	236	0	236	0

Table 3.13: Complementation assays between UV3.4, ST47-6 and VJ72.

Both the mutations in VJ72 and UV3.4 highlight Mp*NEK* as a new gene regulating tip-growth. The phenotype of all three mutants is qualitatively similar in that they form wavy rhizoids of WT diameter, but its penetrance differs between the mutant lines (Figure 7.6 B and Figure 7.6 G-H). Indeed, ST47-6 and VJ72 have a larger coefficient of variation in rhizoid sinuosity than UV3.4 ($Cv_{ST47\text{-}6}$ =39%,Cv_{VJ72} = 8% ; $Cv_{UV3.4}$ =3%), showing that the wavy rhizoid phenotype of ST47-6 and VJ72 is less penetrant than that of UV3.4 .

The effect of the mutations on Mp*NEK* function remains to be investigated in all three mutant lines. Because of the early stop codon in UV3.4, it is likely that UV3.4 is a *nek* loss-of-function mutant. Because of the T-DNA insertion in the promoter region of

MpNEK (Figure 3.7 A), expression of Mp*NEK* is likely to be altered in VJ72. Finally, TAIL PCR in ST47-6 failed to identify any T-DNA insertion at or near the Mp*NEK* locus that could perturb Mp*NEK* function. In the event that there is a T-DNA insertion with a non-functional hygromycin cassette at the Mp*NEK* locus, quantitative PCR would be sufficient to test if ST47-6 is an overexpressing line. However, the causative mutation could be a deletion and whole genome sequencing of ST47-6 would be more informative in this case.

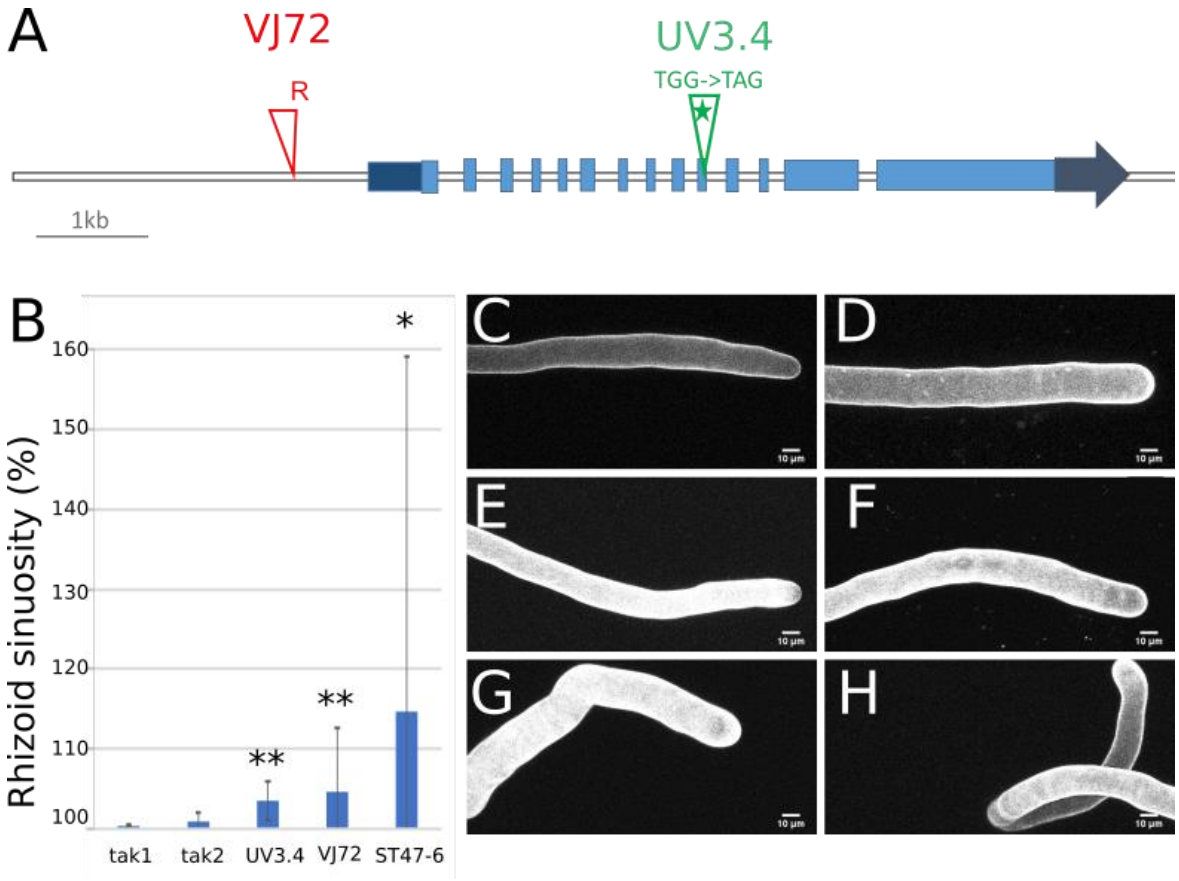

Figure 3.7: Wavy rhizoids phenotype of *nek* mutant lines. Tak1 tak2 3.4. A: Schematic representation of *MpNEK* gene model. UTR regions are represented in dark blue, CDS in light blue. The TPX2 domain spans across the 3 exon represented in brown. VJ72 T-DNA insertion site is indicated in red with the Right border orientation marked with R. UV3.4 early stop codon is indicated by a green star. **B:** Mean rhizoid 3D sinuosity from 10 mature rhizoids. Error bars indicate +/- 1 SD. Single or double stars indicate a Benjamini-Hochberg adjusted p-value from non-parametric Dunn test lower than 0.05 and 0.01 respectively. **C-H:** Mature rhizoids of tak1 (C), tak2 (D), UV3.4 (E), VJ72 (F). Weakly wavy (G) and strongly wavy mature rhizoid of ST47-6 (H).

*3.4.9 UV5.36 has a nonsense mutation in Mp*KLCR

To identify the causative mutation in UV5.36, I applied the non-allelism based mutation discovery pipeline (Table 3.14). Out of 129 049 total mismatches, only 3 were non-synonymous mutations consistent with the UV mutation signature and specific to UV5.36. Of those, only 1 caused an early stop codon and the gene mutated is a homolog of *KINESIN LIGHT CHAIN RELATED* proteins of *Arabidopsis thaliana* (Appendix A9). The nonsense mutation at the *MpKLCR* locus in UV5.36 was validated by Sanger sequencing. Whether the nonsense mutation in Mp*KLCR* is indeed the causative mutation remains to be investigated.

Mutated gene model	**Arabidopsis homolog**	**Annotation of Arabidopsis homolog**	**Type of mutation**
Mp1881s1040	AT4G1084/KLCR1	Kinesin light chain related protein	nonsense
Mp1231s1230	AT1G66320	E3 ubiquitin protein ligase like	missense
Mp3617s1170	No hit	NA	missense

Table 3.14: Complementation assays between UV3.4, ST47-6 and VJ72.

*3.4.10 UV5.5 has no mutation in Mp*WDL *ORF*

To test whether the causative mutations in UV mutant lines of the Mp*WDL* complementation group (Table 3.5) are in the coding sequence of Mp*WDL*, the Mp*WDL* open reading frame was cloned from UV5.5 and sequenced by Sanger sequencing. Surprisingly, no mutation was found compared to tak1 and tak2 ORFs.

3.5 Discussion

3.5.1 Microtubule dynamics regulate tip-growth stability in land plants

Microtubules control tip-growth stability in tip-growing cells of flowering plants and mosses. Reducing microtubule dynamics, either pharmacologically or by disrupting the function of MAP genes, results in unstable tip-growth (Bibikova, Blancaflor, and Gilroy 1999; Schwuchow, Sack, and Hartmann 1990; Hiwatashi, Sato, and Doonan 2014). Here, I show that rhizoids grown on medium supplemented with a drug that inhibit microtubule polymerisation destabilize tip-growth in the liverwort *Marchantia polymorpha*. This shows that microtubules control tip-growth stability in liverworts in addition to mosses and flowering plants. While the most parsimonious interpretation would be that the mechanism controlling microtubule-mediated tip-growth stability is conserved throughout land plants, different mechanisms may have originated independently in several lineages.

The organization of the microtubule cytoskeleton in tip-growing cells of mosses differs substantially from that of flowering plants. Indeed, microtubules are abundant in the apical dome of caulonema cells in mosses, while the apical dome of root hairs and pollen tubes in flowering plants lacks such a prominent microtubule array (Sieberer et al. 2005; Eng and Wasteneys 2014; Hiwatashi, Sato, and Doonan 2014). By comparison, the abundance of microtubules in the apical dome of growing rhizoids in *Marchantia polymorpha* shows that the organisation of the microtubule cytoskeleton in liverworts resembles more that of mosses than that of angiosperms. Assuming that liverworts and mosses are paraphyletic and that liverworts are sister to the stomatophytes (Qiu et al. 2006), this suggests that the presence of microtubules in the apical dome represents an ancestral state of the organization of the microtubule cytoskeleton in tip-growing cells of land plants.

In *Physcomitrella patens*, *kinid1a;kinid1b* double mutants impaired in the formation of the apical microtubule structure form wavy caulonema cells (Hiwatashi, Sato, and Doonan 2014). This suggests that the apical microtubule structure that characterize tip-growing cells of mosses is required to stabilize tip-growth in mosses. Because microtubule-mediated tip-growth stability in flowering plants does not require this bryophyte specific organisation of the microtubule cytoskeleton, it follows that the mechanism that stabilizes tip-growth stability is at least partially different from that of mosses and liverworts. However, to elucidate the evolutionary origin, or origins, of microtubule-mediated tip-growth stability in land plants, one must consider the conservation of function of genes controlling microtubule-mediated tip-growth stability in each lineage.

3.5.2 wdl *mutants suggest a role of microtubule array orientation in tip-growth stability in* Marchantia polymorpha

Promoting microtubule array orientation may be required for microtubule-mediated tip-growth stability in both root hairs and rhizoids. In *Arabidopsis* thaliana, a mutation in the motor domain of the ARM domain kinesin-like gene *MORPHOGENESIS OF ROOT HAIR2* (*MRH2*) causes the formation of wavy and bifurcating root hairs (Yang et al. 2007). In mature root hair of *mrh2-3* mutants, microtubules are more randomly organised (*i.e.* more isotropic). In addition to *mrh2-3*, the *mor1-1* temperature sensitive mutant, forms wavy root hairs and cortical microtubules are misaligned in diffuse growing cells (Whittington et al. 2001). While the phenotype of the microtubule cytoskeleton in growing root hairs of these mutants was not characterised, the correlation of wavy and bifurcating root hairs with the misalignment of cortical microtubules in non-growing root hairs and diffuse growing cells may suggest that microtubule array orientation may

promote tip-growth stability in root hairs. Moreover, the homolog of MOR1 in tobacco, TMBP200 was shown to promote microtubule bundling (Yasuhara et al. 2002), further suggesting that microtubule bundling might participate to the formation of a parallel-arranged longitudinal array of microtubules required to control tip-growth stability.

Here, I identified Mp*WDL* as a gene regulating tip-growth stability in *Marchantia polymorpha*. WAVE DAMPENED2 LIKE proteins form a land plants specific MAP family that promote microtubule bundling *in vitro* and regulate anisotropic growth in *Arabidopsis thaliana* root and light-grown hypocotyl epidermal cell by promoting the longitudinal orientation of the cortical microtubule array (Perrin et al. 2007; X. Liu et al. 2013; Sun, Ma, and Mao 2015). In *Arabidopsis thaliana,* WDL homologs have not been characterised in the context of tip-growth. In *Marchantia polymorpha,* the loss-of-function mutant line *wdl-2* forms wavy rhizoids and exhibits microtubule misalignment in the shank of growing rhizoids: While microtubules are oriented longitudinally in the shank of WT rhizoids, they are more randomly oriented in *wdl-2.* This suggests that the function of WDL proteins in promoting the longitudinal orientation of microtubules may be conserved in cylindrical cells of land plants.

With respect to tip-growth stability, the functional relevance of the longitudinal orientation of microtubules in the shank of tip-growing cells is unclear. By analogy with the microtubule-microfibrils of cellulose alignment paradigm inferred from diffuse growing cells (reviewed in (L. Lei et al. 2014)), longitudinally oriented cortical microtubules are likely to prevent axial growth from taking place in the shank. It is however difficult to understand how axial growth in the shank would result in the wavy rhizoid phenotype of *wdl-2*. I speculate that the disorganisation of microtubules in the shank might perturb indirectly the number and the orientation of microtubules extending in the apical dome of *wdl-2* growing rhizoids. Detailed characterization of the

microtubule phenotype in the apical dome of *wdl-2* growing rhizoids will be required to further investigate the plausible cause of *wdl-2* rhizoid waviness.

3.5.3 nek *mutants suggest a role of microtubule instability in microtubule-mediated tip-growth stability in* Marchantia polymorpha

Promoting microtubule instability may also be a common requirement to stabilize tip-growth in rhizoids and root hairs. In *Arabidopsis thaliana* root hairs, the ARMADILLO REPEAT KINESIN protein *At*ARK1 binds preferentially to the plus-end of growing microtubules and stabilizes tip-growth by promoting catastrophe events and microtubule shrinkage (Eng and Wasteneys 2014). As a result, large endoplasmic microtubule bundles are observed to form in the apical dome of *ark1* root hairs (Eng and Wasteneys 2014). By comparison, in WT plants, bundling of endoplasmic microtubules is typically restricted to the shank of root hairs and only a few highly dynamic microtubules protrude in the apical dome. Moreover, root hairs treated with the microtubule stabilizing drug taxol have a wavy morphology or bifurcate (Bibikova, Zhigilei, and Gilroy 1997). Taken together, this suggests that excessive microtubule stability in the apical dome impairs tip-growth stability. Consistently, lower polymerization rates of endoplasmic microtubules are observed in *ark1* root hairs. Eng et al (2014) proposed that ARK1 may indirectly promote microtubule polymerization by increasing the concentration of free tubulin dimers available for polymerisation. Ultimately, in this model, *At*ARK1 would promote the dynamic instability behaviour of microtubules in root hairs and act to maintain a population of microtubules growing toward the apical dome.

In this study, I identified Mp*NEK* as a gene regulating tip-growth stability in *Marchantia polymorpha* rhizoids. NIMA RELATED KINASE proteins represent a family of MAP

with kinase activity conserved in eukaryotes (O'Connell, Krien, and Hunter 2003). In *Arabidopsis thaliana, At*NEK6 is proposed to prevent the formation of epidermal cell bulging by phosphorylating beta-tubulin and promoting cortical microtubule destabilization (Motose et al. 2011). If the biochemical function of NEK proteins is conserved between land plants, *Mp*NEK may be required for microtubule-mediated tip-growth stability by preventing excessive microtubule stability in growing rhizoids. Testing this hypothesis will require to characterize microtubule dynamics in growing rhizoids of WT and *nek* loss-of-function mutant lines.

*3.5.4 Nonsense mutation in Mp*KLCR *might hint at a role of microtubule-based transport in microtubule-mediated tip-growth stability*

A delicate balance between microtubule bundling and microtubule instability appears to be at play in stabilizing tip-growth in both flowering plants and liverworts. Conceptually, bundling in the shank and dynamic instability in the apical dome could allow to maintain a population of microtubules growing toward the apical membrane and repeatedly targeting polarity markers and/or polar growth effectors. In the fission yeast, the MAP tip1p recruits to the plus-end of growing cytoplasmic microtubules a pair of proteins that effectively link apical plasma-membrane anchored proteins with the actin polymerization machinery, ultimately polarizing the vesicle flow to the site of polar growth (Sieberer, Timmers, and Emons 2005). The localisation of tip1p to the growing plus-ends of endoplasmic microtubules requires the kinesin-like protein tea2p and loss-of-function mutants in either tip1p or its targeting kinesin tea2p exhibit curved cell morphologies and ectopic sites of growth. This so-called tea model of tip-growth in fission yeast is analogous to a hypothetical model where longitudinally arranged endoplasmic

microtubules polymerize toward the apical dome to target polarity markers and/or effectors in plant tip-growing cells.

While neither tip1p nor tea2p have clear homologs in *Arabidopsis thaliana*, an analogous mechanism might possibly participate to tip-growth in plants. Here, I identified a mutant in *Marchantia polymorpha* that has a nonsense mutation in a homolog of KINESIN LIGHT CHAIN (KLC) proteins. In animals, KLC proteins recruit cargo, including protein complexes, to kinesin motor proteins (Verhey, Kaul, and Soppina 2011). While the function of KLC related (KLCR) proteins in plants is unknown, the possibility that the wavy rhizoid phenotype in the mutant line UV5.36 is caused by the nonsense mutation in *Mp*KLCR is certainly intriguing because it would be consistent with a role of microtubule-based transport in tip-growth stability as observed in the fission yeast. First and for all, that the nonsense mutation in Mp*KLCR* causes the wavy rhizoid phenotype of UV5.36 of course remains to be confirmed by complementing the UV5.36 line with Mp*KLCR*.

3.5.5 Concluding remarks

In conclusion, none of the MAPs known to control microtubule-mediated tip-growth stability in *Arabidopsis thaliana* and *Physcomitrell patens* were identified from this mutant screen. However, two different MAPs, *Mp*WDL and *Mp*NEK, were found to control tip-growth stability and likely control the same aspects of microtubule behaviour, based on functional inference from homologous proteins in *Arabidopsis thaliana* and preliminary functional characterization in *Marchantia polymorpha*.

This neither fully supports nor fully invalidates the hypothesis of a common origin of the mechanism controlling microtubule-mediated tip-growth stability in land plants. Indeed,

the mutant screen was likely not saturated and the causative mutation in the vast majority of mutants remains to be identified, leaving open the possibility that *Mp*ARK , *Mp*Kinid and *Mp*MOR1 might also control tip-growth stability in *Marchantia polymorpha*. And inversely, in *Arabidopsis thaliana*, *NEK* and *WDL* gene families are multigenic, leaving open the possibility that functional redundancy has prevented the discovery of their putative role in tip-growth stability in root hairs and pollen tubes.

Chapter 4: General discussion

During the colonization of land, plants have innovated new microtubule cytoskeleton organizations that control specific aspects of cell division and cell differentiation proposed to represent adaptions to living on land (Pickett-heaps et al. 1999; Buschmann and Zachgo 2016; Oda 2015). In chapter 2, I show that a substantial subset of the microtubule-associated proteins (MAP) repertoire regulating microtubule dynamics and the organization of the cortical microtubule array in *Arabidopsis thaliana* originated during the course of streptophyte evolution. Building on these results, I propose that MAP orthogroups that originated during the course of streptophyte evolution exemplify two complementary evolutionary trends: i) innovation of a new MAP orthogroup or ii) recruitment of a preexisting MAP orthogroup to control new organizations of microtubule arrays. As an example of the former evolutionary trend, the MIDD1 orthogroup originates in the LCA of flowering plants and, in *Arabidopsis thaliana,* MIDD1 controls the formation of vessel elements, which are an innovation of flowering plants. In example of the latter evolutionary trend, the MAP70 orthogroup predates the origin of tracheophytes and MAP70 proteins control the formation of tracheary elements in *Arabidopsis thaliana*.

The development of filamentous cells with rooting functions is a ubiquitous characteristic of land plants. It represents an adaptation to living on land in that filamentous rooting cells provide anchorage to the substratum, and water and nutrient uptake (V. a S. Jones and Dolan 2012). Recent studies indicate that part of the gene regulatory network controlling the formation of filamentous rooting cells is conserved between liverworts and flowering plants. Namely, the family of RSL transcription factors controls the formation of root hairs in flowering plants and the formation of rhizoids in bryophytes

(Menand et al. 2007; Proust et al. 2016; Jang et al. 2011; Masucci and Schiefelbein 1994). In addition, genes orthologous to those controlling vesicular trafficking and cell wall biogenesis in root hairs are likely to share the same function in rhizoids in *Marchantia polymorpha*, as suggested by similarities in the morphological phenotype of the corresponding mutants (Honkanen et al. 2016). Altogether, this suggests that a conserved genetic module controls the formation of filamentous rooting cells and the mechanism of cell expansion in these cells.

However, the evolutionary origin of one aspect of the mechanism controlling tip-growth in rhizoids and root hairs is still unclear: namely, the role of microtubules in stabilizing the position of the growing region in tip-growing cells. Pharmacological studies in flowering plants and mosses suggest that finely tuned microtubules dynamics are required to control the spatial stability of the growth point in tip-growing cells in both phyla (Bibikova, Blancaflor, and Gilroy 1999; Schwuchow, Sack, and Hartmann 1990; Hiwatashi, Sato, and Doonan 2014). In chapter 3, I show that the organization of the microtubule cytoskeleton in the apical dome of *Marchantia polymorpha* rhizoids differs from that of root hairs in flowering plants. While the microtubule cytoskeleton in the apical dome of growing root hairs is typically limited to a few endoplasmic microtubules, I observed an abundance of endoplasmic microtubules in the apical dome of growing *Marchantia polymorpha* rhizoids. The recent report of a similar microtubule cytoskeleton organization in the tip-growing caulonema cells of *Physcomitrella patens* (Hiwatashi, Sato, and Doonan 2014) suggests that it represents a bryophyte plesiomorphy. In *Physcomitrella patens*, *kinid1a;kinidab* double mutants in which the formation of this apical microtubule structure is impaired form wavy caulonema cells (Hiwatashi, Sato, and Doonan 2014). This further suggests that this bryophyte specific organization of the microtubule cytoskeleton in the apical dome of tip-growing cells plays a role in

microtubule-mediated tip-growth stability. It would follow that the different organization of the microtubule cytoskeleton of root hairs on one side, and of rhizoids and caulonema cells on the other is indicative of a different mechanism controlling microtubule-mediated tip-growth stability in mosses and flowering plants.

In flowering plants, the mechanism controlling microtubule-mediated tip-growth stability relies on the function of two MAPs. *At*ARK1 and *At*MOR1 stabilize tip-growth, possibly by regulating the dynamic behavior of microtubules and the organization of the microtubule cytoskeleton respectively (Eng and Wasteneys 2014; Whittington et al. 2001; Kawamura and Wasteneys 2008). In chapter 3, I report the identification of 2 new genes regulating tip-growth stability in the liverwort *Marchantia polymorpha*: Mp*WDL* and Mp*NEK*. Similarly to ARK1 and MOR1, NEK and WDL proteins are MAPs and respectively promote microtubule instability and microtubule orientation in *Arabidopsis thaliana* (Motose et al. 2011; X. Liu et al. 2013; Sun, Ma, and Mao 2015). In growing rhizoids, *Mp*WDL was found to localize to microtubules with a bias towards microtubules in the shank rather than in the apical dome. In *Arabidopsis thaliana,* the microtubule bundling and stabilizing activity of WDL proteins is sufficient to promote longitudinal orientation of the cortical microtubule array in hypocotyl and root epidermal cells (X. Liu et al. 2013; Perrin et al. 2007). Consistently, microtubules in the shank of growing rhizoids were arranged more randomly in *wdl-2* compared to WT and the microtubule array had a less pronounced longitudinal orientation. This suggests that Mp*WDL* may promote tip-growth stability in growing rhizoids in a similar way than MOR1 promotes tip-growth stability in growing root hairs in *Arabidopsis thaliana.* While the function of Mp*NEK* in controlling microtubule dynamics remains unknown, it may function similarly to NEK homologs in *Arabidopsis thaliana* and promote microtubule instability

(Motose et al. 2011). Were it so, Mp*NEK* would then execute a similar function than *At*ARK1 in controlling tip-growth stability by promoting microtubule instability.

Altogether, distinct MAP toolkits have been identified to control microtubule-mediated tip-growth stability in *Arabidopsis thaliana*, *Physcomitrella patens* and *Marchantia polymorpha*. The genome of *Marchantia polymorpha* includes two *ARK* and one MOR1 homologous genes; yet, no *ark* or *mor1* mutant was identified from the T-DNA or the UV mutant screen. Such a negative result must be taken with much precaution. Indeed, despite having screened 336 000 T-DNA mutant lines and 120 000 UV mutagenized plants, neither screens is likely to be saturating and the causative mutation in the majority of wavy rhizoid mutants remains to be investigated. Similarly, WDL and NEK proteins have not been implicated with tip-growth in *Arabidopsis thaliana*. Again, the fact that no such function has been reported must be taken with much precaution. The higher number of gene copies in *WDL* and *NEK* orthogroups in *Arabidopsis thaliana* and overlapping patterns of expression could result in functional redundancy and explain why *wdl* and *nek* mutants with impaired tip-growth stability have not yet been identified in *Arabidopsis thaliana*.

With these limitations in mind, one might still want to speculate on the evolutionary implications carried by the observation of distinct MAP genetic toolkit controlling microtubule-mediated tip-growth stability. The function of WDL and NEK proteins in stabilizing tip-growth might be specific to *Marchantia polymorpha* rhizoids, and that of ARK1 and MOR1 be specific to *Arabidopsis thaliana* root hairs. If it is the case, this would suggest that different mechanisms control microtubule-mediated stability in liverworts and flowering plants. In animals, the example of immune cells provides an interesting analogy (reviewed in (Peter and Davidson 2011)). While the function of homologous transcription factors controlling the formation of immune cells in mammals

and fish is conserved, the downstream effector genes differ, with immunoglobulin receptors in mammals and leucine-rich repeat receptors in lampreys. This is conceptually similar with the case of filamentous rooting cells, which form under the control of a conserved family of transcription factors but would appear to have recruited different effector genes to control tip-growth stability.

To conclude, the results of this thesis are consistent with the view that distinct MAP toolkits control microtubule-mediated tip-growth stability in flowering plants and bryophytes. Future work aiming to compare the function of those MAPs in cross-species studies would test this hypothesis and further our understanding of the evolution of mechanisms that control cell growth and morphogenesis.

Appendix

	Oxford University	Joint Genome Insititute
Estimated genome size	**310 Mb (Nasu, *et al* 1997)**	
Number of scaffolds	**4137**	**2957**
Scaffold N50 (L50)	**0.4 Mb (174)**	**1.4 Mb (54)**
Total assembly length	**206 Mb (12% gap)**	**225.8Mb (6% gap)**
% genome in scaffolds > 50kb	**90.0%**	**93.8%**
Number of predicted-coding genes	**17956**	**19287**
Number of contigs in gametophyte transcriptome	**29453**	**24674**

Appendix A1: Comparison of our *Marchantia polymorpha* genome assemblies with that available on the JGI website. Caution is recommended when comparing the N50 values because the two assemblies used a different cut off for minimal scaffold size, resulting in an inflated N50 value in the case of the JGI assembly. Nonetheless, their assembly appears generally less fragmented and contains fewer gaps.

Appendix A2: Rhizoid-mediated anchorage to the soil of WT (left) and *wdl-3* (right). Four weeks-old gametophytes were transferred on soil and further grown for 8 weeks before being uprooted. The different soil mass associated with the rhizoid system of WT and *wdl-3* illustrates that rhizoids anchor the gametophyte to the substratum and suggests that wavy rhizoids cannot.

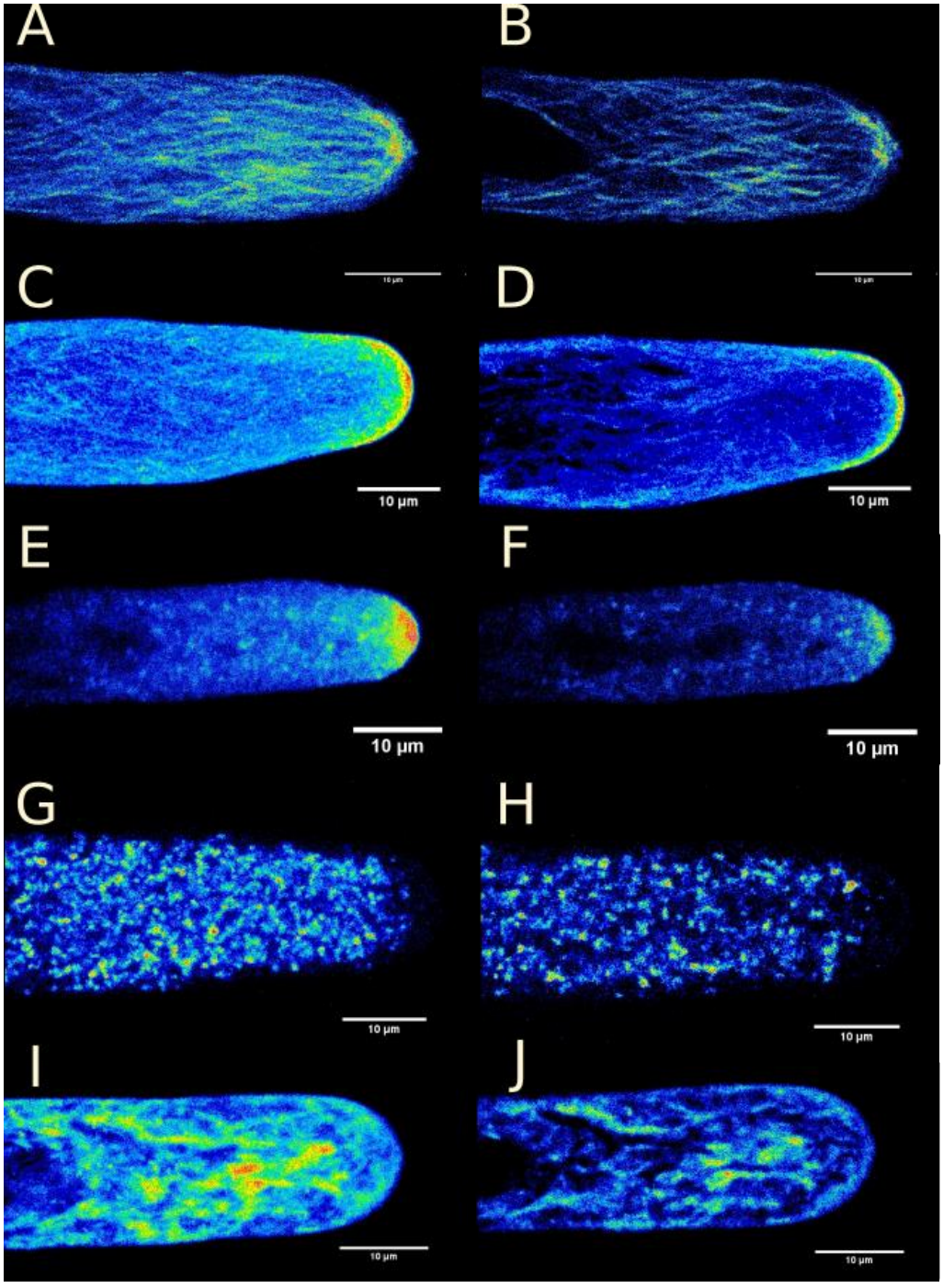

Appendix A3: Cytological organization of growing rhizoids in *Marchantia polymorpha*. Z-maximum projection (**A,C,E,G,I**) and midplane (**B,C,D,F,H,J**) of *proMpEF1a::GFP-MpTUB1* (**A-B),** *proMpWDL::GFP-LifeAct* **(C-D),** *proMpEF1a::YFP-MpRabA4* (**E**-F), *proMpEF1a::YFP-MpSYP6a* (**G-H**) and *pro35S::YFP-HDEL* growing rhizoids. Colour code corresponds to 16 colours scale.

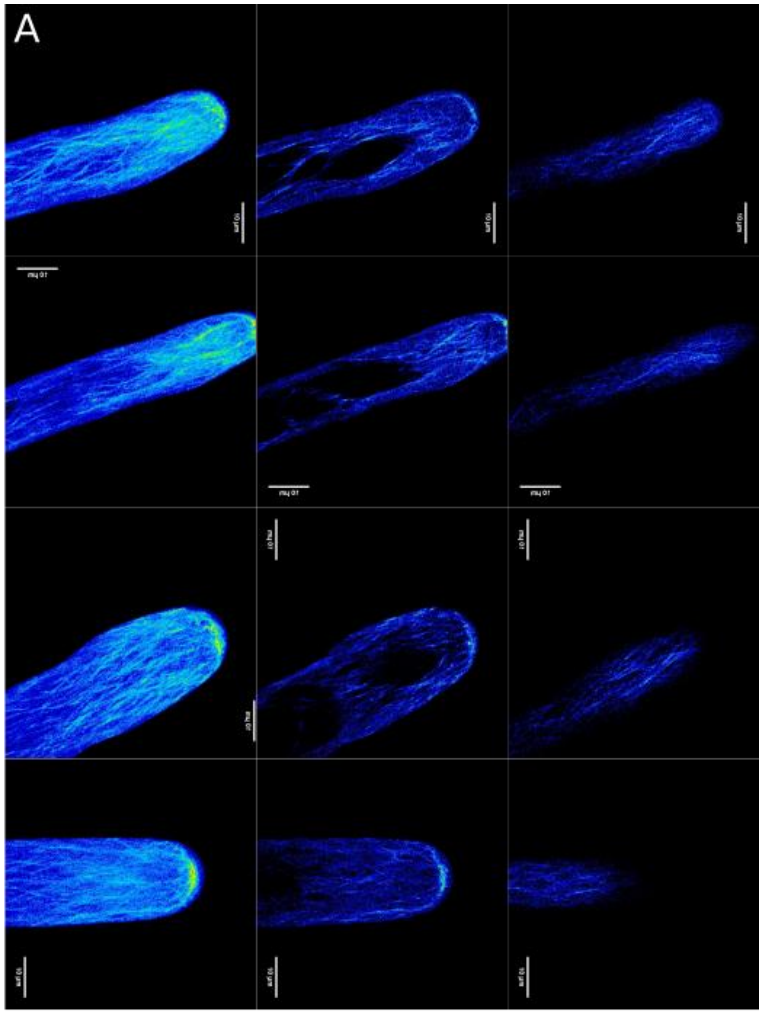

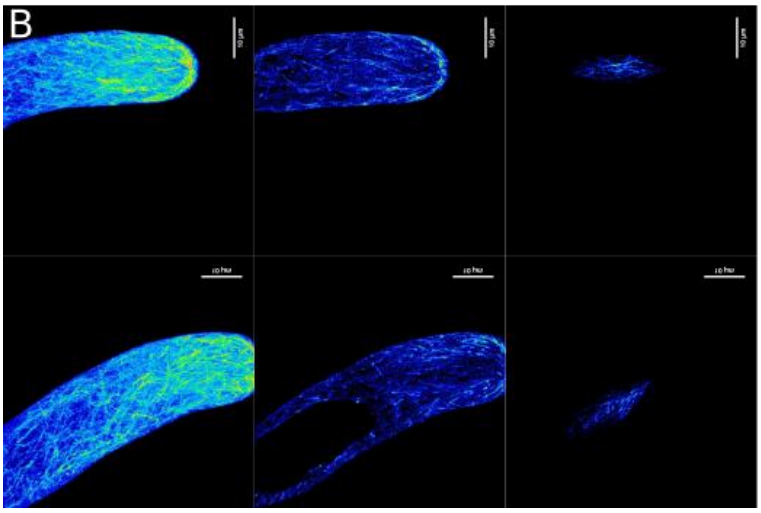

Appendix A4: Microtubule cytoskeleton of WT and *wdl-2* horizontal growing rhizoids. From left to right: Z-maximum projection, midplane and cortical plane of *proMpEF1a::GFP-MpTUB1* growing rhizoids in WT (**A**) and *wdl-2* (**B**) backgrounds.. Colour code corresponds to 16 colours scale.

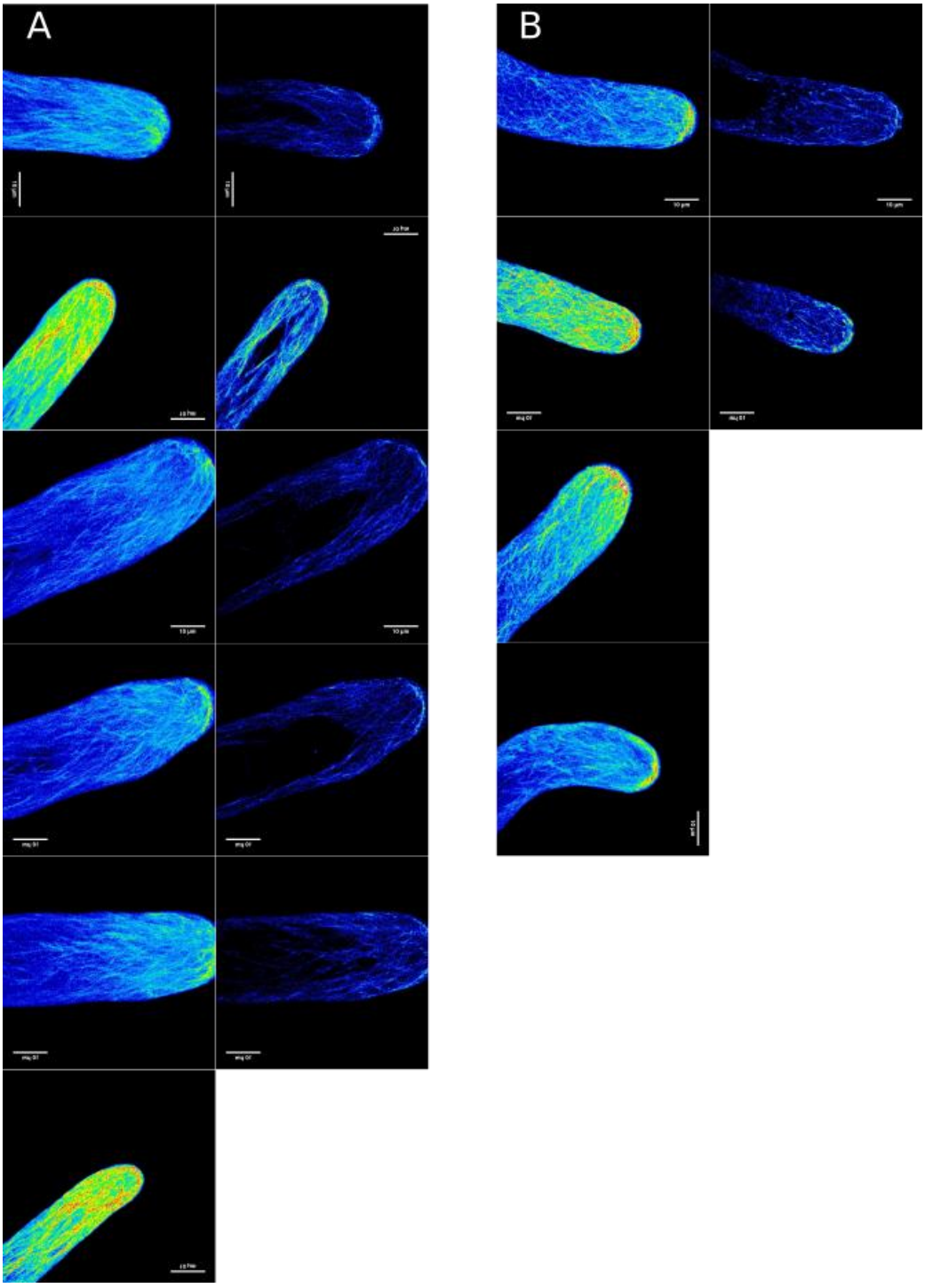

Appendix A5: Microtubule cytoskeleton of WT and *wdl-2* tilted growing rhizoids. From left to right : Z-maximum projection and midplane of *proMpEF1a::GFP-MpTUB1* growing rhizoids in WT (**A**) and *wdl-2* (**B**) backgrounds.. Colour code corresponds to 16 colours scale.

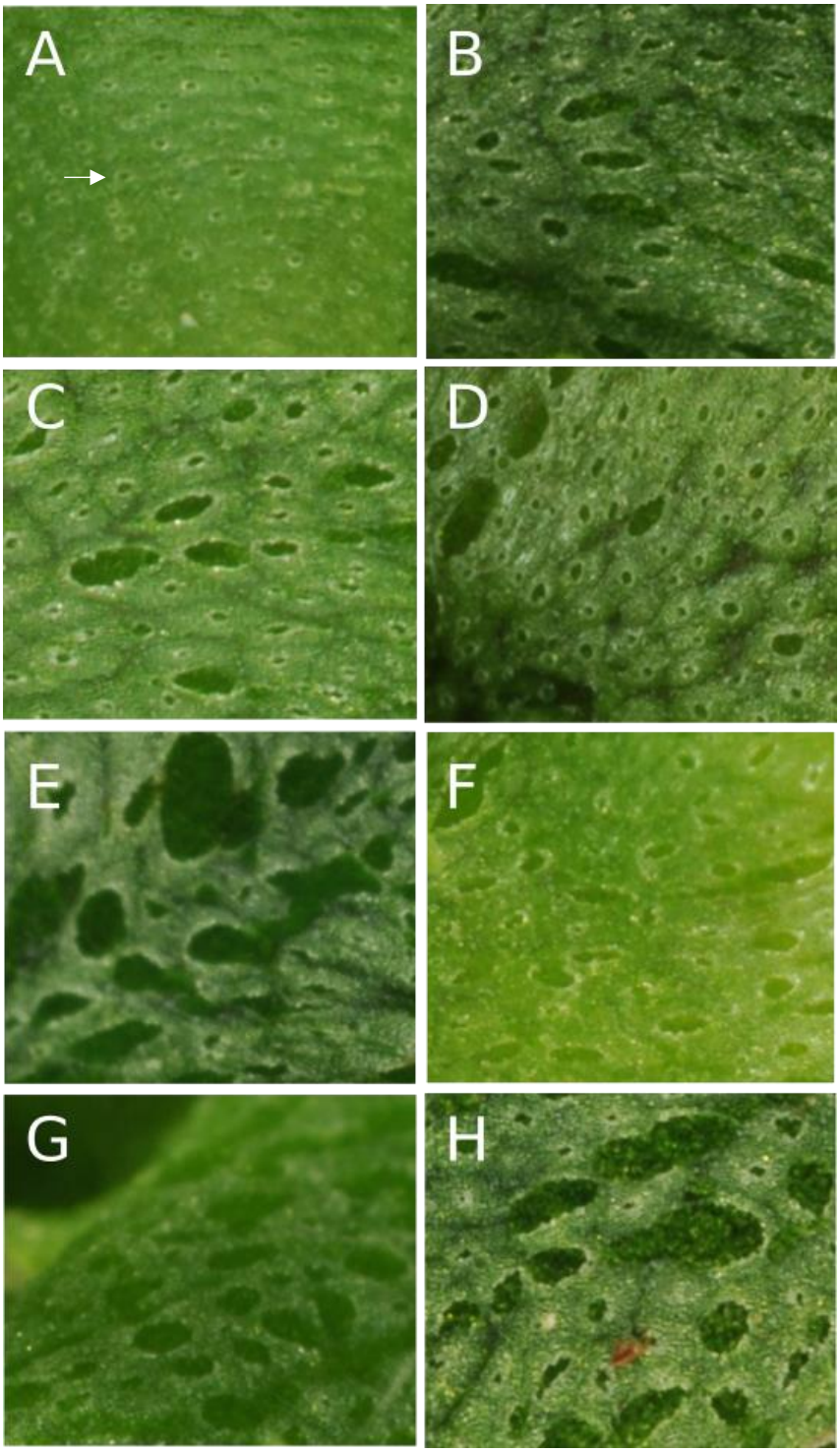

Appendix A6: Dorsal epidermis phenotype of two month-old gametophyte. Tak1 (**A**), *ren-1* (**B**), UV4.31 (**C**), UV4.32 (**D**), UV4.34 (**E**), UV6.3 (**F**), UV6.8 (**G**) and UV5.28 (**H**). The dorsal epidermis shows air pores (A, arrowed), which in mutants (B-D) are stretched.

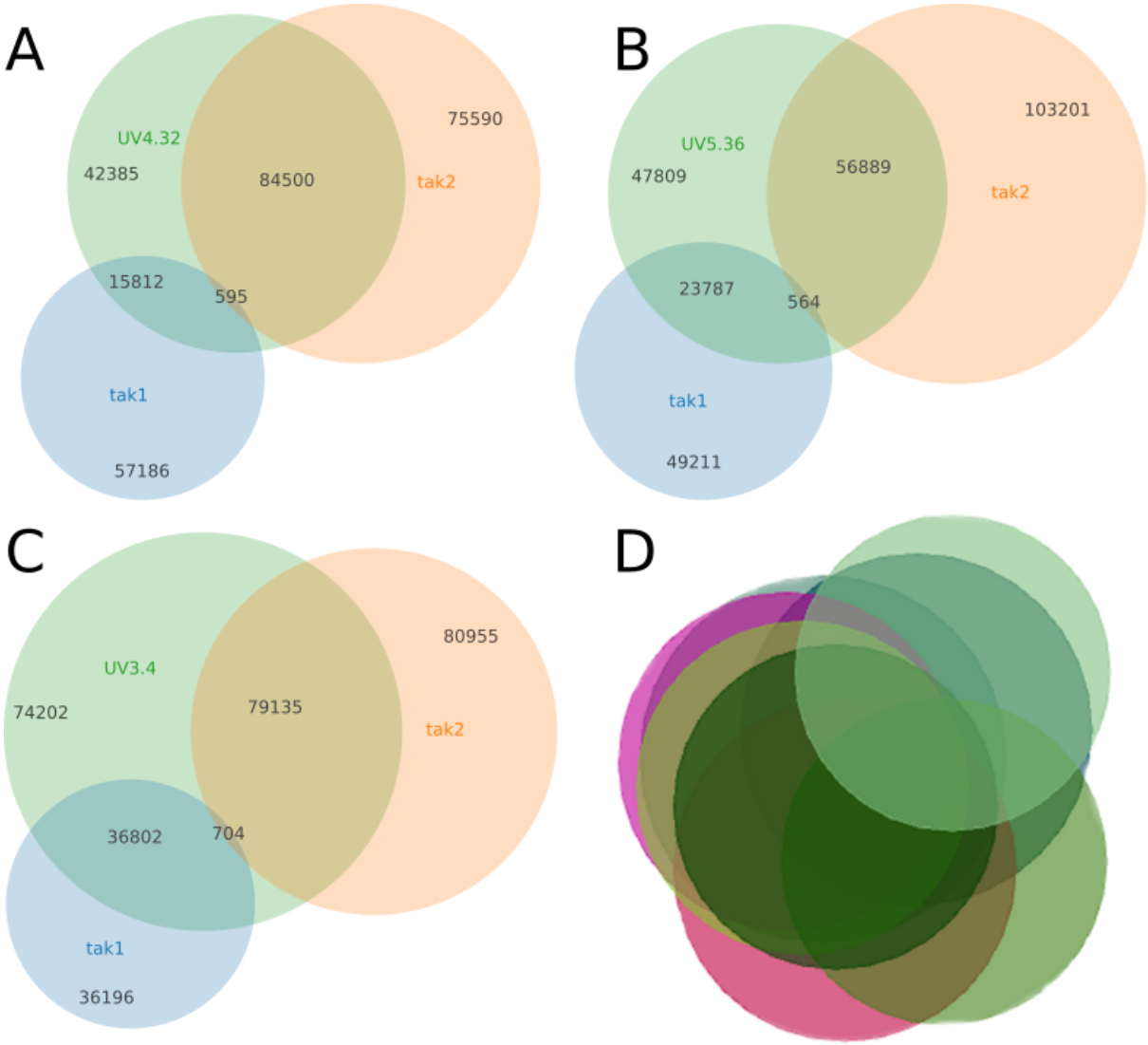

Appendix A7: Overlap between the pools of total mismatches in tak1, tak2 and UV mutants. **A:** UV4.32 compared to tak1 and tak2. **B:** UV5.36 compared to tak1 and tak2. C**:** UV3.4 compared to tak1 and tak2. **D:** non-allelic subtracting UV mutagenized backgrounds compared with each other.

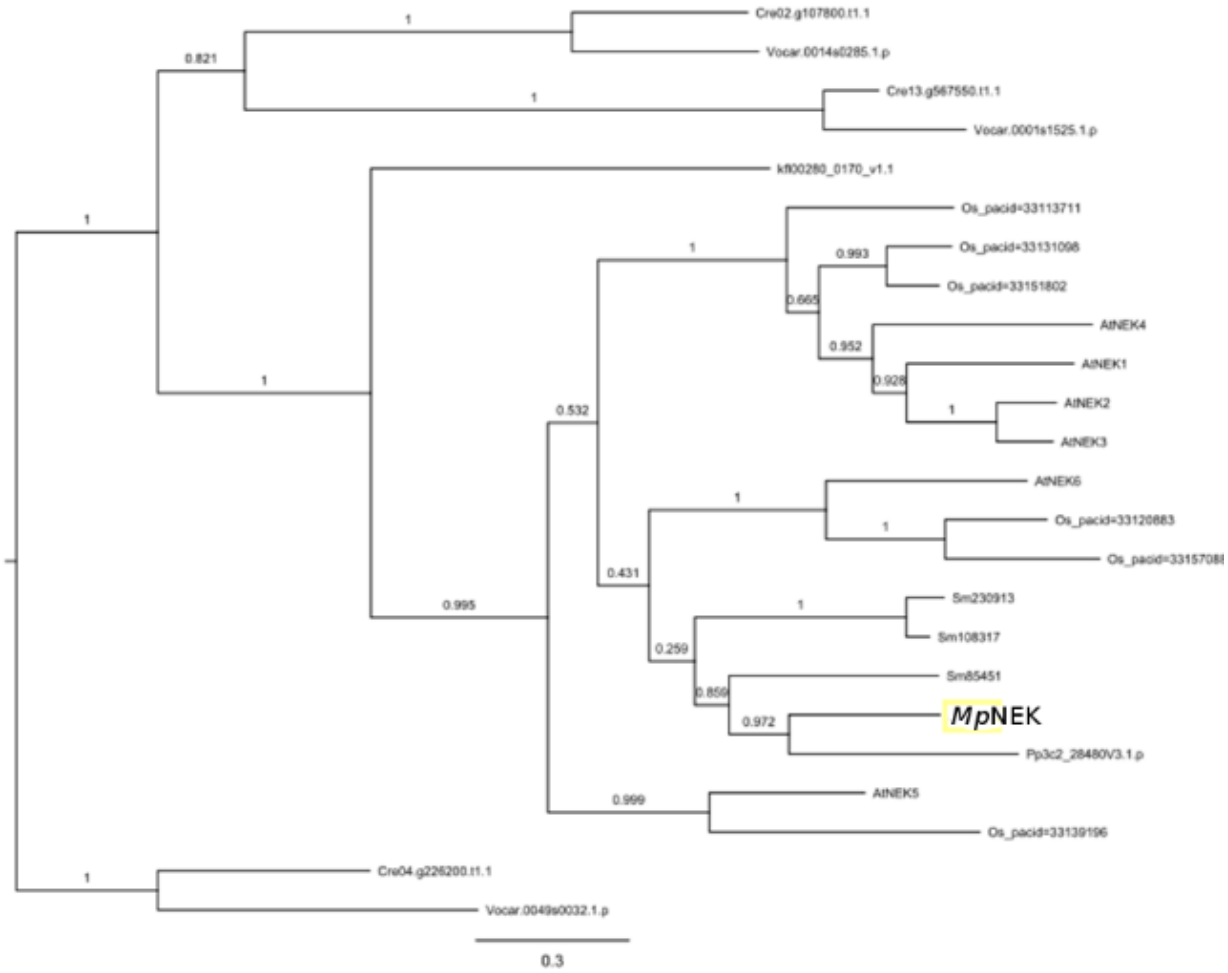

Appendix A8: Phylogenetic tree inferred from full-protein alignment of the NEK orthogroup. The tree is rooted with NEK proteins of chlorophytic algae. Branch support is shown as p-value from SH test.

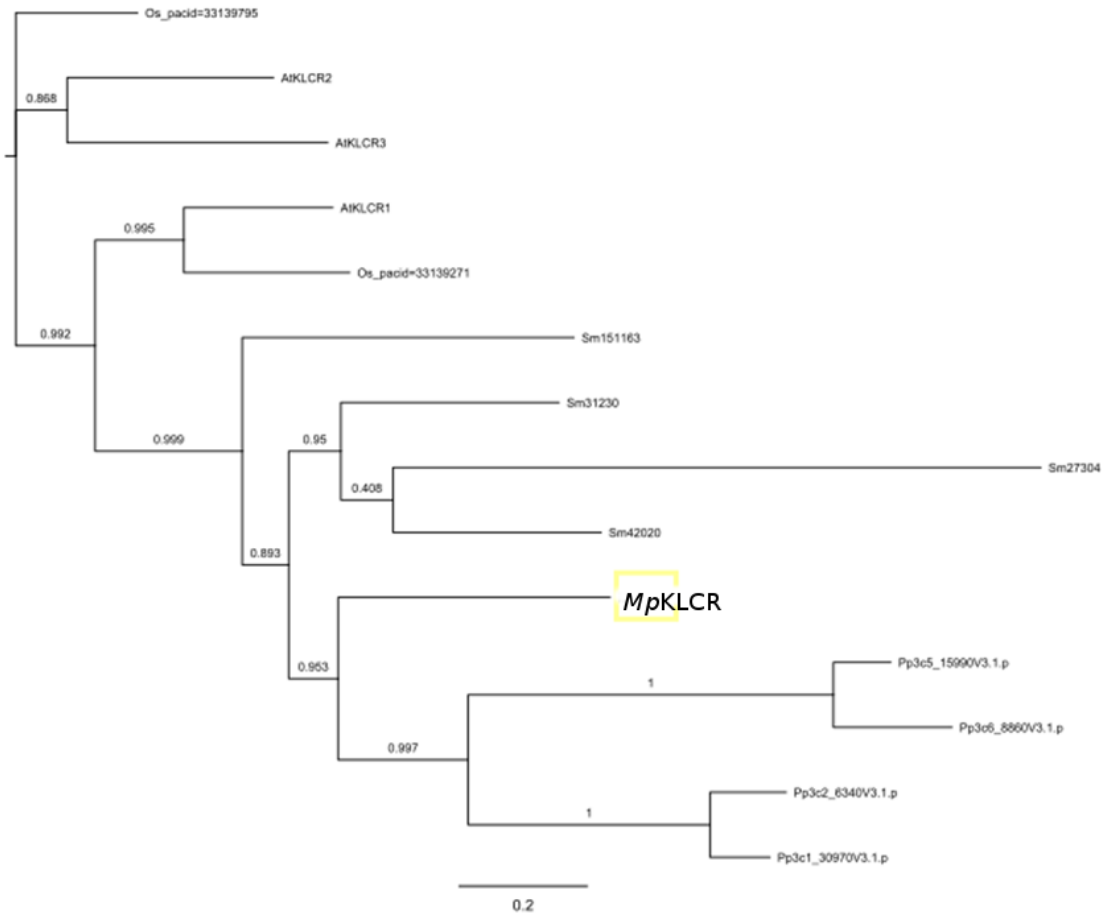

Appendix A9: Phylogenetic tree inferred from full-protein alignment of the KLCR orthogroup. The tree is unrooted. Branch support is shown as p-value from SH test.

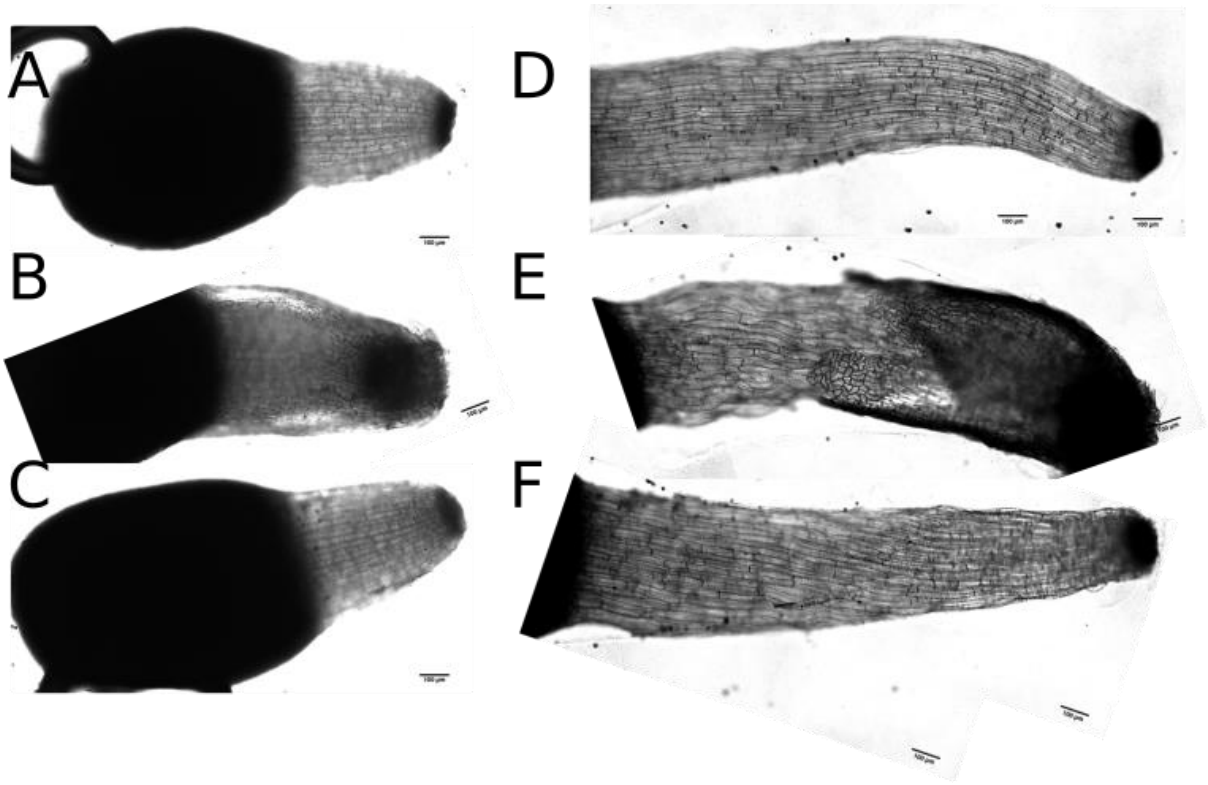

Appendix A9 (preliminary data): Sporophyte elongation phenotype of WT, *wdl-2 -/- and* WDL^{GOF-1} -/-. Immature sporophytes of WT (**A**), *wdl-2 -/-* (**B**) and WDL^{GOF-1} -/- (**C**) were dissected out of archegoniophores and placed in imaging chambers described in 3.3.5. After 14h in constant light, the elongation of the seta was observed.

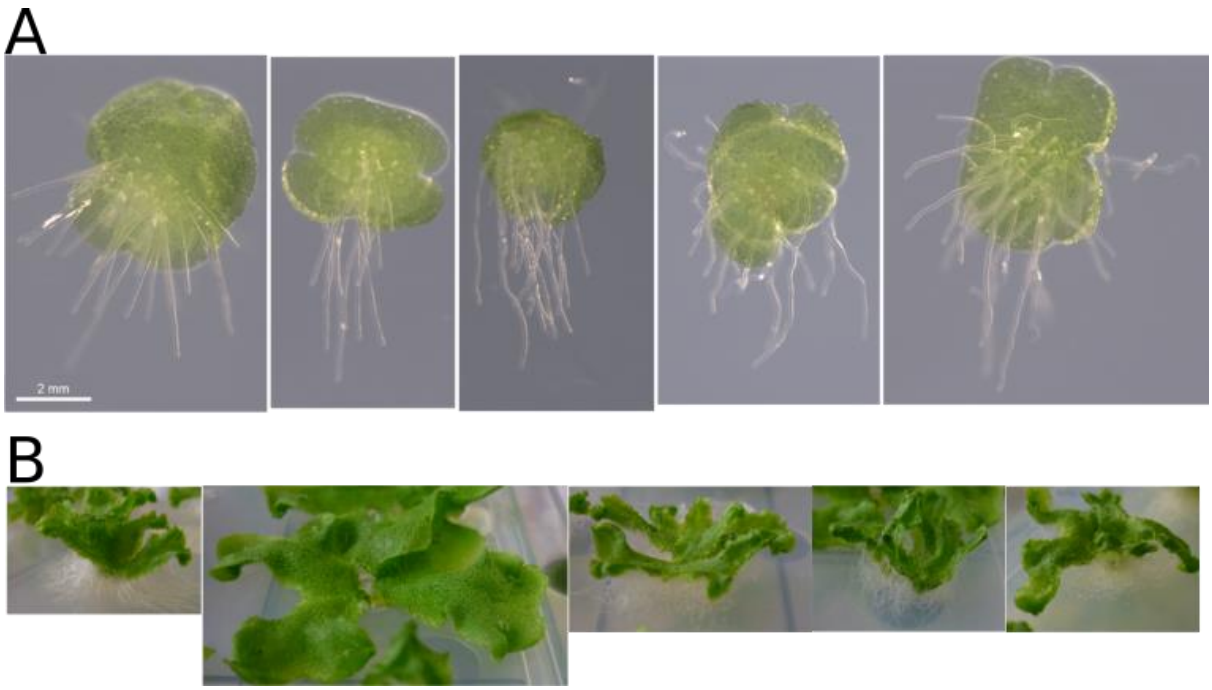

Appendix A10 (preliminary data): Response of *wdl* to light conditions. A: rhizoids from gemmae are negatively phototropic in (from left to right) tak1, *WDLGOF-1*, *wdl-1*, *wdl-2*, *wdl-3*. Plates were grown horizontally and wrapped in black cardboard paper to only let through light that came from one side, here from top side of the picture. **B**: three weeks-old thallus etiolation phenotype of (from left to right) tak1, *WDLGOF-1*, *wdl-1*, *wdl-2*, *wdl-3*. All genotypes investigated formed narrow thallus branches that grew upward; this is the typical etiolation phenotype. By contrast, *WDLGOF-1* formed a thallus of normal width that grew horizontal; this is the typical non-etiolating phenotype.

References

Al-Bassam, Jawdat, Hwajin Kim, Gary Brouhard, Antoine van Oijen, Stephen C. Harrison, and Fred Chang. 2010. “CLASP Promotes Microtubule Rescue by Recruiting Tubulin Dimers to the Microtubule.” *Developmental Cell* 19 (2). Elsevier Ltd: 245–58. doi:10.1016/j.devcel.2010.07.016.

Ambrose, Chris, Jun F. Allard, Eric N. Cytrynbaum, and Geoffrey O. Wasteneys. 2011. “A CLASP-Modulated Cell Edge Barrier Mechanism Drives Cell-Wide Cortical Microtubule Organization in Arabidopsis.” *Nature Communications* 2 (May). Nature Publishing Group: 430. doi:10.1038/ncomms1444.

Ambrose, Chris, and Geoffrey O Wasteneys. 2014. “Microtubule Initiation from the Nuclear Surface Controls Cortical Microtubule Growth Polarity and Orientation in Arabidopsis Thaliana.” *Plant & Cell Physiology* 0 (0): 1–10. doi:10.1093/pcp/pcu094.

Ambrose, J. C., T. Shoji, A. M. Kotzer, J. A. Pighin, and G. O. Wasteneys. 2007. “The Arabidopsis CLASP Gene Encodes a Microtubule-Associated Protein Involved in Cell Expansion and Division.” *The Plant Cell* 19 (9): 2763–75. doi:10.1105/tpc.107.053777.

Anderhag, P., P. K. Hepler, and M. D. Lazzaro. 2000. “Microtubules and Microfilaments Are Both Responsible for Pollen Tube Elongation in the Conifer Picea Abies (Norway Spruce).” *Protoplasma* 214 (3–4): 141–57. doi:10.1007/BF01279059.

Ayaz, Pelin, Sarah Munyoki, Elisabeth A. Geyer, Felipe Andrés Piedra, Emily S. Vu, Raquel Bromberg, Zbyszek Otwinowski, Nick V. Grishin, Chad A. Brautigam, and Luke M. Rice. 2014. “A Tethered Delivery Mechanism Explains the Catalytic Action of a Microtubule Polymerase.” *eLife* 3: e03069. doi:10.7554/eLife.03069.

Ayaz, Pelin, Xuecheng Ye, Patrick Huddleston, Chad a Brautigam, and Luke M Rice. 2012. “A TOG : Aβ-Tubulin Complex Structure Reveals Conformation-Based Mechanisms for a Microtubule Polymerase.” *Science* 337 (6096): 857–60. doi:10.1126/science.1221698.

Baluška, František, Ján Salaj, Jaideep Mathur, Markus Braun, Fred Jasper, Josef Šamaj, Nam-

Hai Chua, Peter W Barlow, and Dieter Volkmann. 2000. “Root Hair Formation: F-Actin-Dependent Tip Growth Is Initiated by Local Assembly of Profilin-Supported F-Actin Meshworks Accumulated within Expansin-Enriched Bulges.” *Developmental Biology* 227 (2): 618–32. doi:10.1006/dbio.2000.9908.

Bashline, Logan, Lei Lei, Shundai Li, and Ying Gu. 2014. “Cell Wall, Cytoskeleton, and Cell Expansion in Higher Plants.” *Molecular Plant* 7 (4). The Authors. All rights reserved.: 586–600. doi:10.1093/mp/ssu018.

Bhaskara, Govinal Badiger, Tuan-Nan Wen, Thao Thi Nguyen, and Paul E Verslues. 2017. “Protein Phosphatase 2Cs and Microtubule-Associated Stress Protein 1 Control Microtubule Stability, Plant Growth, and Drought Response.” *The Plant Cell* 29 (1): 169–91. doi:10.1105/tpc.16.00847.

Bibikova, Tatiana N., Elison B. Blancaflor, and Simon Gilroy. 1999. “Microtubules Regulate Tip Growth and Orientation in Root Hairs of Arabidopsis Thaliana.” *Plant Journal* 17 (6): 657–65. doi:10.1046/j.1365-313X.1999.00415.x.

Bibikova, Tatiana N., Angelica Zhigilei, and Simon Gilroy. 1997. “Root Hair Growth in Arabidopsis Thaliana Is Directed by Calcium and an Endogenous Polarity.” *Planta* 203 (4): 495–505. doi:10.1007/s004250050219.

Bichet, Adeline, Thierry Desnos, Simon Turner, Olivier Grandjean, and Herman Höfte. 2001. “BOTERO1 Is Required for Normal Orientation of Cortical Microtubules and Anisotropic Cell Expansion in Arabidopsis.” *Plant Journal* 25 (2): 137–48. doi:10.1046/j.1365-313X.2001.00946.x.

Bloch, Daria, Meirav Lavy, Yael Efrat, Idan Efroni, Keren Bracha-Drori, Mohamad Abu-Abied, Einat Sadot, and Shaul Yalovsky. 2005. “Ectopic Expression of an Activated RAC in Arabidopsis Disrupts Membrane Cycling.” *Molecular Biology of the Cell* 16 (8): 1–13. doi:10.1091/mbc.E04.

Bosch, Maurice, Alice Y Cheung, and Peter K Hepler. 2005. “Pectin Methylesterase, a Regulator of Pollen Tube Growth.” *Plant Physiology* 138 (3): 1334–46. doi:10.1104/pp.105.059865.nor.

Bosch, Maurice, and Peter K Hepler. 2005. “Pectin Methylesterases and Pectin Dynamics in Pollen Tubes.” *The Plant Cell* 17 (12): 3219–26. doi:10.1105/tpc.105.037473.

Bradski, G. n.d. “No Title.” *Dr. Dobb’s Journal of Software Tools*.

Burk, D H, B Liu, R Q Zhong, W H Morrison, and Z H Ye. 2001. “A Katanin-like Protein Regulates Normal Cell Wall Biosynthesis and Cell Elongation.” *Plant Cell* 13 (4): 807–27. #.

Burkart, Graham M, Tobias I Baskin, and Magdalena Bezanilla. 2015. “A Family of ROP Proteins That Suppresses Actin Dynamics, and Is Essential for Polarized Growth and Cell Adhesion.” *Journal of Cell Science* 128 (14): 2553–64. doi:10.1242/jcs.172445.

Buschmann, Henrik, Michael Holtmannsp??tter, Agnes Borchers, Martin Timothy O’Donoghue, and Sabine Zachgo. 2016. “Microtubule Dynamics of the Centrosome-like Polar Organizers from the Basal Land Plant Marchantia Polymorpha.” *New Phytologist* 209 (3): 999–1013. doi:10.1111/nph.13691.

Buschmann, Henrik, and Sabine Zachgo. 2016. “The Evolution of Cell Division: From Streptophyte Algae to Land Plants.” *Trends in Plant Science* 21 (10). Elsevier Ltd: 872–83. doi:10.1016/j.tplants.2016.07.004.

Cannon, Maura C, Kimberly Terneus, Qi Hall, Li Tan, Yumei Wang, Benjamin L Wegenhart, Liwei Chen, Derek T A Lamport, Yuning Chen, and Marcia J Kieliszewski. 2008. “Self-Assembly of the Plant Cell Wall Requires an Extensin Scaffold.” *Proceedings of the National Academy of Sciences* 105 (6): 2226–31. doi:10.1073/pnas.0711980105.

Catarino, Bruno, Alexander J. Hetherington, David M. Emms, Steven Kelly, and Liam Dolan. 2016. “The Stepwise Increase in the Number of Transcription Factor Families in the

Precambrian Predated the Diversification of Plants on Land." *Molecular Biology and Evolution* 33 (11): 2815–19. doi:10.1093/molbev/msw155.

Chan, J., C. G. Jensen, L. C. Jensen, M. Bush, and C. W. Lloyd. 1999. "The 65-kDa Carrot Microtubule-Associated Protein Forms Regularly Arranged Filamentous Cross-Bridges between Microtubules." *Proceedings of the National Academy of Sciences of the United States of America* 96 (26): 14931–36. doi:10.1073/pnas.96.26.14931.

Chebli, Youssef, Minako Kaneda, Rabah Zerzour, and Anja Geitmann. 2012. "The Cell Wall of the Arabidopsis Pollen Tube--Spatial Distribution, Recycling, and Network Formation of Polysaccharides." *Plant Physiology* 160 (4): 1940–55. doi:10.1104/pp.112.199729.

Chen, Liangliang, Yuancheng Peng, Juan Tian, Xiaohong Wang, Zhaosheng Kong, Tonglin Mao, Ming Yuan, and Yunhai Li. 2016. "TCS1, a Microtubule-Binding Protein, Interacts with KCBP/ZWICHEL to Regulate Trichome Cell Shape in Arabidopsis Thaliana." *PLoS Genetics* 12 (10): 1–21. doi:10.1371/journal.pgen.1006266.

Chen, Tong, Nianjun Teng, Xiaoqin Wu, Yuhua Wang, Wei Tang, Jozef Šamaj, František Baluška, and Jinxing Lin. 2007. "Disruption of Actin Filaments by Latrunculin B Affects Cell Wall Construction in Picea Meyeri Pollen Tube by Disturbing Vesicle Trafficking." *Plant and Cell Physiology* 48 (1): 19–30. doi:10.1093/pcp/pcl036.

Cheung, Alice Y., and Hen-ming Wu. 2008. "Structural and Signaling Networks for the Polar Cell Growth Machinery in Pollen Tubes." *Annual Review of Plant Biology* 59 (1): 547–72. doi:10.1146/annurev.arplant.59.032607.092921.

Cho, Hyung-Taeg, and Daniel J Cosgrove. 2002. "Regulation of Root Hair Initiation and Expansin Gene Expression in Arabidopsis." *The Plant Cell* 14 (12): 3237–53. doi:10.1105/tpc.006437.

Cleveland, William S. 1979. "Robust Locally Weighted Regression and Smoothing Scatterplots." *Journal of the American Statistical Association* 74 (368): 829–36.

doi:10.2307/2286407.

Cosgrove, Daniel J., Lian Chao Li, Hyung Taeg Cho, Susanne Hoffmann-Benning, Richard C. Moore, and Douglas Blecker. 2002. “The Growing World of Expansins.” *Plant and Cell Physiology* 43 (12): 1436–44. doi:10.1093/pcp/pcf180.

Cosgrove, Daniel J, Patricia Bedinger, and Daniel M Durachko. 1997. “Group I Allergens of Grass Pollen as Cell Wall-Loosening Agents.” *Proceedings of the National Academy of Sciences* 94 (12): 6559–64. doi:10.1073/pnas.94.12.6559.

Damme, Daniël Van, Kris Van Poucke, Emmanuel Boutant, Christophe Ritzenthaler, Dirk Inzé, and Danny Geelen. 2004. “In Vivo Dynamics and Differential Microtubule-Binding Activities of MAP65 Proteins.” *Plant Physiology* 136 (4): 3956–67. doi:10.1104/pp.104.051623.

De Bodt, Stefanie, Steven Maere, and Yves Van De Peer. 2005. “Genome Duplication and the Origin of Angiosperms.” *Trends in Ecology and Evolution* 20 (11): 591–97. doi:10.1016/j.tree.2005.07.008.

de Graaf, Barend H J, Alice Y Cheung, Tatyana Andreyeva, Kathryn Levasseur, Marcia Kieliszewski, and Hen-ming Wu. 2005. “Rab11 GTPase-Regulated Membrane Trafficking Is Crucial for Tip-Focused Pollen Tube Growth in Tobacco.” *The Plant Cell* 17 (9): 2564–79. doi:10.1105/tpc.105.033183.

Demkiv, O.T., E.L. Kordyum, O.R. Kardash, and O.Ya. Khorkavtsiv. 1999. “Gravitropism and Phototropism in Protonemata of the Moss Pohlia Nutans (Hedw.) Lindb.” *Advances in Space Research* 23 (12): 1999–2004. doi:10.1016/S0273-1177(99)00349-X.

Derksen, J., T. Rutten, I. K. Lichtscheidl, A. H N de Win, E. S. Pierson, and G. Rongen. 1995. “Quantitative Analysis of the Distribution of Organelles in Tobacco Pollen Tubes: Implications for Exocytosis and Endocytosis.” *Protoplasma* 188 (3–4): 267–76. doi:10.1007/BF01280379.

Dimitrov, A., M. Quesnoit, S. Moutel, I. Cantaloube, C. Pous, and F. Perez. 2008. “Detection of GTP-Tubulin Conformation in Vivo Reveals a Role for GTP Remnants in Microtubule Rescues.” *Science* 322 (5906): 1353–56. doi:10.1126/science.1165401.

Drevensek, S., M. Goussot, Y. Duroc, a. Christodoulidou, S. Steyaert, E. Schaefer, E. Duvernois, et al. 2012. “The Arabidopsis TRM1-TON1 Interaction Reveals a Recruitment Network Common to Plant Cortical Microtubule Arrays and Eukaryotic Centrosomes.” *The Plant Cell* 24 (1): 178–91. doi:10.1105/tpc.111.089748.

Dumais, Jacques. 2013. “Modes of Deformation of Walled Cells.” Article. *Journal of Experimental Botany* 64 (15): 4681–95. doi:10.1093/jxb/ert268.

Dumais, Jacques, Sidney L. Shaw, Charles R. Steele, Sharon R. Long, and Peter M. Ray. 2006. “An Anisotropic-Viscoplastic Model of Plant Cell Morphogenesis by Tip Growth.” *International Journal of Developmental Biology* 50 (2–3): 209–22. doi:10.1387/ijdb.052066jd.

Emms, David M., and Steven Kelly. 2015. “OrthoFinder: Solving Fundamental Biases in Whole Genome Comparisons Dramatically Improves Orthogroup Inference Accuracy.” *Genome Biology* 16 (1). Genome Biology: 157. doi:10.1186/s13059-015-0721-2.

Emons, Anne Mie C, and Niek van Maaren. 1987. “Helicoidal Cell-Wall Texture in Root Hairs.” *Planta* 170 (2): 145–51. doi:10.1007/BF00397882.

Endler, Anne, Christopher Kesten, René Schneider, Yi Zhang, Alexander Ivakov, Anja Froehlich, Norma Funke, and Staffan Persson. 2015. “A Mechanism for Sustained Cellulose Synthesis during Salt Stress.” *Cell* 162 (6): 1353–64. doi:10.1016/j.cell.2015.08.028.

Eng, Ryan Christopher, and Geoffrey O Wasteneys. 2014a. “The Microtubule plus-End Tracking Protein ARMADILLO-REPEAT KINESIN1 Promotes Microtubule Catastrophe in Arabidopsis.” *The Plant Cell* 26 (8): 3372–86. doi:10.1105/tpc.114.126789.

———. 2014b. “The Microtubule plus-End Tracking Protein ARMADILLO-REPEAT KINESIN1 Promotes Microtubule Catastrophe in Arabidopsis.” *The Plant Cell* 26 (8): 3372–86. doi:10.1105/tpc.114.126789.

Esseling, J J. 2003. “Nod Factor-Induced Root Hair Curling: Continuous Polar Growth towards the Point of Nod Factor Application.” *Plant Physiol* 132 (4): 1982–88. doi:10.1104/pp.103.021634.

Etzold, Helmut. 1965. “Der Polarotropismus Und Phototropismus Der Chloronemen von Dryopteris Filix Mas (L.) Schott.” *Planta* 64 (3): 254–80. doi:10.1007/BF00394953.

Fache, V., J. Gaillard, D. Van Damme, D. Geelen, E. Neumann, V. Stoppin-Mellet, and M. Vantard. 2010. “Arabidopsis Kinetochore Fiber-Associated MAP65-4 Cross-Links Microtubules and Promotes Microtubule Bundle Elongation.” *The Plant Cell* 22 (11): 3804–15. doi:10.1105/tpc.110.080606.

Foissner, Ilse, Franz Grolig, and Gerhard Obermeyer. 2002. “Reversible Protein Phosphorylation Regulates the Dynamic Organization of the Pollen Tube Cytoskeleton: Effects of Calyculin A and Okadaic Acid.” *Protoplasma* 220 (1–2): 1–15. doi:10.1007/s00709-002-0032-9.

Furt, Fabienne, Kyle Lemoi, Erkan Tüzel, and Luis Vidali. 2012. “Quantitative Analysis of Organelle Distribution and Dynamics in Physcomitrella Patens Protonemal Cells.” *BMC Plant Biology* 12 (1): 70. doi:10.1186/1471-2229-12-70.

Galway, M E, J W Heckman, and J W Schiefelbein. 1997. “Growth and Ultrastructure of Arabidopsis Root Hairs: The rhd3 Mutation Alters Vacuole Enlargement and Tip Growth.” *Planta* 201 (2): 209–18. doi:10.1007/BF01007706.

Gardiner, John. 2013. “The Evolution and Diversification of Plant Microtubule-Associated Proteins.” *Plant Journal* 75 (2): 219–29. doi:10.1111/tpj.12189.

Hartman, J. J., and Ronald D. Vale. 1999. “Microtubule Disassembly by ATP-Dependent

Oligomerization of the AAA Enzyme Katanin." *Science* 286 (5440): 782–85. doi:10.1126/science.286.5440.782.

Hashimoto, Takashi. 2015. "Microtubules in Plants." *The Arabidopsis Book* 13: e0179. doi:10.1199/tab.0179.

Held, Michael A., Li Tan, Abdolreza Kamyabi, Michael Hare, Elena Shpak, and Marcia J. Kieliszewski. 2004. "Di-Isodityrosine Is the Intermolecular Cross-Link of Isodityrosine-Rich Extensin Analogs Cross-Linked in Vitro." *Journal of Biological Chemistry* 279 (53): 55474–82. doi:10.1074/jbc.M408396200.

Hiwatashi, Yuji, Yoshikatsu Sato, and John H Doonan. 2014. "Kinesins Have a Dual Function in Organizing Microtubules during Both Tip Growth and Cytokinesis in Physcomitrella Patens." *The Plant Cell* 26 (3): 1256–66. doi:10.1105/tpc.113.121723.

Honkanen, Suvi, Victor A.S. Jones, Giulia Morieri, Clement Champion, Alexander J. Hetherington, Steve Kelly, Hélène Proust, Denis Saint-Marcoux, Helen Prescott, and Liam Dolan. 2016. "The Mechanism Forming the Cell Surface of Tip-Growing Rooting Cells Is Conserved among Land Plants." *Current Biology*, 3238–44. doi:10.1016/j.cub.2016.09.062.

Hwang, Jae-Ung, Ying Gu, Yong-Jik Lee, and Zhenbiao Yang. 2005. "Oscillatory ROP GTPase Activation Leads the Oscillatory Polarized Growth of Pollen Tubes." *Molecular Biology of the Cell* 16 (November): 5385–99. doi:10.1091/mbc.E05.

Hwang, Jae-Ung, Guang Wu, An Yan, Yong-Jik Lee, Claire S Grierson, and Zhenbiao Yang. 2010. "Pollen-Tube Tip Growth Requires a Balance of Lateral Propagation and Global Inhibition of Rho-Family GTPase Activity." *Journal of Cell Science* 123 (Pt 3): 340–50. doi:10.1242/jcs.039180.

Ishizaki, Kimitsune, Ryuichi Nishihama, Minoru Ueda, Keisuke Inoue, Sakiko Ishida, Yoshiki Nishimura, Toshiharu Shikanai, and Takayuki Kohchi. 2015. "Development of Gateway

Binary Vector Series with Four Different Selection Markers for the Liverwort Marchantia Polymorpha." *PLoS ONE* 10 (9): 1–13. doi:10.1371/journal.pone.0138876.

Ito, Kanako, Junling Ren, and Tomomichi Fujita. 2014. "Conserved Function of Rho-Related Rop/RAC GTPase Signaling in Regulation of Cell Polarity in Physcomitrella Patens." *Gene* 544 (2). Elsevier B.V.: 241–47. doi:10.1016/j.gene.2014.04.057.

Jang, Geupil, Keke Yi, Nuno D Pires, Benoît Menand, and Liam Dolan. 2011. "RSL Genes Are Sufficient for Rhizoid System Development in Early Diverging Land Plants." Article. *Development* 138 (11): 2273–81. doi:10.1242/dev.060582.

Jauh, GuangYuh, and ElizabethM. Lord. 1996. "Localization of Pectins and Arabinogalactan-Proteins in Lily (Lilium Longiflorum L.) Pollen Tube and Style, and Their Possible Roles in Pollination." *Planta* 199 (2): 251–61. doi:10.1007/BF00196566.

Jenkins, G I, and D J Cove. 1983. "Phototropism and Polarotropism of Primary Chloronemata of the Moss Physcomitrella Patens: Responses of the Wild-Type." *Planta* 158 (4): 357–64. doi:10.1007/BF00397338.

Jiang, Lixi, Shu-lan Yang, Li-fen Xie, Ching San Puah, Xue-qin Zhang, and Wei-cai Yang. 2005. "VANGUARD1 Encodes a Pectin Methylesterase That Enhances Pollen Tube Growth in the Arabidopsis Style and Transmitting Tract" 17 (February): 584–96. doi:10.1105/tpc.104.027631.2.

Jones, Mark A, Jun-Jiang Shen, Ying Fu, Hai Li, Zhenbiao Yang, and Claire S Grierson. 2002. "The Arabidopsis Rop2 GTPase Is a Positive Regulator of Both Root Hair Initiation and Tip Growth." *The Plant Cell* 14 (April): 763–76. doi:10.1105/tpc.010359.

Jones, Victor a S, and Liam Dolan. 2012. "The Evolution of Root Hairs and Rhizoids." Article. *Annals of Botany* 110 (2): 205–12. doi:10.1093/aob/mcs136.

Kang, Erfang, Mingzhi Zheng, Yan Zhang, Ming Yuan, Shaul Yalovsky, Lei Zhu, and Ying Fu. 2017. *The Microtubule-Associated Protein MAP18 Affects ROP2 GTPase Activity during*

Root Hair Growth. *Plant Physiology*. doi:10.1104/pp.16.01243.

Kawamura, E., and G. O. Wasteneys. 2008. "MOR1, the Arabidopsis Thaliana Homologue of Xenopus MAP215, Promotes Rapid Growth and Shrinkage, and Suppresses the Pausing of Microtubules in Vivo." *Journal of Cell Science* 121 (24): 4114–23. doi:10.1242/jcs.039065.

Ke, Danxia, Xiangyong Li, Yapeng Han, Lin Cheng, Hongyu Yuan, and Lei Wang. 2016. "ROP6 Is Involved in Root Hair Deformation Induced by Nod Factors in Lotus Japonicus." *Plant Physiology and Biochemistry* 108. Elsevier Masson SAS: 488–98. doi:10.1016/j.plaphy.2016.08.015.

Keech, O., E. Pesquet, L. Gutierrez, A. Ahad, C. Bellini, S. M. Smith, and P. Gardestrom. 2010. "Leaf Senescence Is Accompanied by an Early Disruption of the Microtubule Network in Arabidopsis." *Plant Physiology* 154 (4): 1710–20. doi:10.1104/pp.110.163402.

Ketelaar, T., M. E. Galway, B. M. Mulder, and A. M C Emons. 2008. "Rates of Exocytosis and Endocytosis in Arabidopsis Root Hairs and Pollen Tubes." *Journal of Microscopy* 231 (2): 265–73. doi:10.1111/j.1365-2818.2008.02031.x.

Kirchhelle, Charlotte, Cheung Ming Chow, Camille Foucart, Helia Neto, York Dieter Stierhof, Monika Kalde, Carol Walton, et al. 2016. "The Specification of Geometric Edges by a Plant Rab GTPase Is an Essential Cell-Patterning Principle During Organogenesis in Arabidopsis." *Developmental Cell* 36 (4): 386–400. doi:10.1016/j.devcel.2016.01.020.

Kollmar, Martin. 2016. "Fine-Tuning Motile Cilia and Flagella: Evolution of the Dynein Motor Proteins from Plants to Humans at High Resolution." *Molecular Biology and Evolution* 33 (12): 3249–67. doi:10.1093/molbev/msw213.

Korolev, Andrey V., Jordi Chan, Mike J. Naldrett, John H. Doonan, and Clive W. Lloyd. 2005. "Identification of a Novel Family of 70 kDa Microtubule-Associated Proteins in Arabidopsis Cells." *Plant Journal* 42 (4): 547–55. doi:10.1111/j.1365-

313X.2005.02393.x.

Korolev, Andrey V, Henrik Buschmann, John H Doonan, and Clive W. Lloyd. 2007. "AtMAP70-5, a Divergent Member of the MAP70 Family of Microtubule-Associated Proteins, Is Required for Anisotropic Cell Growth in Arabidopsis." *J. Cell Sci.* 120 (Pt 13): 2241–47. doi:10.1242/jcs.007393.

Kost, Benedikt, Emmanuel Lemichez, Pius Spielhofer, Yan Hong, Kimberly Tolias, Christopher Carpenter, and Nam-hai Chua. 1999. "Rac Homologues and Compartmentalized Phosphatidylinositol 4,5-Bisphophate Act in a Common Pathway to Refulate Polar Pollen Tube Growth." *The Journal of Cell Biology* 145 (2): 317–30.

Kwasniewski, Miroslaw, and Iwona Szarejko. 2006. "Molecular Cloning and Characterization of B -Expansin Gene Related to Root Hair Formation in Barley." *Plant Physiol.* 141 (July): 1149–58. doi:10.1104/pp.106.078626.).

Lampugnani, Edwin R., Isabel E. Moller, Andrew Cassin, Daniel F. Jones, Poh Ling Koh, Sunil Ratnayake, Cherie T. Beahan, Sarah M. Wilson, Antony Bacic, and Ed Newbigin. 2013. "In Vitro Grown Pollen Tubes of Nicotiana Alata Actively Synthesise a Fucosylated Xyloglucan." *PLoS ONE* 8 (10): 1–10. doi:10.1371/journal.pone.0077140.

Lee, Kieran J D, Yoichi Sakata, Shaio-Lim Mau, Filomena Pettolino, Antony Bacic, Ralph S Quatrano, Celia D Knight, and J Paul Knox. 2005. "Arabinogalactan Proteins Are Required for Apical Cell Extension in the Moss Physcomitrella Patens." *The Plant Cell* 17 (November): 3051–65. doi:10.1105/tpc.105.034413.

Lei, Lei, Shundai Li, Logan Bashline, and Ying Gu. 2014. "Dissecting the Molecular Mechanism Underlying the Intimate Relationship between Cellulose Microfibrils and Cortical Microtubules." *Frontiers in Plant Science* 5 (March): 1–8. doi:10.3389/fpls.2014.00090.

Lei, Ming-Juan, Qi Wang, Xiaolin Li, Aimin Chen, Li Luo, Yajun Xie, Guan Li, et al. 2015.

"The Small GTPase ROP10 of Medicago Truncatula Is Required for Both Tip Growth of Root Hairs and Nod Factor-Induced Root Hair Deformation." *The Plant Cell* 27 (3): 806–22. doi:10.1105/tpc.114.135210.

Li, Hai, Yakang Lin, Rachel M Heath, Michael X Zhu, and Zhenbiao Yang. 1999. "Control of Pollen Tube Tip Growth by a Rop GTPase-Dependent Pathway That Leads to Tip-Localized Calcium Influx." *The Plant Cell* 11 (September): 1731–42. doi:10.1105/tpc.11.9.1731.

Li, Haoge, Baojuan Sun, Michiko Sasabe, Xingguang Deng, Yasunori Machida, Honghui Lin, Y. R. Julie Lee, and Bo Liu. 2017. "Arabidopsis MAP65-4 Plays a Role in Phragmoplast Microtubule Organization and Marks the Cortical Cell Division Site." *New Phytologist* 215 (1): 187–201. doi:10.1111/nph.14532.

Li, J., X. Wang, T. Qin, Y. Zhang, X. Liu, J. Sun, Y. Zhou, et al. 2011. "MDP25, A Novel Calcium Regulatory Protein, Mediates Hypocotyl Cell Elongation by Destabilizing Cortical Microtubules in Arabidopsis." *The Plant Cell* 23 (12): 4411–27. doi:10.1105/tpc.111.092684.

Lin, Changfa, Hee Seung Choi, and Hyung Taeg Cho. 2011. "Root Hair-Specific Expansin A7 Is Required for Root Hair Elongation in Arabidopsis." *Molecules and Cells* 31 (4): 393–97. doi:10.1007/s10059-011-0046-2.

Lin, Deshu, Lingyan Cao, Zhenzhen Zhou, Lei Zhu, David Ehrhardt, Zhenbiao Yang, and Ying Fu. 2013. "Rho GTPase Signaling Activates Microtubule Severing to Promote Microtubule Ordering in Arabidopsis." *Current Biology* 23 (4). Elsevier Ltd: 290–97. doi:10.1016/j.cub.2013.01.022.

Lindeboom, J. J., M. Nakamura, A. Hibbel, K. Shundyak, R. Gutierrez, T. Ketelaar, A. M. C. Emons, B. M. Mulder, V. Kirik, and D. W. Ehrhardt. 2013. "A Mechanism for Reorientation of Cortical Microtubule Arrays Driven by Microtubule Severing." *Science* 342 (6163): 1245533–1245533. doi:10.1126/science.1245533.

Liu, Wei, Ai Min Chen, Li Luo, Jie Sun, Lian Pu Cao, Guan Qiao Yu, Jia Bi Zhu, and Yan Zhang Wang. 2010. “Characterization and Expression Analysis of Medicago Truncatula ROP GTPase Family during the Early Stage of Symbiosis.” *Journal of Integrative Plant Biology* 52 (7): 639–52. doi:10.1111/j.1744-7909.2010.00944.x.

Liu, Xiaomin, Tao Qin, Qianqian Ma, Jingbo Sun, Ziqiang Liu, Ming Yuan, and Tonglin Mao. 2013. “Light-Regulated Hypocotyl Elongation Involves Proteasome-Dependent Degradation of the Microtubule Regulatory Protein WDL3 in Arabidopsis.” *The Plant Cell* 25 (5): 1740–55. doi:10.1105/tpc.113.112789.

Lovy-Wheeler, Alenka, Luis Cárdenas, Joseph G. Kunkel, and Peter K. Hepler. 2007. “Differential Organelle Movement on the Actin Cytoskeleton in Lily Pollen Tubes.” *Cell Motility and the Cytoskeleton* 64 (September 2006): 217–32. doi:10.1002/cm.20181.

Lovy-Wheeler, Alenka, Kathleen L. Wilsen, Tobias I. Baskin, and Peter K. Hepler. 2005. “Enhanced Fixation Reveals the Apical Cortical Fringe of Actin Filaments as a Consistent Feature of the Pollen Tube.” *Planta* 221 (1): 95–104. doi:10.1007/s00425-004-1423-2.

Lucas, Jessica R., Stephanie Courtney, Mathew Hassfurder, Sonia Dhingra, Adam Bryant, and Sidney L. Shaw. 2011. “Microtubule-Associated Proteins MAP65-1 and MAP65-2 Positively Regulate Axial Cell Growth in Etiolated *Arabidopsis* Hypocotyls.” *The Plant Cell* 23 (5): 1889–1903. doi:10.1105/tpc.111.084970.

Lundh, F, M Ellis, and others. 2012. “Python Imaging Library (PIL).” Secret Labs AB,< http://www. pythonware. com/products/pil.

Mandelkow, Eckhard, and Eva Maria Mandelkow. 1995. “Microtubules and Microtubule-Associated Proteins.” *Current Opinion in Cell Biology* 7 (1): 72–81. doi:10.1016/0955-0674(95)80047-6.

Mao, Guojie, Henrik Buschmann, John H Doonan, and Clive W Lloyd. 2006. “The Role of MAP65-1 in Microtubule Bundling during Zinnia Tracheary Element Formation.” *Journal*

of Cell Science 119 (Pt 4): 753–58. doi:10.1242/jcs.02813.

Masucci, J D, and J W Schiefelbein. 1994. “The rhd6 Mutation of Arabidopsis Thaliana Alters Root-Hair Initiation through an Auxin- and Ethylene-Associated Process.” Article. *Plant Physiology* 106 (4): 1335–46. http://www.pubmedcentral.nih.gov/articlerender.fcgi?artid=159671&tool=pmcentrez&rendertype=abstract.

Menand, Benoît, Grant Calder, and Liam Dolan. 2007. “Both Chloronemal and Caulonemal Cells Expand by Tip Growth in the Moss Physcomitrella Patens.” *Journal of Experimental Botany* 58 (7): 1843–49. doi:10.1093/jxb/erm047.

Menand, Benoît, Keke Yi, Stefan Jouannic, Laurent Hoffmann, Eoin Ryan, Paul Linstead, Didier G Schaefer, and Liam Dolan. 2007. “An Ancient Mechanism Controls the Development of Cells with a Rooting Function in Land Plants.” Article. *Science* 316 (5830). American Association for the Advancement of Science: 1477–80. doi:10.1126/science.1142618.

Molendijk, Arthur J., Friedrich Bischoff, Chadalavada S.V. Rajendrakumar, Jiří Friml, Markus Braun, Simon Gilroy, and Klaus Palme. 2001. “Arabidopsis Thaliana Rop GTPases Are Localized to Tips of Root Hairs and Control Polar Growth.” *EMBO Journal* 20 (11): 2779–88. doi:10.1093/emboj/20.11.2779.

Motose, Hiroyasu, Takahiro Hamada, Kaori Yoshimoto, Takashi Murata, Mitsuyasu Hasebe, Yuichiro Watanabe, Takashi Hashimoto, Tatsuya Sakai, and Taku Takahashi. 2011. “NIMA-Related Kinases 6, 4, and 5 Interact with Each Other to Regulate Microtubule Organization during Epidermal Cell Expansion in Arabidopsis Thaliana.” *Plant Journal* 67 (6): 993–1005. doi:10.1111/j.1365-313X.2011.04652.x.

Murata, Takashi, and Masamitsu Wada. 1989. “Organization of Cortical Microtubules and Microfibril Deposition in Response to Blue-Light-Induced Apical Swelling in a Tip-Growing Adiantum Protonema Cell.” *Planta* 178 (3): 334–41. doi:10.1007/BF00391861.

Nakajima, Keiji, Tomomi Kawamura, and Takashi Hashimoto. 2006. “Role of the SPIRAL1 Gene Family in Anisotropic Growth of Arabidopsis Thaliana.” *Plant and Cell Physiology* 47 (4): 513–22. doi:10.1093/pcp/pcj020.

Nakamura, Masayoshi, David W Ehrhardt, and Takashi Hashimoto. 2010. “Microtubule and Katanin-Dependent Dynamics of Microtubule Nucleation Complexes in the Acentrosomal Arabidopsis Cortical Array.” *Nature Cell Biology* 12 (11). Nature Publishing Group: 1064–70. doi:10.1038/ncb2110.

Newcomb, E.H., and H.T. Bonnet. 1965. “Cytoplasmic Microtubules and Wall Microfibril Orientation in Root Hairs Orientation of Radish.” *The Journal of Cell Biology*, no. 16: 575–89.

Nguema-Ona, Eric, Sílvia Coimbra, Maïté Vicré-Gibouin, Jean-Claude Mollet, and Azeddine Driouich. 2012. “Arabinogalactan Proteins in Root and Pollen-Tube Cells: Distribution and Functional Aspects.” *Annals of Botany* 110 (2): 383–404. doi:10.1093/aob/mcs143.

O’Connell, Matthew J., Michael J.E. Krien, and Tony Hunter. 2003. “Never Say Never. The NIMA-Related Protein Kinases in Mitotic Control.” *Trends in Cell Biology* 13 (5): 221–28. doi:10.1016/S0962-8924(03)00056-4.

Oda, Yoshihisa. 2015. “Cortical Microtubule Rearrangements and Cell Wall Patterning.” *Frontiers in Plant Science* 6 (April): 1–7. doi:10.3389/fpls.2015.00236.

Oda, Yoshihisa, and Hiroo Fukuda. 2012. “Initiation of Cell Wall Pattern by a Rho- and Microtubule-Driven Symmetry Breaking.” *Science (New York, N.Y.)* 337 (6100): 1333–36. doi:10.1126/science.1222597.

Oda, Yoshihisa, and Hiroo Fukuda. 2013a. “Rho of Plant GTPase Signaling Regulates the Behavior of Arabidopsis Kinesin-13A to Establish Secondary Cell Wall Patterns.” *The Plant Cell* 25 (November): 1–13. doi:10.1105/tpc.113.117853.

Oda, Yoshihisa, and Hiroo Fukuda. 2013b. “Spatial Organization of Xylem Cell Walls by ROP

GTPases and Microtubule-Associated Proteins.” *Current Opinion in Plant Biology* 16 (6). Elsevier Ltd: 743–48. doi:10.1016/j.pbi.2013.10.010.

Oda, Yoshihisa, Yuki Iida, Yuki Kondo, and Hiroo Fukuda. 2010. “Wood Cell-Wall Structure Requires Local 2D-Microtubule Disassembly by a Novel Plasma Membrane-Anchored Protein.” *Current Biology* 20 (13). Elsevier Ltd: 1197–1202. doi:10.1016/j.cub.2010.05.038.

Oda, Yoshihisa, Tetsuro Mimura, and Seiichiro Hasezawa. 2005. “Regulation of Secondary Cell Wall Development by Cortical Microtubules during Tracheary Element Differentiation in Arabidopsis Cell Suspensions.” *Plant Physiology* 137 (3): 1027–36. doi:10.1104/pp.104.052613.

Parton, R. M., a. F. Dyer, N. D. Read, and a. J. Trewavas. 2000. “Apical Structure of Actively Growing Fern Rhizoids Examined by DIC and Confocal Microscopy.” *Annals of Botany* 85: 233–45. doi:10.1006/anbo.1999.1027.

Parton, R M, S Fischer-Parton, M K Watahiki, and a J Trewavas. 2001. “Dynamics of the Apical Vesicle Accumulation and the Rate of Growth Are Related in Individual Pollen Tubes.” *Journal of Cell Science* 114 (Pt 14): 2685–95. doi: .

Perrin, Robyn M, Yan Wang, Christen Y L Yuen, Jessica Will, and Patrick H Masson. 2007. “WVD2 Is a Novel Microtubule-Associated Protein in Arabidopsis Thaliana.” *The Plant Journal : For Cell and Molecular Biology* 49 (6): 961–71. doi:10.1111/j.1365-313X.2006.03015.x.

Pesquet, Edouard, Andrey V. Korolev, Grant Calder, and Clive W. Lloyd. 2010. “The Microtubule-Associated Protein AtMAP70-5 Regulates Secondary Wall Patterning in Arabidopsis Wood Cells.” *Current Biology* 20 (8). Elsevier Ltd: 744–49. doi:10.1016/j.cub.2010.02.057.

Peter, Isabelle S, and Eric H Davidson. 2011. “Evolution of Gene Regulatory Networks

Controlling Body Plan Development." Article. *Cell* 144 (6). Elsevier Inc.: 970–85. doi:10.1016/j.cell.2011.02.017.

Pickett-heaps, Author Jeremy D, Brian E S Gunning, Roy C Brown, Betty E Lemmon, Jeremy D Pickett-heaps, Brian E S Gunning, Roy C Brown, Betty E Lemmon, and A N N L Cleary. 1999. "The Cytoplast Concept in Dividing Plant Cells : Cytoplasmic Domains and the Evolution of Spatially Organized Cell Division." *Ameri* 86 (2): 153–72.

Proust, H??l??ne, Suvi Honkanen, Victor A S Jones, Giulia Morieri, Helen Prescott, Steve Kelly, Kimitsune Ishizaki, Takayuki Kohchi, and Liam Dolan. 2016. "RSL Class I Genes Controlled the Development of Epidermal Structures in the Common Ancestor of Land Plants." *Current Biology* 26 (1): 93–99. doi:10.1016/j.cub.2015.11.042.

Qiu, Y.-L., L. Li, B. Wang, Z. Chen, V. Knoop, M. Groth-Malonek, O. Dombrovska, et al. 2006. "The Deepest Divergences in Land Plants Inferred from Phylogenomic Evidence." *Proceedings of the National Academy of Sciences* 103 (42): 15511–16. doi:10.1073/pnas.0603335103.

Reiss, Hans Dieter, Eberhard Schnepf, and Werner Herth. 1984. "The Plasma Membrane of the Funaria Caulonema Tip Cell: Morphology and Distribution of Particle Rosettes, and the Kinetics of Cellulose Synthesis." *Planta* 160 (5): 428–35. doi:10.1007/BF00429759.

Rensing, Stefan A, Julia Ick, Jeffrey A Fawcett, Daniel Lang, Andreas Zimmer, Yves Van de Peer, and Ralf Reski. 2007. "An Ancient Genome Duplication Contributed to the Abundance of Metabolic Genes in the Moss Physcomitrella Patens." *BMC Evolutionary Biology* 7 (1): 130. doi:10.1186/1471-2148-7-130.

Röckel, Nina, Sebastian Wolf, Benedikt Kost, Thomas Rausch, and Steffen Greiner. 2008. "Elaborate Spatial Patterning of Cell-Wall PME and PMEI at the Pollen Tube Tip Involves PMEI Endocytosis, and Reflects the Distribution of Esterified and de-Esterified Pectins." *Plant Journal* 53 (1): 133–43. doi:10.1111/j.1365-313X.2007.03325.x.

Rojas, Enrique R., Scott Hotton, and Jacques Dumais. 2011. “Chemically Mediated Mechanical Expansion of the Pollen Tube Cell Wall.” *Biophysical Journal* 101 (8). Biophysical Society: 1844–53. doi:10.1016/j.bpj.2011.08.016.

Roll-Mecak, Antonina, and Ronald D. Vale. 2008. “Structural Basis of Microtubule Severing by the Hereditary Spastic Paraplegia Protein Spastin.” *Nature* 451 (7176): 363–67. doi:10.1038/nature06482.

Rossum, G. van. 1995. “Python Tutorial, Technical Report CS-R9526.” Centrum voor Wiskunde en Informatica (CWI), Amsterdam.

Rounds, Caleb M, and Magdalena Bezanilla. 2013. “Growth Mechanisms in Tip-Growing Plant Cells.” *Annual Review of Plant Biology* 64: 243–65. doi:10.1146/annurev-arplant-050312-120150.

Sack, Fred D. 1993. “Gravitropism in Protonemata of the Moss Ceratodon.” *Memoirs of the Torrey Botanical Club* 25 (1): 36–44.

Sasabe, Michiko, Ken Kosetsu, Mikiko Hidaka, Akinori Murase, and Yasunori Machida. 2011. “Arabidopsis Thaliana MAP65-1 and MAP65-2 Function Redundantly with MAP65-3/PLEIADE in Cytokinesis Downstream of MPK4.” *Plant Signaling & Behavior* 6 (5): 743–47. doi:10.4161/psb.6.5.15146.

Schaefer, Estelle, Katia Belcram, Magalie Uyttewaal, Yann Duroc, Magali Goussot, David Legland, Elise Laruelle, Marie-Ludivine de Tauzia-Moreau, Martine Pastuglia, and David Bouchez. 2017. “The Preprophase Band of Microtubules Controls the Robustness of Division Orientation in Plants.” *Science* 356 (6334): 186–89. doi:10.1126/science.aal3016.

Schwuchow, J., F. D. Sack, and E. Hartmann. 1990. “Microtubule Distribution in Gravitropic Protonemata of the Moss Ceratodon.” *Protoplasma* 159 (1): 60–69. doi:10.1007/BF01326635.

Seabold, Skipper, and Josef Perktold. 2010. “Statsmodels: Econometric and Statistical

Modeling with Python." In *9th Python in Science Conference*.

Seifert, Georg J, and Keith Roberts. 2007. "The Biology of Arabinogalactan Proteins." *Annual Review of Plant Biology* 58: 137–61. doi:10.1146/annurev.arplant.58.032806.103801.

Seshadri, Aravind. 2006. "Simulated Annealing for Traveling Salesman Problem," 1–14.

Shaw, S L, J Dumais, and S R Long. 2000. "Cell Surface Expansion in Polarly Growing Root Hairs of Medicago Truncatula." *Plant Physiology* 124 (3): 959–70. doi:10.1104/pp.124.3.959.

Sherrier, D. Janine, and Kathryn A. VandenBosch. 1994. "Secretion of Cell Wall Polysaccharides in Vicia Root Hairs." *The Plant Journal* 5 (2): 185–95.

Shpak, E, J F Leykam, and M J Kieliszewski. 1999. "Synthetic Genes for Glycoprotein Design and the Elucidation of Hydroxyproline-O-Glycosylation Codes." *Proceedings of the National Academy of Sciences of the United States of America* 96 (26): 14736–41. doi:10.1073/pnas.96.26.14736.

Sieberer, Björn J., Tijs Ketelaar, John J. Esseling, and a. M C Emons. 2005. "Microtubules Guide Root Hair Tip Growth." *New Phytologist* 167 (3): 711–19. doi:10.1111/j.1469-8137.2005.01506.x.

Sieberer, Björn J, Antonius C J Timmers, and Anne Mie C Emons. 2005. "Nod Factors Alter the Microtubule Cytoskeleton in Medicago Truncatula Root Hairs to Allow Root Hair Reorientation." *Molecular Plant-Microbe Interactions : MPMI* 18 (11): 1195–1204. doi:10.1094/MPMI-18-1195.

Smertenko, Andrei P, Hsin-yu Chang, Vera Wagner, Despina Kaloriti, Stepan Fenyk, Seiji Sonobe, Clive Lloyd, Marie-Theres Hauser, and Patrick J Hussey. 2004. "The Arabidopsis Microtubule-Associated Protein AtMAP65-1: Molecular Analysis of Its Microtubule Bundling Activity." *The Plant Cell* 16 (8): 2035–47. doi:10.1105/tpc.104.023937.

Struk, Sylwia, and Pankaj Dhonukshe. 2014. "MAPs: Cellular Navigators for Microtubule

Array Orientations in Arabidopsis." *Plant Cell Reports* 33 (1): 1–21. doi:10.1007/s00299-013-1486-2.

Su, Shih Heng, and Patrick J. Krysan. 2016. "A Double-Mutant Collection Targeting MAP Kinase Related Genes in Arabidopsis for Studying Genetic Interactions." *Plant Journal* 88 (5): 867–78. doi:10.1111/tpj.13292.

Sun, J, Q Ma, and T Mao. 2015. "Ethylene Regulates the Arabidopsis Microtubule-Associated Protein WAVE-DAMPENED2-LIKE5 in Etiolated Hypocotyl Elongation." *Plant Physiol* 169 (1): 325–37. doi:10.1104/pp.15.00609.

Tabuchi, Akira, Lian Chao Li, and Daniel J. Cosgrove. 2011. "Matrix Solubilization and Cell Wall Weakening Byβ-Expansin (Group-1 Allergen) from Maize Pollen." *Plant Journal* 68 (3): 546–59. doi:10.1111/j.1365-313X.2011.04705.x.

Tian, Guo W., Min Huei Chen, Adi Zaltsman, and Vitaly Citovsky. 2006. "Pollen-Specific Pectin Methylesterase Involved in Pollen Tube Growth." *Developmental Biology* 294 (1): 83–91. doi:10.1016/j.ydbio.2006.02.026.

Timmers, Antonius C J, Pascal Vallotton, Claudia Heym, and Diedrik Menzel. 2007. "Microtubule Dynamics in Root Hairs of Medicago Truncatula." *European Journal of Cell Biology* 86 (2): 69–83. doi:10.1016/j.ejcb.2006.11.001.

Valentin, Romain, Carole Cerclier, Nathalie Geneix, V??ronique Agui??-B??ghin, C??dric Gaillard, Marie Christine Ralet, and Bernard Cathala. 2010. "Elaboration of Extensin-Pectin Thin Film Model of Primary Plant Cell Wall." *Langmuir* 26 (12): 9891–98. doi:10.1021/la100265d.

Van Der Walt, S., Johannes L Schönberger, Juan Nunez-Iglesias, François Boulogne, Joshua D Warner, Neil Yager, Emmanuelle Gouillart, and Tony Yu. 2014. "Scikit-Image: Image Processing in Python." *PeerJ* 2: e453. doi:10.7717/peerj.453.

van der Walt, S, S C Colbert, and G Varoquaux. 2011. "The NumPy Array: A Structure for

Efficient Numerical Computation." *Computing in Science Engineering* 13 (2): 22–30. doi:10.1109/MCSE.2011.37.

Vassileva, V N. 2005. "Microtubule Dynamics in Living Root Hairs: Transient Slowing by Lipochitin Oligosaccharide Nodulation Signals." *The Plant Cell Online* 17 (6): 1777–87. doi:10.1105/tpc.105.031641.

Velasquez, S M, M M Ricardi, J G Dorosz, P V Fernandez, A D Nadra, L Pol-Fachin, J Egelund, et al. 2011. "O-Glycosylated Cell Wall Proteins Are Essential in Root Hair Growth." *Science* 332 (6036): 1401–3. doi:10.1126/science.1206657.

Velasquez, Silvia M., Eliana Marzol, Cecilia Borassi, Laercio Pol-Fachin, Martiniano Maria Ricardi, Silvina Mangano, Silvina Paola Denita Juarez, et al. 2015. "Low Sugar Is Not Always Good: Impact of Specific O-Glycan Defects on Tip Growth in Arabidopsis." *Plant Physiology* 168 (July): 808–13. doi:10.1104/pp.114.255521.

Verhey, Kristen J., Neha Kaul, and Virupakshi Soppina. 2011. "Kinesin Assembly and Movement in Cells." *Annual Review of Biophysics* 40 (1): 267–88. doi:10.1146/annurev-biophys-042910-155310.

Vidali, Luis, Caleb M. Rounds, Peter K. Hepler, and Magdalena Bezanilla. 2009. "Lifeact-mEGFP Reveals a Dynamic Apical F-Actin Network in Tip Growing Plant Cells." *PLoS ONE* 4 (5). doi:10.1371/journal.pone.0005744.

Wada, Masamitsu, and L. Andrew Staehelin. 1981. "Freeze-Fracture Observations on the Plasma Membrane, the Cell Wall and the Cuticle of Growing Protonemata of Adiantum Capillus-Veneris L." *Planta* 151 (5): 462–68. doi:10.1007/BF00386540.

Wang, Bin, Li Huey Yeun, Jia Yu Xue, Yang Liu, Jean Michel Ané, and Yin Long Qiu. 2010. "Presence of Three Mycorrhizal Genes in the Common Ancestor of Land Plants Suggests a Key Role of Mycorrhizas in the Colonization of Land by Plants." *New Phytologist* 186 (2): 514–25. doi:10.1111/j.1469-8137.2009.03137.x.

Wang, Wei, Li Wang, Chen Chen, Guangyan Xiong, Xiao Yun Tan, Ke Zhen Yang, Zi Chen Wang, Yihua Zhou, De Ye, and Li Qun Chen. 2011. "Arabidopsis CSLD1 and CSLD4 Are Required for Cellulose Deposition and Normal Growth of Pollen Tubes." *Journal of Experimental Botany* 62 (14): 5161–77. doi:10.1093/jxb/err221.

Wang, X., L. Zhu, B. Liu, C. Wang, L. Jin, Q. Zhao, and M. Yuan. 2007. "Arabidopsis MICROTUBULE-ASSOCIATED PROTEIN18 Functions in Directional Cell Growth by Destabilizing Cortical Microtubules." *The Plant Cell Online* 19 (3): 877–89. doi:10.1105/tpc.106.048579.

Wasteneys, Geoffrey O., and J. Christian Ambrose. 2009. "Spatial Organization of Plant Cortical Microtubules: Close Encounters of the 2D Kind." *Trends in Cell Biology* 19 (2): 62–71. doi:10.1016/j.tcb.2008.11.004.

Whittington, a T, O Vugrek, K J Wei, N G Hasenbein, K Sugimoto, M C Rashbrooke, and G O Wasteneys. 2001. "MOR1 Is Essential for Organizing Cortical Microtubules in Plants." *Nature* 411 (6837): 610–13. doi:10.1038/35079128.

Winter, Debbie, Ben Vinegar, Hardeep Nahal, Ron Ammar, Greg V. Wilson, and Nicholas J. Provart. 2007. "An 'electronic Fluorescent pictograph' Browser for Exploring and Analyzing Large-Scale Biological Data Sets." *PLoS ONE* 2 (8): 1–12. doi:10.1371/journal.pone.0000718.

Won, Su Kyung, Sang Bong Choi, Simple Kumari, Misuk Cho, Sang Ho Lee, and Hyung Taeg Cho. 2010. "Root Hair-Specific EXPANSIN B Genes Have Been Selected for Graminaceae Root Hairs." *Molecules and Cells* 30 (4): 369–76. doi:10.1007/s10059-010-0127-7.

Wong, Jeh Haur, and Takashi Hashimoto. 2017. "Novel Arabidopsis Microtubule-Associated Proteins Track Growing Microtubule plus Ends." *BMC Plant Biology* 17 (1). BMC Plant Biology: 33. doi:10.1186/s12870-017-0987-5.

Yang, Guohua, Peng Gao, Hua Zhang, Shanjin Huang, and Zhi-Liang Zheng. 2007. “A Mutation in MRH2 Kinesin Enhances the Root Hair Tip Growth Defect Caused by Constitutively Activated ROP2 Small GTPase in Arabidopsis.” *PloS One* 2 (10): e1074. doi:10.1371/journal.pone.0001074.

Yao, Maki, Yoshinori Wakamatsu, Tomohiko J Itoh, Tsubasa Shoji, and Takashi Hashimoto. 2008. “Arabidopsis SPIRAL2 Promotes Uninterrupted Microtubule Growth by Suppressing the Pause State of Microtubule Dynamics.” *Journal of Cell Science* 121 (Pt 14): 2372–81. doi:10.1242/jcs.030221.

Yasuhara, Hiroki, Masaaki Muraoka, Hiroki Shogaki, Hitoshi Mori, and Seiji Sonobe. 2002. “TMBP200, a Microtubule Bundling Polypeptide Isolated from Telophase Tobacco BY-2 Cells Is a MOR1 Homologue.” *Plant & Cell Physiology* 43 (6): 595–603.

Yuasa, Koji, Kiminori Toyooka, Hiroo Fukuda, and Ken Matsuoka. 2005. “Membrane-Anchored Prolyl Hydroxylase with an Export Signal from the Endoplasmic Reticulum.” *Plant Journal* 41 (1): 81–94. doi:10.1111/j.1365-313X.2004.02279.x.

Zhang, Quan, Erica Fishel, Tyler Bertroche, and Ram Dixit. 2014. “Erratum: Microtubule Severing at Crossover Sites by Katanin Generates Ordered Cortical Microtubule Arrays in Arabidopsis (Current Biology (2013) 23 (2191-2195)).” *Current Biology* 24 (8). Elsevier Ltd: 917. doi:10.1016/j.cub.2014.03.057.

Zhu, L., Y. Zhang, E. Kang, Q. Xu, M. Wang, Y. Rui, B. Liu, M. Yuan, and Y. Fu. 2013. “MAP18 Regulates the Direction of Pollen Tube Growth in Arabidopsis by Modulating F-Actin Organization.” *The Plant Cell* 25 (3): 851–67. doi:10.1105/tpc.113.110528.